Interplay between spin transition and gas sorption in compartmentalized coordination polymers

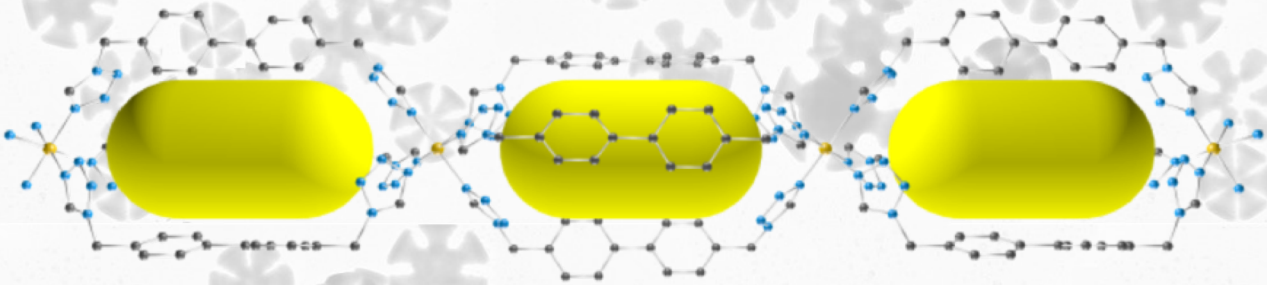

Supervised by:
Prof. Eugenio Coronado Miralles
Dr. Guillermo Mínguez Espallargas

Néstor Calvo Galve
Universitat de València
Paterna, January 2019

PhD thesis in Nanoscience and Nanotechnology

Interplay between spin transition and gas sorption in compartmentalized coordination polymers

Instituto de Ciencia Molecular (ICMol)

Universitat de València

******

Memoria presentada por Néstor Calvo Galve para aspirar al grado de Doctor en Nanociencia y Nanotecnología

Enero 2019

******

Dirigida por:

Prof. Eugenio Coronado Miralles

Dr. Guillermo Mínguez Espallargas

D. EUGENIO CORONADO MIRALLES, catedrático del Departamento de Química Inorgánica de la Universitat de València y D. GUILLERMO MÍNGUEZ ESPALLARGAS, doctor por la University of Sheffield y actualmente investigador del Instituto de Ciencia Molecular, de la Universitat de València.

CERTIFICAN:

Que la memoria presentada por D. Néstor Calvo Galve con título "Interplay between spin transition and gas sorption in compartmentalized coordination polymers" corresponde a su Tesis Doctoral y ha sido realizada bajo su dirección en el Instituto de Ciencia Molecular, autorizando mediante este escrito la presentación de la misma para optar al grado de Doctor.

En Paterna, a 14 de Enero de 2019.

Dr. Eugenio Coronado Miralles Dr. Guillermo Mínguez Espallargas

AGRADECIMIENTOS

Mucha gente ha participado directa o indirectamente en la ayuda para poder realizar esta tesis, así que esto va para largo. En primer lugar, me gustaría agradecer a mi familia directa: mis padres y mi hermano. Porque pese a los problemas vividos, estoy seguro que sin ellos no hubieran sido posibles todos estos años en la universidad.

A Eugenio Coronado, por darme la oportunidad de realizar la tesis en su grupo. Las posibilidades científicas que brindan estar en el grupo UIMM del ICMol la verdad es que son innumerables y desde luego, cuando hay un problema con el magnetismo Eugenio siempre sabe la respuesta.

A Guillermo Mínguez, una de las personas más brillantes que he conocido y que es un pozo sin fin de conocimientos. Es increíble todas las cosas que sabe y me ha enseñado a lo largo de estos años, sin duda creo que he crecido mucho en todos los aspectos durante el doctorado gracias a ti. Y no solo te agradezco como director, pues las dosis de humor diarias y necesarias no han faltado, además del apoyo moral en los momentos más difíciles. Muchas gracias por todo.

A Mónica Giménez, con la que empecé a "cacharrear" y me enseñó toda la parte del laboratorio en mis inicios. Siempre estuviste dispuesta a ayudarme y la verdad la adaptación al grupo y a la manera de trabajar en el laboratorio fue mucho más sencilla gracias a ti. Has vuelto ahora hecha toda una científica con mayúsculas y estoy seguro que te espera un futuro brillante.

A Íñigo, pues sin su ayuda gran parte de este trabajo no se hubiera podido realizar. Fue un placer conocerte en persona y las dosis de humor tampoco faltaban contigo. También agradecer al grupo del Prof. Fernando Rey y en especial a Miguel Palomino por las medidas de adsorción y separación de gases. También han ayudado en gran medida a la realización de esta tesis. Y a Mónica Jiménez, por la ayuda en la difracción de neutrones.

A todo el equipo técnico del grupo UIMM. Gracias Alejandra por la ayuda en las medidas de superficie, Xevi por los pedidos (aunque a veces a regañadientes), Ángel por estar siempre disponible para cualquier ayuda. Gracias también a Gloria y Chema por las medidas de SQUID, Manuel por la ayuda con cualquier problema informático, Paco por todos los papeleos del master y doctorado. También gracias a Cristian, que ha sido el último en llegar y siempre está ayudando con cualquier incidencia mecánica.

A los compañeros del master, pese a que tras 5 semanas en Toledo se me han quitado las ganas de volver, con vosotros las cuestas fueron mucho más divertidas. Las escuelas fueron épicas y la verdad han quedado anécdotas graciosas para toda la vida.

A muchos compañeros de carrera, pese a haber perdido el contacto con muchos, afortunadamente lo mantengo con algunos (Javi, Alexis, Víctor). La verdad es que son años que se recuerdan con mucho cariño.

A Elena, una de las mejores personas que he conocido y creo que ha debido ser la que más abrazos me ha dado en la vida. Se agradece mucho todo el cariño que das a la gente y estoy muy orgulloso de las decisiones que tomaste para hacer el master de docencia y poder dedicarte a ello. Estoy seguro que vas a ser una profesora increíble.

A Lopera, otra persona increíble y que es imposible no reírse a su lado. Las historias inverosímiles que cuenta nos hacen reír a carcajadas siempre a todos, sin duda eres un personaje sacado de los libros de Bukowsky. Y además de las risas, en los momentos serios siempre has estado ahí.

A Jose, que pese a haber tenido nuestros roces durante todos estos años (mítica la zapatilla volando en Toledo), es otra persona que siempre está ahí para preguntar cualquier cosa, ya que se estudia tanto las bases de cualquier organismo que sabe más que el que las escribe. Las risas con él y los troleos nunca han faltado.

A Lucía, que se convirtió en mi gran amiga durante la carrera. Demasiadas risas haciendo los trabajos de química-física. La tuya es una de esas amistades que durarán toda la vida, muchas gracias por TODO. Estoy muy orgulloso que consigas todo lo que te propones, llegarás todo lo lejos que quieras.

Llega el turno a los compañeros del UIMM, espero no dejarme a nadie. Si es así lo siento. A las compañeras de pecera originales (Verónica, Yan, Patricia). A Michele, los últimos post-doc llegados Manel, Eleni. También a Edurne, una lástima que no hubieras llegado antes, nos hubiéramos echado buenas

risas en el 2.7. A CMG por trolearme los días que me quedaba hasta las 10 de la noche o los sábados y domingos en navidad. A Katia, porque su TOC es muy divertido. Además, es un público fácil para mis contextualizadas historias. A Roger, porque hablar de dinero con él siempre te saca unas risas. También es una persona que cuando toca hablar serio, es el primero. A Ramón, otro compañero de algunos fines de semana. Si uno quiere escapar al foco de las bromas, llame a Ramón para que se las lleve todas (jajaja). A Mario, por sus "yeeee locoooo" diarios. A SeNa, que tiene las respuestas más rápidas e ingeniosas cuando le intentas trolear. A recién llegados como María.

A los compañeros de LA pecera. Al último en llegar, Alejandro, porque esa violencia verbal durante los últimos meses de tesis ha sido muy desestresante. A Cella, el primo lejano del pueblo. Los meses de cadenas de bromas fueron muy divertidos, además de los montajes y troleos realizados a otras personas. Y me dejo los dos últimos para el final.

A Javi, porque las mofadas en estos años han sido infinitas. Un gran compañero y un gran amigo, con toda la producción científica que has hecho en este tiempo y la que te queda estoy seguro que te espera un gran futuro como investigador. Has sabido dar el punto de risas perfecto al día a día para poder sobrellevar la realización de esta tesis, muchísimas gracias.

A Eugenia, continuadora de mi trabajo en el ICMol y una grandísima persona. Estoy seguro que con tu perseverancia, tus ganas incansables de trabajar y tu buen hacer, los resultados científicos excepcionales que te mereces llegarán. Ha sido un placer compartir contigo las charlas de ciencia y de no ciencia, las

risas, los días de cine y los infinitos pinchos de tortilla durante todos estos años (¡y espero que durante muchos más!). Muchas gracias por todo.

A mi amiga Daniela, que pese a perdernos la pista durante años al acabar el instituto, nos pudimos reencontrar años después y continuar una amistad que durará para toda la vida. Pese a que estemos a miles de kilómetros nunca perderemos el contacto.

A mi amigo Antonio, por todas las palabras cultas que me has enseñado, además de todo el saber que atesoras de cosas que la mente de un científico ni piensa en ellas. Ha sido un placer poderte enseñar un poquito de ajedrez.

A todos los compañeros del club de ajedrez Camp de Morvedre. La verdad creo que son ya casi 20 años allí y las dosis de risas y locuras vividas a lo largo de estos años son inolvidables.

SUMMARY

The work described in this thesis is motivated by the intention of developing multifunctional compartmentalized coordination polymers and study their magnetic and gas sorption properties. A rational ligand design has been developed in order to accomplish the objectives of the different chapters. The ligands provide flexible structures and appropriate moieties to produce the spin-crossover behaviour. Three different ligands have been used and are:

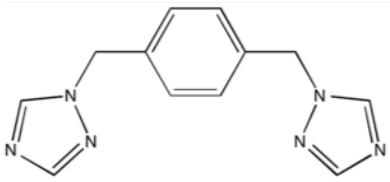

1,4-bis(triazol-1-ylmethyl)benzene

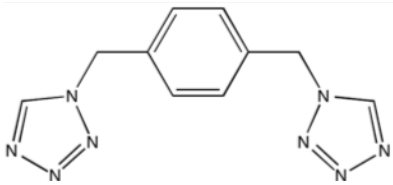

1,4-bis(tetrazol-1-ylmethyl)benzene

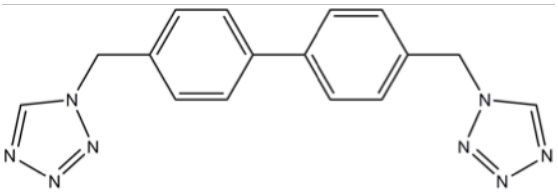

4,4'-bis((1H-tetrazol-1-yl)methyl)-1,1'-biphenyl

The ligand 1,4-bis(triazol-1-ylmethyl)benzene (btix) has been combined with the ligand 1,4-bis(tetrazol-1-ylmethyl)benzene (btzx) to produce new spin transitions on a coordination polymer. Btzx has been used to synthesize two previously reported coordination polymers and study their magnetic and gas sorption/separation properties and with 4,4'-bis((1H-tetrazol-1-yl)methyl)-1,1'-biphenyl (btzbp), other two isostructural but larger coordination polymers have been obtained, enhancing the gas capacity of the previous

reported systems. In addition, this system has been studied under microfluidic conditions.

First of all, a general introduction to coordination polymers is presented in *chapter 1*, focusing on the particular type of coordination polymers presenting magnetism and spin-crossover. *Chapter 2* presents how compartmentalized coordination polymers are perfect materials to study gas sorption and gas separation. In addition, with the presence of spin-crossover behaviour, it will be discussed how the inclusion of different gases can affect the spin transition temperature.

Chapter 3 presents how the synthesis of chemical mixtures of different ligands can effectively tune the spin transition temperature.

In *chapter 4* it is shown how the chemical design of a larger ligand can afford an enhancement of the gas sorption properties of different coordination polymers.

Finally, in *chapter 5* the study of the crystallization processes on compartmentalized coordination polymers has been performed using microfluidics approaches. Interesting pathways of growing have been found and how the different synthesis processes can affect to the growing of the microcrystals will be discussed.

The work described in this dissertation has given rise to the following publications:

"A mixed-ligand approach for spin-crossover modulation in a linear Fe^{II} coordination polymer". N. Calvo Galve, E. Coronado, M. Giménez-Marqués, G. Mínguez Espallargas. *Inorg. Chem.* **2014**, *53*, 4482-4490.

"Isostructural compartmentalized spin-crossover coordination polymers for gas confinement". N. Calvo Galve, M. Giménez-Marqués, M. Palomino, S. Valencia, F. Rey, G. Mínguez Espallargas, E. Coronado. *Inorg. Chem. Front.* **2016**, *3*, 808-813.

"Gas confinement in compartmentalized coordination polymers for highly selective sorption". M. Giménez-Marqués, N. Calvo Galve, M. Palomino, S. Valencia, F. Rey, G. Sastre, I. J. Vitórica-Yrezábal, M. Jiménez-Ruiz, J. A. Rodríguez-Velamazán, M. A. González, J. L. Jordá, E. Coronado, G. Mínguez Espallargas. *Chem. Sci.* **2017**, *8*, 3109-3120.

"Unveiling pathway complexity in the growth of a spin-crossover MOF via engineered liquid-liquid interfacial reactions". N. Calvo Galve, A. Abrishamkar, A. Sorrenti, E. Coronado, A. J. deMello, G. Mínguez Espallargas, J. Puigmartí-Luís. *Submitted*.

Table of Contents

Chapter 1:
Introduction

1.1 Coordination polymers and MOFs

Coordination polymers are hybrid organic-inorganic materials formed by a metal and surrounding organic ligands connected by coordination bonds to form 1D, 2D or 3D topologies (figure 1.1). The most studied metals in coordination polymers are the transition metals and combined with a huge library of organic ligands, the possibilities of constructing coordination polymers are almost infinite. Chemical design is the key to construct coordination polymers with desired properties and with the possibility to combine such a numerous building blocks, the properties of these materials are very varied and extensive.

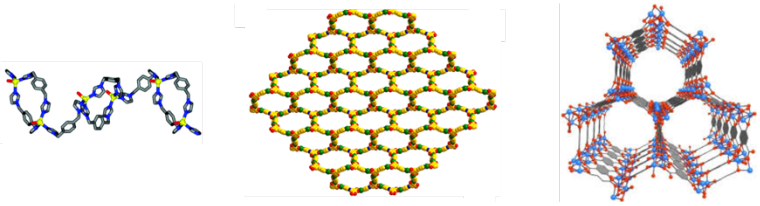

Figure 1.1. Different dimensionality in coordination polymers.

One of the properties that can present these materials is the porosity. When it occurs, the coordination polymer is called porous coordination polymer or metal-organic framework (MOF)[1] and the porosity in these compounds can be presented in different dimensionalities (figure 1.2). These materials present a lot of applications based on their varied properties, like high chemical stability, magnetism, catalysis, proton conductivity, nanofabrication, optics, gas storage and separation, among others.[2]

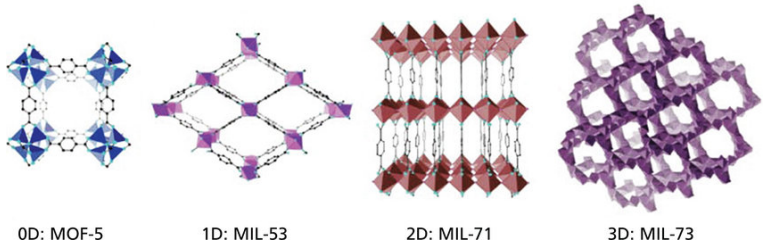

Figure 1.2. Different dimensionalities of the inorganic SBUs in MOFs.

Unfortunately, the presence of strong covalent and coordination bonds in these materials do not ensure them to present good thermal stability, in fact, over all the MOFs reported (>80.000), only a minority are high temperature stable.[3,4] In addition, chemical stability is necessary to ensure endurance against solvents and other chemical agents. One of the first examples of MOF with a high chemical stability is the zeolitic imidazolate framework-8 (ZIF-8),[5] reported in 2006 and presenting stability in front of boiling methanol, benzene, water and concentrated NaOH at 100 ºC (figure 1.3).

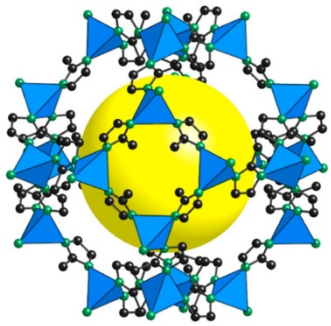

Figure 1.3. Structure of ZIF-8. The yellow sphere represents empty space.

The presence in MOFs of high surface areas, large pores and active sites make them perfect candidates for catalysis. The first example reported was in 1994,[6]

involving the cyanosilylation of aldehydes in a Cd-based framework. Since then, many examples of catalytic MOFs have been reported. Another interesting use for MOFs is in fuel cell applications, taking advantage of proton-conducting properties presented in some of these materials. The first measured conductivity were performed by Kitagawa and co-workers in 2002.[7] The compound was an oxoamidato derivative, although the conductivity results were not so good. Further investigations on MOFs established that in order to obtain good proton conductivities, the presence of carboxylic acids is necessary.

Porosity in MOFs make them perfect candidates for gas storage. The first example of permanent porosity on a MOF was obtained in 1998 by Yaghi and co-workers with the measurement of nitrogen and carbon dioxide isotherms on a layered zinc terephthalate MOF, Zn(BDC).[8] The next year, the same group reported MOF-5, presenting robustness and high porosity (figure1.4).[9]

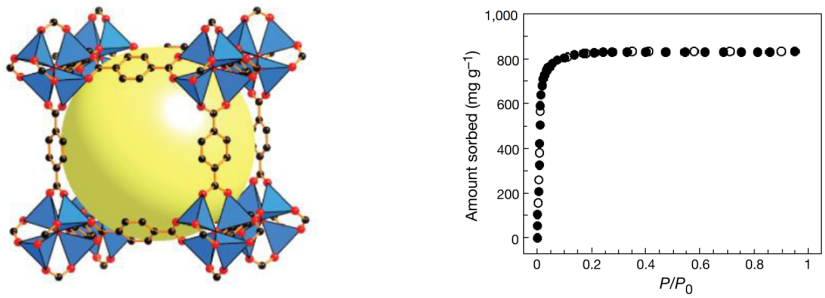

Figure 1.4. Structure of MOF-5. The yellow sphere represents empty space (left). N_2 sorption isotherm for MOF-5 (right).

The structure consists on $Zn_4O(CO_2)_6$ octahedral secondary building units linked by six chelating 1,4-benzenedicarboxylate (BDC^{2-}) units, forming a cubic framework. The BET surface is 2320 m^2/g, which is substantially higher than those commonly found for zeolites or activated carbons. Still, the efforts of the MOF community to produce high porous materials developed the gas capacity of the materials over the years. In 2004 Yaghi and co-workers reported the MOF-177, of formula $Zn_4O(BTB)_2$, being BTB the 4,4,4´-benzene-1,3,5-triyl-tribenzoate ligand.[10] It established the BET record at that time, being 3780 m^2/g (figure 1.5).

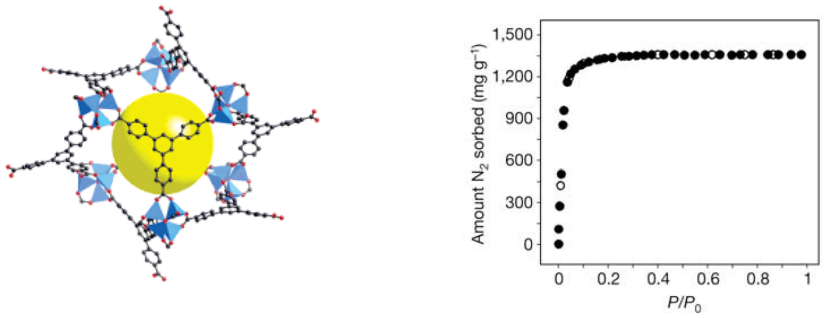

Figure 1.5. Structure of MOF-177. The yellow sphere represents empty space (left). N_2 sorption isotherm for MOF-177 (right).

Based on the same topological structures, in 2010 they doubled the value of BET reporting the MOF-210,[11] which has the formula $(Zn_4O)_3(BTE)_4(BPDC)_3$, being BTE = 4,4,4´-(benzene-1,3,5-triyl-tris(ethyne-2,1-diyl))tribenzoate and BPDC = biphenyl-4,4´-dicarboxylate. Not only increasing the storage capacity has been developed over the years but also, more interestingly, the possibility to use these materials for gas separation.

1.2 Ultra-microporous MOFs

The possibility in MOFs to present reversible gas adsorption make them perfect candidates to study separation of distinct gas mixtures. A special class of MOFs has been used in the recent years for gas separation, known as ultra-microporous MOFs.[12] Instead of synthesizing MOFs with wide pore size, these MOFs present pore aperture size below 5-7 Å, presenting notable performances as separating agents due to the small pore size and shape. These ultra-micropores can be tuned with the properties of the gases to separate (size, shape and electronic properties). However, these materials not only present advantages, but also can present problems due to slow kinetics in the gas sorption process, the quantity of gas adsorbed, pore gate opening effects and breathing. Different strategies are being used for achieving the gas separation and are listed in the next sections.

1.2.1 Thermodynamic separation

Thermodynamic separation is one of the most common strategies. It is based on the different affinities of the different components in the gas mixture and the framework.

One of the most important mixtures to separate in the industry is the one formed by acetylene (C_2H_2) and carbon dioxide (CO_2). Acetylene is extensively used in the petrochemical and electronic industries. The production of highly pure acetylene presents the problem of carbon dioxide contamination, so a high-efficient separation of these two gases is needed. Kitagawa *et al.* reported in 2005[13] the selective sorption of acetylene

compared to carbon dioxide in a previously studied copper MOF, $Cu_2(pzdc)_2(pyz)$.[14,15] (figure 1.6).

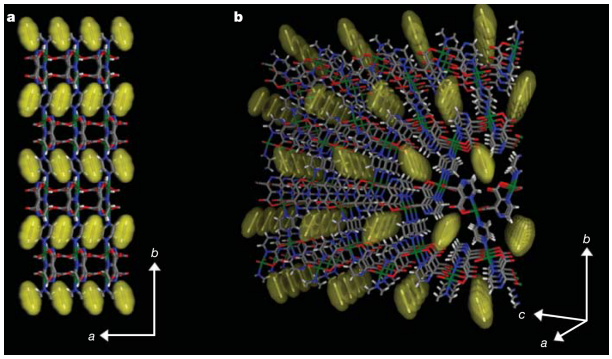

Figure 1.6. Structure of $Cu_2(pzdc)_2(pyz)$ with C_2H_2 inside. View down the *c* axis (a) and view down the *a* axis (b).

The structure is defined by 2D layers formed by Cu(pzdc) units pillared by pyrazine molecules and resulting in 1D channels of 6 x 4 Å of pore dimension. Individual gas sorption isotherms for acetylene and carbon dioxide revealed an indicative preferential sorption of the first one, confirmed by the measure of the heat of adsorption for each one, derived from the Clausius-Clapeyron equation. The location of the acetylene molecules in the structure were described using Rietveld refinements and reveals that the gas molecules are located in the middle of the channels forming strong hydrogen bonds between their hydrogen atoms and the oxygen atoms of the framework. It was the first example of a material capable of preferential adsorption of acetylene in front of carbon dioxide.

However, as CO_2 is the main impurity that should be removed to obtain pure C_2H_2 gas, it would be more convenient to design a material that presents an inverse selectivity, that is, preferential sorption of CO_2 among C_2H_2. This rare inverse selectivity was accomplished by the same group, Kitagawa and co-workers reported in 2016 a MOF presenting this particularity.[16] The material is formed by [Mn(bdc)(dpe)] units, with an interpenetrated structure that display disrupted 1D channels, resulting in the formation of isolated cages. (figure1.7).

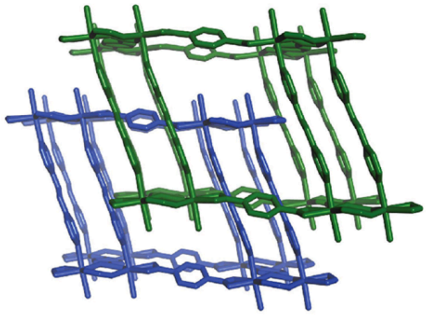

Figure 1.7. Interpenetrated structure of [Mn(bdc)(dpe)].

The material shows carbon dioxide adsorption (21.6 weight % at 195 K), but in the gas sorption isotherm for acetylene, only sorption is showed until reaching certain pressure, revealing a gate opening effect (figure 1.8). IAST calculation and gas breakthrough experiments for CO_2/C_2H_2 mixtures fully

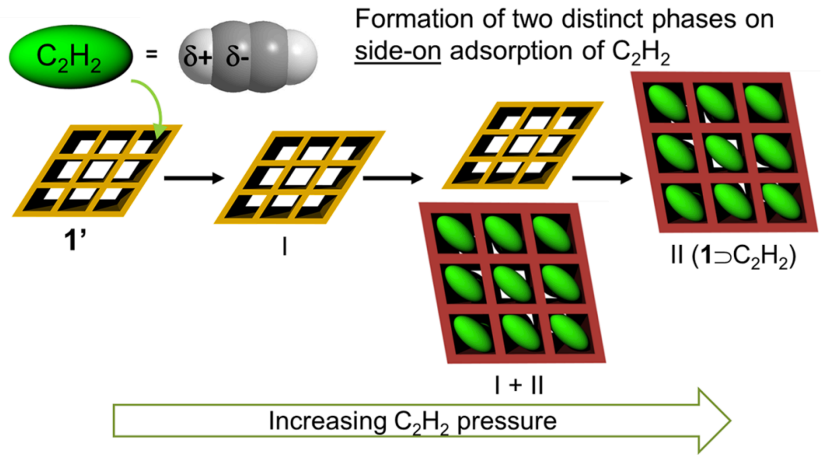

Figure 1.8. Gate-opening effect observed in the C_2H_2 adsorption by [Mn(bdc)(dpe)].

confirm a preferential selectivity for CO_2. Authors hypothesized about this preferential sorption with the interaction between the quadrupole moment of the gases and the framework in the small cage. The opposite quadrupolar moment of both gases, $-4.30 \cdot 10^{26}$ [esu·cm^2] for CO_2 and $6.03 \cdot 10^{26}$ [esu·cm^2] for C_2H_2, can explain the differences observed in sorption at low pressures, being the interaction for CO_2 positive (attracting it) and negative for C_2H_2 (refusing it). This situation is only perturbed by a structure transformation at high pressures, permitting the access of acetylene molecules to the pores.

Another important mixture to separate in industry is the acetylene/ethylene mixture. Ethylene is used in the industry of polymers and another chemical reagents, but during the production of it some impurities are generated,

including acetylene. Hu and co-workers reported in 2017 a MOF named UTSA-100,[17] presenting 1D channels of 4.3 Å and small cages between the channels with a pore aperture of 3.3 Å (figure 1.9).

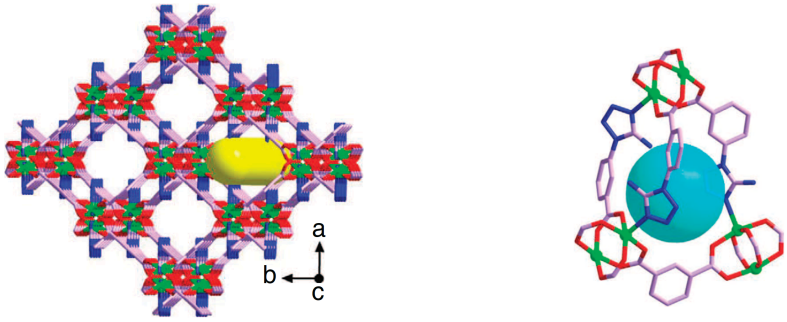

Figure 1.9. Channels (left) and cages (right) in UTSA-100.

The adsorption isotherms showed moderate acetylene uptake in comparison with ethylene, confirming the preferential selectivity with IAST and breakthrough experiments. DFT calculations revealed the reason for this preferential sorption: a strong hydrogen bonding between the oxygen atoms of the MOF and the hydrogen atoms of the acetylene.

1.2.2 Kinetic separation

In gas separation, kinetics takes advantage of the diffusivity problems of some gases to move along the pores of a material. Normally, this approach is used with gases that have similar size and functionality.

Kinetics is useful to separate mixtures of linear alkanes. One example of this kind is provided by fcu-MOF-1. Its structure is formed by the connection of $[Tb_6(\mu_3\text{-}OH)_8(O_2C\text{–})_6(N_4C)_6]$ and 2-fluoro-4-(1*H*-tetrazol-5-yl)benzoic acid

that generates a 3D periodic MOF with two types of polyhedral cages (octahedral and tetrahedral), with pore diameters of 5-6 Å (figure 1.10).[18] This material was reported by Eddaoudi *et al.* in 2013 and in 2015 the same group studied the material for ethane, propane and *n*-butane adsorption.[19] The adsorption isotherms of ethane, propane and *n*-butane showed a preferential adsorption of the C_{2+} hydrocarbons. In addition, the kinetic study showed that the adsorption kinetics for *n*-butane is much slower than for methane, as confirmed by breakthrough experiments that present almost an infinite selectivity in the mixture butane/methane.

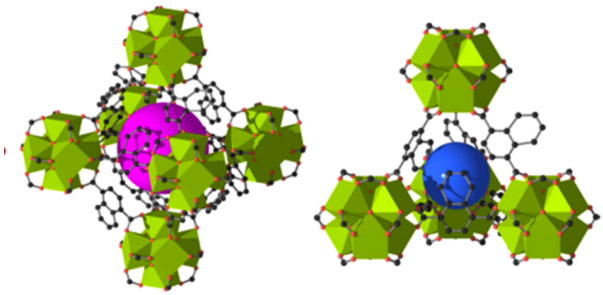

Figure 1.10. Crystal structure of fcu-MOF-1 showing the octahedral (left) and tetrahedral (right) cages.

Separation of propylene and propane were investigated using the previous described ZIF-8 material. Adsorption experiments showed similar sorption capabilities for both gases in ZIF-8, but further investigations in the kinetic sorption process of each gas revealed that propylene diffuses much faster (by two orders of magnitude) than propane. This has been explained due to the smaller kinetic diameter for propylene, that is allowed to pass more easily

through the aperture of the ZIF-8 pores, diffusing much faster and allowing the separation of both gases.

1.3 Magnetic MOFs

Over years, the inclusion of magnetic properties on coordination polymers have been extensively used. The infinite possibilities to tune the coordination polymers are of great interest to combine magnetic behaviour with other interesting properties. In MOFs, the presence of porosity open the possibility of synthesizing multifunctional materials in which magnetism can be tuned by the presence of guest molecules. This topic has recently been reviewed.[20] The magnetic MOFs can be divided in materials presenting long-range order magnetism, single-molecule magnetic behaviour and spin-crossover phenomena. The first and the second class of materials will be discussed in this section and the last one will be extensively discussed more in detail in the later sections as this is the approach used in this *thesis*.

1.3.1 Long-range magnetic order in MOFs

The presence of porosity and magnetism in a material is challenging due to the fact that whereas porosity normally needs long linkers to produce wide pores, magnetism needs short distances between the metal centers to produce strong magnetic exchange. Different strategies have been developed to carry out this combination of opposite properties, which will be discussed below.

The first one is the use of short linkers. The smallest ligand used in the synthesis of magnetic coordination polymers is the cyanide (CN^-) group and

the first example of a material combining porosity and long-range order magnetism was reported by Long *et al.* in 2002.[21] The compound is formed by $Co_3[Co(CN)_5]_2$ units and presents a magnetic ordering at 38 K with a BET surface area of 480 $m^2\ g^{-1}$ by N_2 sorption, although the gas sorption does not modify the magnetism. Years later, the same group reported two analogous materials, $CsNi[Cr(CN)_6]$ and $Cr_3[Cr(CN)_6]_2 \cdot 6\ H_2O$.[22] Their crystal structures can be seen on figure 1.11. These authors observed that the sorption of O_2 causes an increase in the ordering temperature due to a ferromagnetic coupling between the paramagnetic oxygen molecules and the $[Cr(CN)_6]^{3-}$ units (figure 1.12). That demonstrates that the inclusion of guest molecules inside a porous structure can modify the intrinsic magnetic properties of the material.

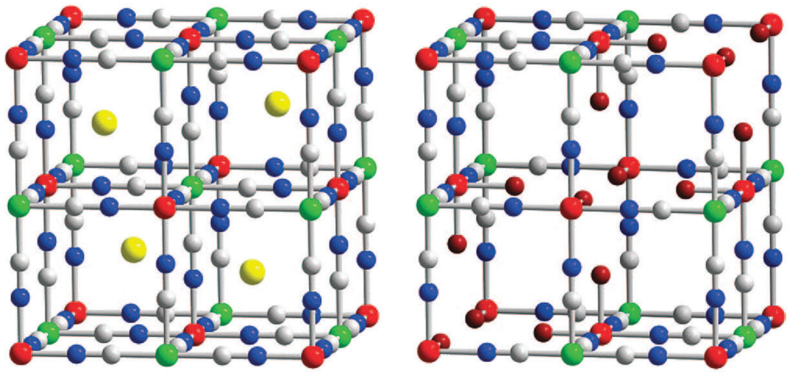

Figure 1.11. Crystal structure of $CsNi[Cr(CN)_6]$ (left) and $Cr_3[Cr(CN)_6]_2 \cdot 6\ H_2O$ (right).

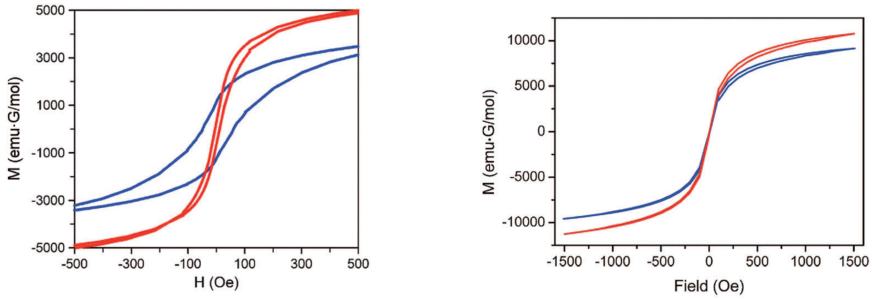

Figure 1.12. left: Magnetic hysteresis loops measured at 5 K of bare $Cr_3[Cr(CN)_6]_2 \cdot 6\ H_2O$ (blue) and loaded with O_2 (red). Right: Magnetic hysteresis loops measured at 2 K of bare $CsNi[Cr(CN)_6]$ (blue) and loaded with O_2 (red).

Other small linkers used in the construction of materials with long-range magnetic order are the heterocyclic family of diazines. In 2008, Navarro and co-workers reported the modification of the magnetic properties upon guest inclusion on a Cu(II) MOF.[23] The compound presents the formula $[Cu(F\text{-}pymo)_2(H_2O)_{1.25}]_n$ being F-pymo = 5-fluoropyrimidin-2-olate. The structure presents helical channels filled with water molecules (figure 1.13). The material presents antiferromagnetic interactions, and it orders as a canted antiferromagnet below T_N = 24 K. Upon the removal of the water molecules, T_N decreases to 22 K and different gas molecules can be located inside the empty channels, causing changes in T_N. For example, CO_2 causes an increase in T_N to 29 K, which has been associated to the structural changes induced by the CO_2 molecules.

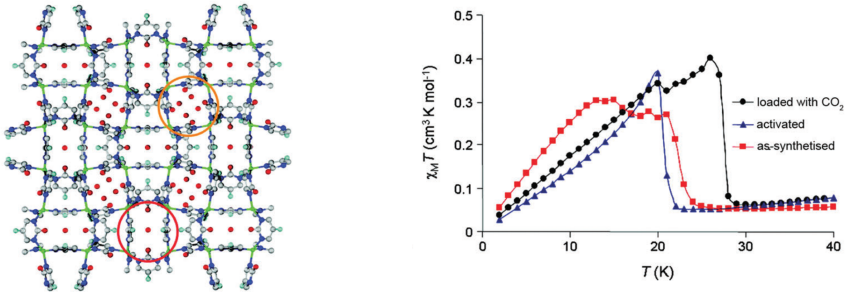

Figure 1.13. Crystal structure of $[Cu(F\text{-}pymo)_2(H_2O)_{1.25}]_n$ (left) and its magnetism modified by CO_2 adsorption (right).

However, the preparation of MOFs presenting magnetic capacity is not restricted to the exclusive use of short linkers. Another methodology is the use of short ligands to extend the metal connection along 1D or 2D dimensions and another large ligand to extend the structure and create large pores. The family of MOF-74 is a perfect example of this methodology. This has the general formula $M_2(dhtp)(H_2O)_2$ (dhtp = 2,5-dihydroxyterephtalate) and exhibits great BET areas with diverse metal centers (Zn,[24] Co,[25] Ni,[26] Mg,[27] Mn,[28] Cu[29]). The crystal structure presents a honeycomb distribution with channels of 11 Å (figure 1.14). The Fe derivative was reported in 2012 by Long *et al.*[30] The magnetic exchange of the material is modified upon sorption of 1 bar of different hydrocarbons and, depending on the strength of the interaction between the gas and the framework, the modification is different. With weakly interacting gases, the ferromagnetic exchange slightly decreases but with strongly interacting gases, the ferromagnetic coupling changes to antiferromagnetic.

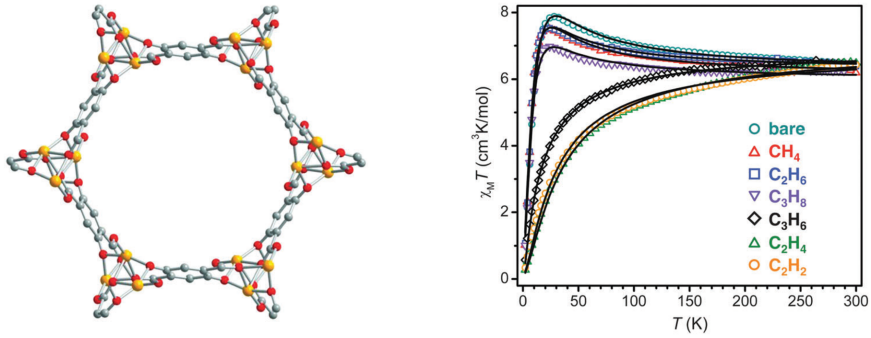

Figure 1.14. Crystal structure of MOF-74 (left) and modification of the magnetic properties of Fe-MOF-74 upon sorption of gases.

Another completely different approach is the use of metallo-ligands, as has been reported by Pardo *et al.* in 2012.[31,32] They used oxomato-based dinuclear Cu^{II} metallacyclic complexes, with weak ferromagnetic coupling between the Cu^{II} ions. These complexes can coordinate to Mn^{II} ions yielding a 3D MOF, presenting pores in which selective separation of gases or vapors are performed. The structure can be seen on figure 1.15 and a 3D ferromagnetic ordering is observed, resulting from the antiferromagnetic coupling between the Mn^{II} and the Cu^{II} ions through the oxamato bridges and the interlayer ferromagnetic interaction across the double amidate bridges.

The last approach to produce long range magnetic order in coordination polymers is the use of radicals as ligands.[33] The first example was reported by the group of Veciana in 2003.[34] They synthesized a MOF using a polychlorinated triphenylmethyl tricarboxylic acid radical (ptmtc). The structure, named MOROF-1, orders as a 2D ferrimagnet with $T_c < 2K$ and with Cu^{II} centers forming a square pyramidal coordination geometry,

coordinated to two organic radicals and each radical connected to three metal centers, forming a 2D structure (figure 1.16).

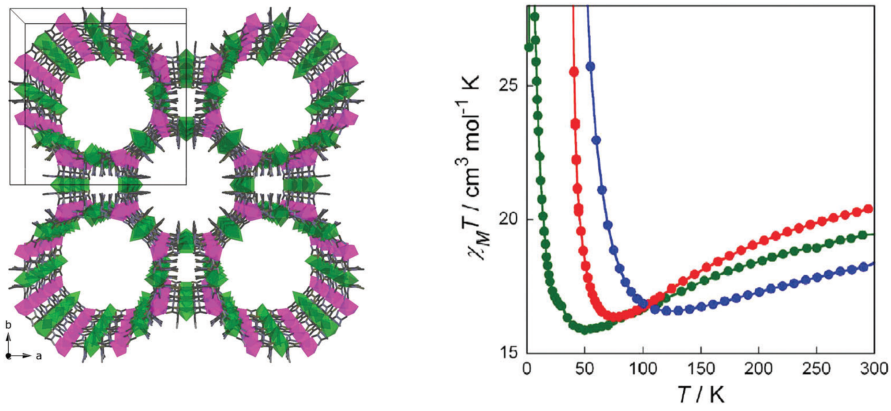

Figure 1.15. Crystal structure of the coordination polymer from reference 31 (left) and its magnetic properties (right).

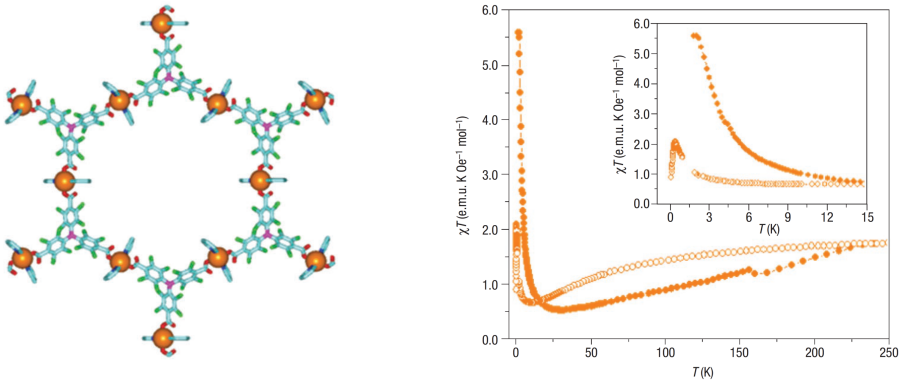

Figure 1.16. Crystal structure of MOROF-1 (left) and its magnetic properties (right).

1.3.2 Single-molecule magnets in MOFs nodes

Single-molecule magnets (SMMs) are magnetic molecules that present slow relaxation of the magnetization at low temperatures. Typically, the basic units to form the SMMs are polynuclear magnetic clusters with a large spin value and high magnetic anisotropy, but more recently a new family has been developed based on mononuclear metal complexes with highly anisotropic magnetic ions. The last family known as single-ion magnets (SIMs), has in addition a lot of interest in the field of quantum computing, due to the fact that they can be considered as quantum bits. With the increase in the interest for connecting SMMs with organic linkers to study the interplay between the generated connected network, the combination of such an interesting property like porosity appears promising for study these materials.

The first example of a 3D network using Mn_4 clusters was reported in 2004 by Clérac *et al.*[35] Subtle modifications in these types of networks cause changes in the dimensionality and magnetic properties but normally all the structures present lack of porosity. Only in 2016 Kou *et al.* reported the first MOF presenting SMM behaviour.[36]

This situation has changed recently when the SIMs where discovered.[37,38] They are based on mononuclear metal complexes composed of highly anisotropic magnetic ions, principally lanthanoids. The first example of MOF based on this type of magnetic molecules was reported in our group in 2014 by Baldoví *et al*.[39] The general formula of the SIM-MOF is $Ln(bipyNO)_4(TfO)_3$ being bipyNO = 4,4´-bypyridyl-N,N-dioxide, TfO = triflate anion and Ln a lanthanide. The structure can be observed in figure 1.17

and is composed by a porous cationic framework formed by the organic ligand with lanthanoid SIMs in the nodes. The triflate counter anions are located in the pores of the 3D structure.

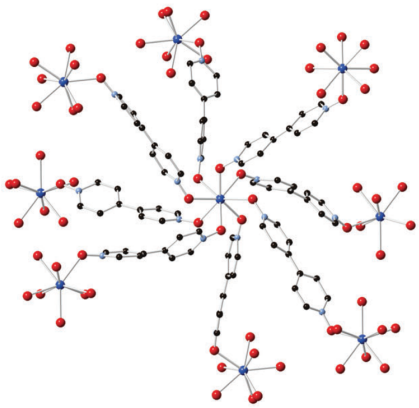

Figure 1.17. Crystal structure of $Ln(bipyNO)_4(TfO)_3$.

Further investigations in our group have focused on an anion exchange in these systems, replacing the triflate anions in the pores by POMs or $[AuCl_4]^-$ units using a single-crystal-to-single-crystal methodology.[40]

The last example of magnetic MOFs is provided by the porous materials exhibiting spin-crossover (SCO) behaviour. This is the approach used in this *thesis* and will be discussed in detail in the next sections, introducing first in detail the spin-crossover phenomenon.

1.4 Spin-crossover phenomenon

The observation of a spin transition occurring with a change of the temperature was observed for the first time in the 1930s by Cambi, almost at the same time that the physicist Hans Bethe and John Hasbrouck van Vleck developed the Crystal Field Theory (CFT). CFT was used to explain the behaviour of transition metal complexes, treating the metal as a positive charge and the surrounding ligands as negative ones. With the CFT, the degeneracy of the d orbitals of the metal was removed by the inclusion of an electric field produced by the surrounding ligands. This feature was explained, but not the bonding between the metal and the ligands. This theory evolved, with the help of the Molecular Orbital Theory (MOT), to the Ligand Field Theory (LFT). The most studied type of coordination compounds is the one of transition metals surrounded by ligands in an octahedral environment. A transition metal present five degenerated *d*-orbitals: d_{xy}, d_{xz}, d_{yz}, d_{z^2} and $d_{x^2}-d_{y^2}$. A transition metal in an octahedral coordination environment suffer the breaking on the degeneracy of its d orbitals, splitting them on two series: the irreducible representation t_{2g} formed by d_{xy}, d_{xz} and d_{yz} and the irreducible representation e_g formed by d_{z^2} and $d_{x^2}-d_{y^2}$ (figure 1.18). t_{2g} are non-bonding orbitals, then placed at lower energy than the e_g ones that are anti-bonding. The total difference in energy between both series of orbitals is named ligand field splitting, represented by the greek letter Δ and its magnitude is measured in terms of 10Dq. This splitting depends on factors like the type of metal and its oxidation state, the type of bonding ligand and the metal-ligand distance.

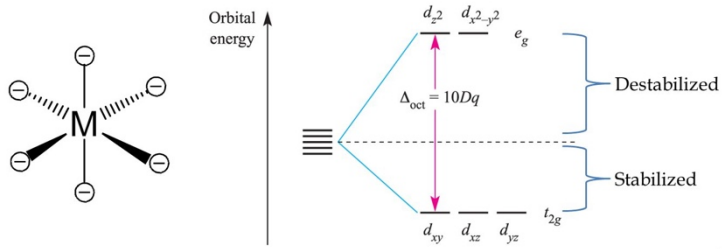

Figure 1.18. Break of the degeneracy levels of the d orbitals of a transition metal when it is placed into an octahedral ligand field.

SCO can exist in first series transition metals with an electronic configuration of d^4 to d^7 in an octahedral ligand field. One of the most studied ions exhibiting SCO is Fe(II). This particular cation presents six electrons in the d orbitals which can be distributed in low spin (LS) or high spin (HS) configurations. This depends basically on two parameters: the pairing energy between the electrons, P, and Δ. When P is large compared to Δ, then the electrons fill the orbitals according the Hund's rule, that is, maximizing the spin multiplicity (S = 2) and resulting in a paramagnetic HS configuration. On the contrary, when Δ is large compared to P, the electrons are all paired in the t_{2g} orbitals (S = 0), resulting in the diamagnetic LS configuration (figure 1.19). In some coordination compounds, Δ and P are very close, so a spin transition can occur between the two states with a slight perturbation of Δ, the so-called spin-crossover. This perturbation can be exerted by an external perturbation such temperature, light, magnetic field, pressure, electric field or guest-inclusion of molecules.

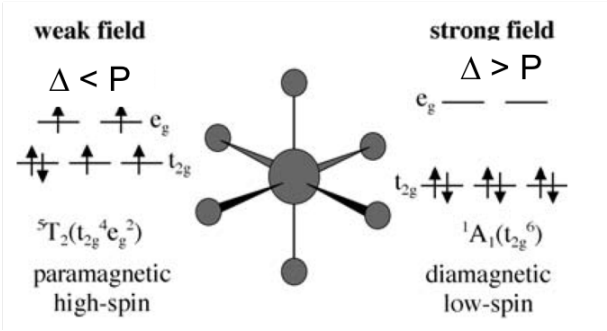

Figure 1.19. Electronic configurations of the two possible ground states for Fe (II) in an octahedral complex.

1.5 Spin-crossover coordination polymers

As already stated, the multifunctional behaviour of coordination polymers and MOFs have attracted a lot of interest for these materials since decades. The possibility of including bi-stability in coordination polymers turned spin-crossover an interesting property to be incorporated to these materials. Despite the fact that a lot of examples of monomeric spin-crossover compounds have been published, it was not until the 1990s when some examples of polymeric compounds have been reported. One of the first was reported on 1995, when José Antonio Real and co-workers published an extended structure of a spin-crossover Fe (II) coordination polymer.[41] They used the tvp ligand (figure 1.20), a dipyridyl derivative, to form interlocking 2D frameworks of formula $[Fe(tvp)_2(NCS)_2] \cdot CH_3OH$.

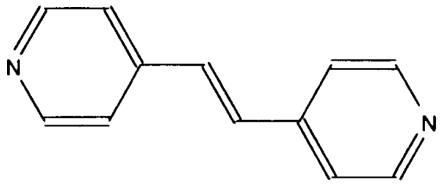

Figure 1.20. Tvp ligand used in the formation of $[Fe(tvp)_2(NCS)_2] \cdot CH_3OH$.

Interestingly, the cooperativity of the SCO phenomenon has shown to be dependent on the quality of the coordination polymers. Thus, coordination polymers are infinite frameworks and the cooperative nature of the spin-crossover can be affected by crystal defects, which often lead toi ncomplete SCO transitions. Sharp transitions are obtained when a good elastic cooperativity in the lattice exist, propagating efficiently the transition through the framework.

To produce a good propagation of spin-crossover through the crystal lattice, sometimes rigidity and suitable coordination ligands, like cyanide anions, are necessary. On this respect, a particular group of coordination polymers that present these particularities are the called Hofmann clathrates. The general formula of these compounds is $\{Ni(NH_3)_2[Ni(CN)_4]\} \cdot 2\ G$ (figure 1.21), being G a guest molecule, normally benzene, pyrrole, thiophene or furan. These compounds were discovered at the beginning of the twenty century but until the 1950s their structures has not been solved by Powell and Rayner.[42,43]

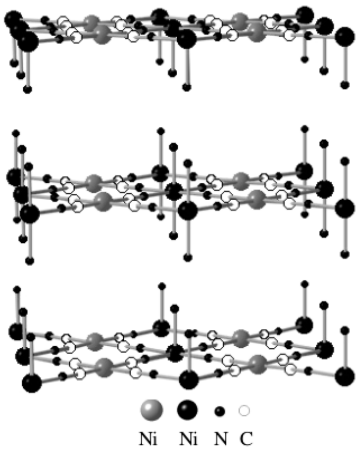

Figure 1.21. Perspective view of the 2D Hofmann clathrate $\{Ni(NH_3)_2[Ni(CN)_4]\} \cdot 2\ G$.

In the decade of the 80s, Iwamoto *et al.* synthesize derivatives of the Hofmann clathrates by effective substitution of the metal centers by other divalent ones and in addition they increase the dimensionality to 3D substituting the amino groups.[44,45] With the inclusion of iron (II) metallic centers and nitrogenated ligands, the possibility to produce some clathrate with spin-crossover transition appeared, and then was reported the first example in 1996 by Kitazawa and co-workers.[46] The formula of the compound is $\{Fe(py)_2[Ni(CN)_4]\}$ (py = pyridine), presenting a more efficient crystal packing with the iron (II) center of a given layer situated in the vertical of the nickel (II) atoms of the layers immediately below and above (figure 1.22).

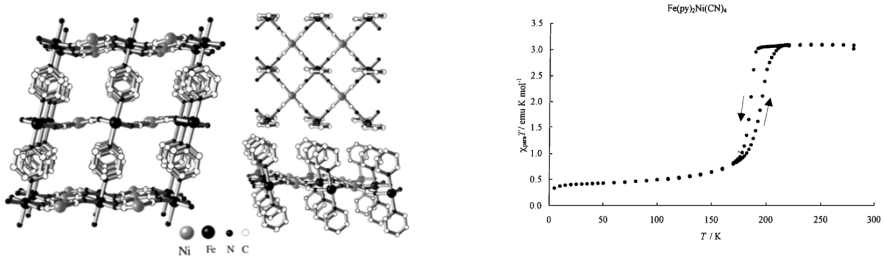

Figure 1.22. Different perspectives of the {$Fe(py)_2[Ni(CN)_4]$} system (left) and its spin transition (right).

The compound presents a sharp spin transition with $T_{1/2}$ = 190 K, with a thermal hysteresis of 10 K. Soon, Niel *et al.* reported two novel derivatives substituting the nickel center with palladium and platinum. At the same time these authors also increased the dimensionality of the system by substituting the pyridine ligand with pyrazine (pz) (figure 1.23).[47] Now, the pz ligand bridges the iron (II) centers of consecutive layers, achieving a pillaring of the 2D metal-cyanide sheets by vertical columns of the pz bridge to give the 3D structure. In terms of magnetic behaviour, the pz derivatives present higher $T_{1/2}$ and stronger cooperativity, with larger hysteresis loops (figure 1.24). These differences can be related to an increased internal pressure produced by the extended dimensionality.

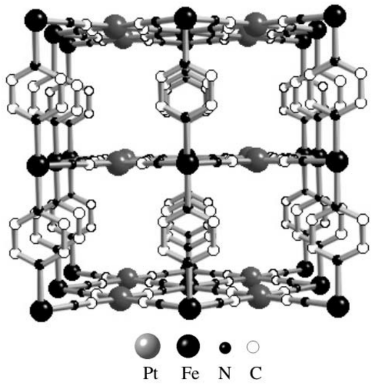

Figure 1.23. Fragment of the $\{Fe(pz)_2[M(CN)_4]\}\cdot 2\ H_2O$ (M = Ni, Pd or Pt) system.

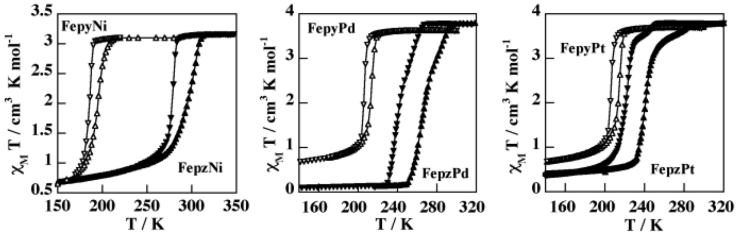

Figure 1.24. $\chi_M T$ vs T plots for the 2D $\{Fe(py)_2[M(CN)_4]$ (white triangles) and the 3D $\{Fe(pz)_2[M(CN)_4]\}$ (black triangles) derivatives.

1.6 Spin-crossover coordination polymers with tetrazole moieties

Tetrazoles are five-membered aromatic heterocycles with four nitrogens and have good coordination behaviour due to the sp^2 N-donors. In combination with Fe (II) centers, they have a proper ligand field to produce spin-crossover behaviour in Fe (II) octahedral coordination environments. Some examples of mononuclear Fe (II) compounds formed by 1-alkyl-substituted tetrazoles showing SC behaviour were reported in the 80s and 90s,[48–59] but the field of

coordination polymers with iron (II) and tetrazoles presenting SCO behaviour has not been exploited until 2000. Van Koningsbruggen and co-workers have published a 1D coordination polymer of formula $[Fe(btzp)_3](ClO_4)_2$, where btzp is the bis-tetrazole ligand.[60] It shows a gradual spin-crossover behaviour with $T_{1/2}$, defined as the temperature where the molar fractions of HS and LS are both equal to 0.5, is 130 K (figure 1.25). The decade of 2000 was very productive not only in the publication of many Fe (II) tetrazole 1D coordination polymers presenting SCO, but 2D and 3D derivatives too.

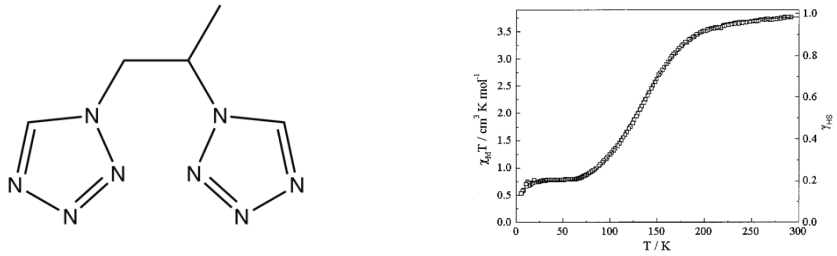

Figure 1.25. Btzp ligand used by van Koningsbruggen and co-workers (left) and the spin transition curve of $[Fe(btzp)_3](ClO_4)_2$ (right).

The same group expanded the study of this family of coordination polymers with bis-tetrazole ligands. In 2001, they expanded the field of Fe (II) tetrazole spin-crossover coordination polymers with the report of a 3D structure, $[Fe(btzb)_3](ClO_4)_2$, where btzb is another bis-tetrazole ligand, with an alkyl chain of four carbons (figure 1.26).[61]

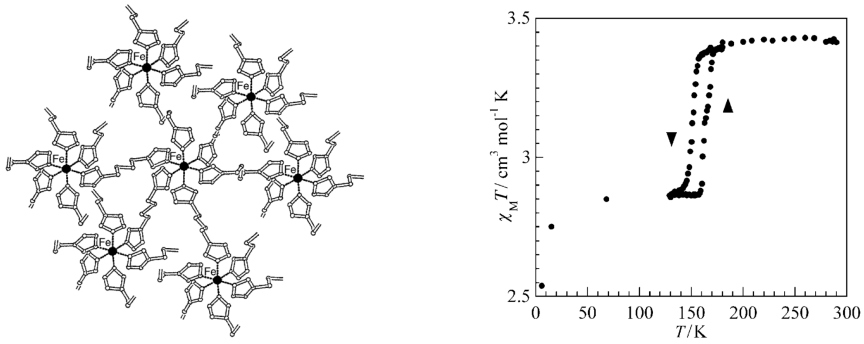

Figure 1.26. A model of the 3D structure for $[Fe(btzb)_3](ClO_4)_2$ (left) and its transition curve (right).

They reported in 2002 an isostructural compound to $[Fe(btzp)_3](ClO_4)_2$, a 1D coordination polymer of formula $[Fe(btze)_3](BF_4)_2$, being btze = 1,2-(tetrazol-1-yl)ethane. (figure 1.27).[62] The spin transition curve is slightly more abrupt than in the isostructural 1,2-propane derivative.

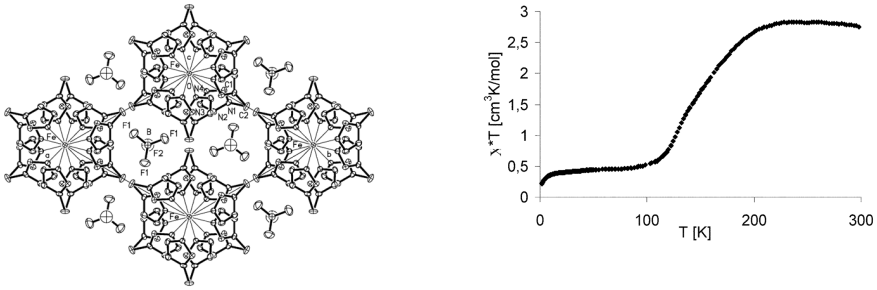

Figure 1.27. Crystal structure of $[Fe(btze)_3](BF_4)_2$ (left) and its transition curve (right).

Weinberger and co-workers continued the work of Van Koningsbruggen in the field of Fe^{II} spin-crossover aliphatic bis-tetrazole derivatives. The 1,3-propane derivative was not reported until 2013. It has the formula

$[Fe(3ditz)_3](BF_4)_2$, being 3ditz = 1,3-bis(tetrazol-1-yl)propane. Its crystal structure is isoreticular to that of ethane and 1,2-propane derivatives (figure 1.28).[63] The transition curve is complete and abrupt, being the transition sharper than that encountered in the ethane, butane and 1,2-propane derivatives.

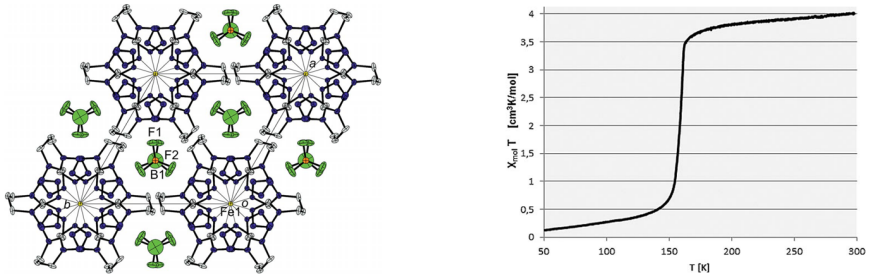

Figure 1.28. Crystal structure of $[Fe(3ditz)_3](BF_4)_2$ (left) and its transition curve (right).

In 2004 Van Koningsbruggen and co-workers synthesized a coordination polymer isostructural to the previous reported $[Fe(btzb)_3](ClO_4)_2$ with formula $[Fe(btzb)_3](PF_6)_2 \cdot$ solvent.[64] The magnetic properties of this coordination polymer shows a two-step sharp and complete transition, in contrast with its perchlorate derivative that shows an incomplete one. (figure 1.29).

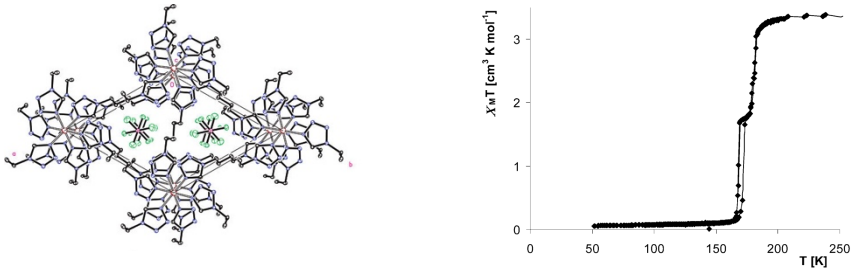

Figure 1.29. Crystal structure of $[Fe(btzb)_3](PF_6)_2 \cdot$ solvent (left) and its transition curve (right).

In 2006 they complete the study of aliphatic bis-tetrazole ligands with a study where the number of carbon atoms of the aliphatic spacer was changed.[65] The general formula of the family of coordination polymers synthesized is $[Fe(nditz)_3](ClO_4)_2$, with $4 \leq n \leq 9$. All the structures are 3D, isostructural to the previous reported $[Fe(btzb)_3](ClO_4)_2$ and $[Fe(btzb)_3](PF_6)_2$. The most interesting conclusion of this study is the observation of two different behaviours, depending on the number of carbon atoms (odd or even) in the organic ligand (figure 1.30).

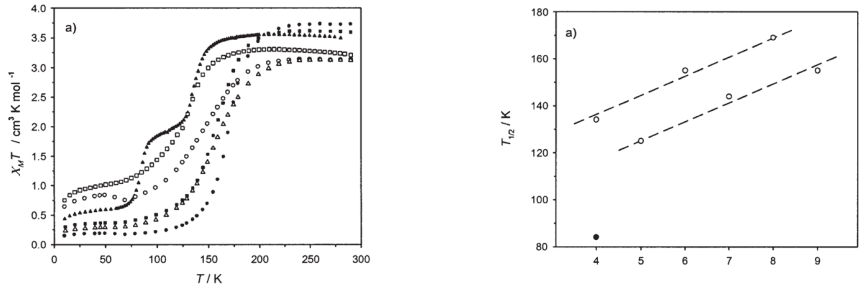

Figure 1.30. Spin transition curves (left) and comparision of $T_{1/2}$ as function of n (right) for the $[Fe(nditz)_3](ClO_4)_2$ family.

The first behaviour was observed in the compounds with odd-number of carbon atoms. They show a $\chi_M T$ value at room temperature equal to 3 cm^{-3} K mol^{-1} and more gradual transitions. The second behaviour was observed in the compounds with even-number of carbon atoms. They show a $\chi_M T$ value at room temperature equal to 3.75 cm^3 mol^{-1} K and sharper transitions.

In 2007 they used a branched alkane ligand to synthesize [Fe(μ-btzmp)$_2$(btzmp)$_2$](ClO$_4$)$_2$, being btzmp = 1,2-bis(tetrazol-1-yl)-2-methylpropane.[66] This compound shows 1D chains only connected by two ligands, whereas the another two remains monocoordinated (figure 1.31). The spin transition is abrupt and almost complete.

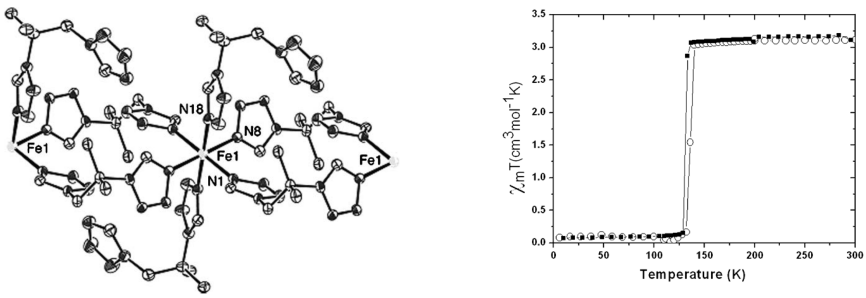

Figure 1.31. Labelled ORTEP representation of [Fe(μ-btzmp)$_2$(btzmp)$_2$](ClO$_4$)$_2$ (left) and its transition curve (right).

Not only aliphatic bis-tetrazole ligands have been studied by Peter Weinberger and co-workers, but also cycloalkanes. Very recently in 2018, they used the ligand ppditz (1,3-bis((1*H*-tetrazol-1-yl)methyl)bicyclo[1.1.1]pentane (figure 1.32) to obtain a family of three different coordination polymers of general formula [Fe(ppditz)$_3$](X)$_2$ (X =

BF_4, ClO_4 or PF_6).[67] The well-known structure of 1D chains with Fe^{II} connected by 3 bridging tetrazole ligands is formed and the transition curve for the three derivatives synthesized is very similar, regardless of the counterion used.

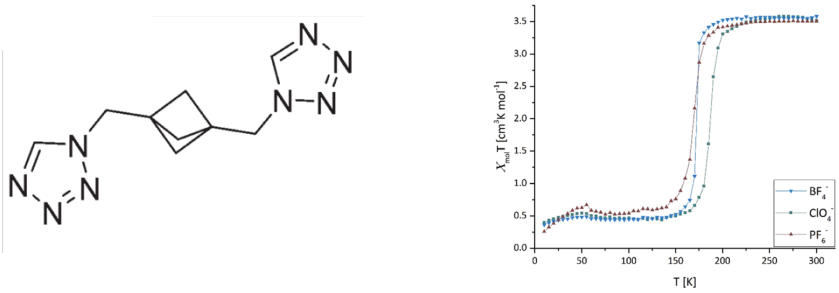

Figure 1.32. ppditz ligand (left) and transition curves for the $[Fe(ppditz)_3](X)_2$ family (right).

Notice that other functional groups have been inserted between the tetrazole moieties. Quesada *et al.* reported in 2007 the 2D material $[Fe(btzpol)_{1.8}(btzpol\text{-}OBF_3)_{1.2}](BF_4)_{0.8} \cdot (H_2O)_{0.8}(CH_3CN)$, being btzpol = 1,3-bis (tetrazol-1-yl)-2-propanol.[68] The connection between the iron centers is made by 1 ligand in one direction, and 2 in the perpendicular, allowing a layered structure (figure 1.33).

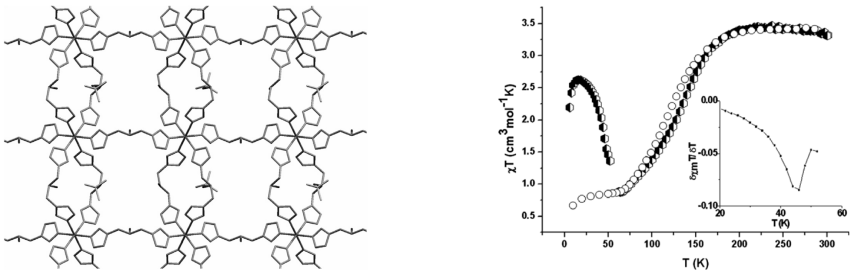

Figure 1.33. Representation of the Fe (II) 2D layered structure (left) and its magnetic properties (right).

The transition is gradual but $T_{1/2}$ is 112 K, a value which is unusual compared with the family of alkane bis-tetrazole derivatives.

Aromatic rings have also been inserted between the tetrazole moieties. Quesada and co-workers reported in 2008 an interesting work using the ligand btzx (*m*-Xylylenebis(tetrazole).[69] They synthesized the family of coordination polymers $[Fe(btzx)_3](X)_2$ (X= PF_6, CF_3SO_3 or ClO_4) and studied how the counter-ion affect the spin-transition (figure 1.34). The family presents the 1D chain arrangement observed previously for this type of coordination polymers with three ligands serving as bridges between the Fe^{II} centers.

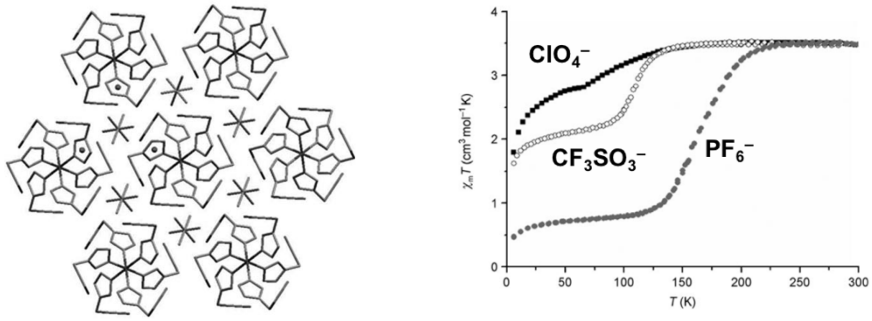

Figure 1.34. Hexagonal packing of the 1D chains for $[Fe(btzx)_3](PF_6)_2$ and transition curves for the $[Fe(btzx)_3](X)_2$ family (right).

Our group has made important advances in the inclusion of aromatic rings between the bis-tetrazole moieties, but they will be discussed in detail later on this thesis.

1.7 Spin-crossover modification through chemical stimuli in coordination polymers

After the establishment of coordination polymers exhibiting spin-crossover behaviour, the next step in the outlook for these materials was the search of tuning the transition temperature with a chemical stimulus. For this purpose, the coexistence of porosity with spin-crossover in the material is the perfect approach for this magnetic modification. In principle, these two behaviours are opposite in conceptually terms: while porosity needs far metal centers to produce large pores, spin-crossover needs a good connection between them to enhance the cooperativity and propagate the spin-crossover through the lattice. Despite this contradiction, it was demonstrated that both

characteristics can coexist in MOF-like materials.[70,71] In a first example,[70] the Hofmann derivative $[Fe(pz)Ni(CN)_4] \cdot 2\ H_2O$ (where pz is pyrazine, figure 1.35) shows that previous heating and losing of the two water molecules, it can locate inside molecules of gases (N_2, O_2, CO_2) and vapors of solvents (methanol, ethanol, acetone, acetonitrile and toluene).

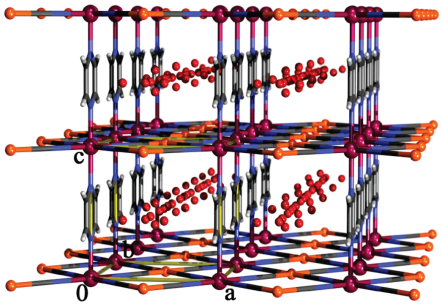

Figure 1.35. Fragment of the $\{Fe(pz)_2[Ni(CN)_4]\} \cdot 2\ H_2O$ system. 1D channels are filled with disordered water molecules.

The loss of the two water molecules provokes a rearrangement in the structure, thus modifying the spin transition. Upon sorption of the different guests, almost no modification of the magnetic properties has been observed by the gases, but dramatic changes have been observed for the solvents, as can be seen on figure 1.36.

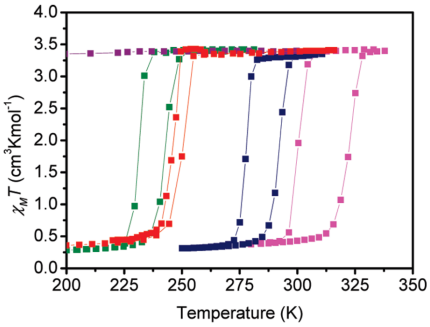

Figure 1.36. Temperature dependence of $\chi_M T$ after the sorption of 0.6 Toluene (purple), 1.2 Acetone (green), 1.5 Ethanol (red), 1.8 Methanol (blue) and 1.0 Acetonitrile (pink) for $\{Fe(pz)_2[Ni(CN)_4]\}\cdot$ Xsolvent.

Similar behaviour has been observed in a second $Fe(pz)_2[Pt(CN)_4]$ loaded with different gases and solvent molecules.[71] No effect on the spin transition has been observed by the gas molecules, and almost all solvents stabilize the high-spin state, remaining the loaded compounds paramagnetic all over the temperatures. Only CS_2 has a direct effect on the spin transition, modifying the original transition (figure 1.37). The system remains at low-spin in the range of 2-298 K. When CS_2 molecules are lost, the system presents some "memory" effect, remaining at low-spin until 330 K and undergoing a transition to high-spin at higher temperatures.

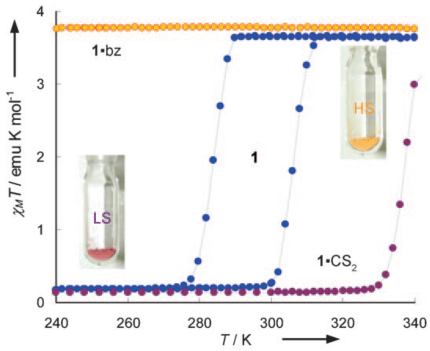

Figure 1.37. Temperature dependence of $\chi_M T$ for bare material $\{Fe(pz)_2[Pt(CN)_4]\}$ (blue), 1.0 Benzene (yellow), 1.0 CS_2 (purple).

Real *et al.* did further investigations on the latter system, reporting in 2013 how the gas sorption of SO_2 inside the pores subtle modifies the spin transition.[72] The SO_2 molecules interact with the Pt atom, modifying the ligand field of the iron (II) center, then changing the spin transition (figure 1.38).

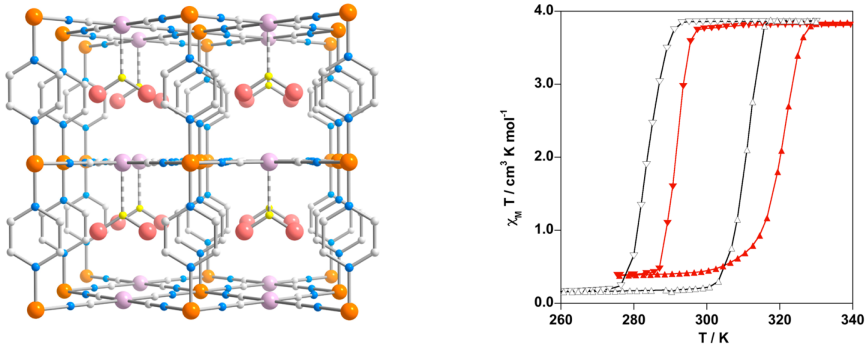

Figure 1.38. SO_2 molecules interacting with Pt atoms (left) and $\chi_M T$ plot for bare (black) and 1.0 SO_2 (red) (right).

However, the first study in which gas sorption has shown the ability to modify the spin transition on a coordination polymer was reported by our group in 2013.[73] The approach of using discrete compartments to enhance the interaction between the gas and the framework was successfully performed, synthesizing the coordination polymer $[Fe(btzx)_3](ClO_4)_2$ (btzx = 1,4-bis(tetrazol-1-ylmethyl)benzene). The coordination polymer presents the 1D linear chain structure observed in the family of linear alkane Fe^{II} bis-tetrazole coordination polymers, but now the benzene rings generates isolated voids where gas sorption studies can be performed. The material presents preferential sorption of CO_2 *vs* N_2, and the adsorption of CO_2 modify the original spin transition of the bare material. (figure 1.39).

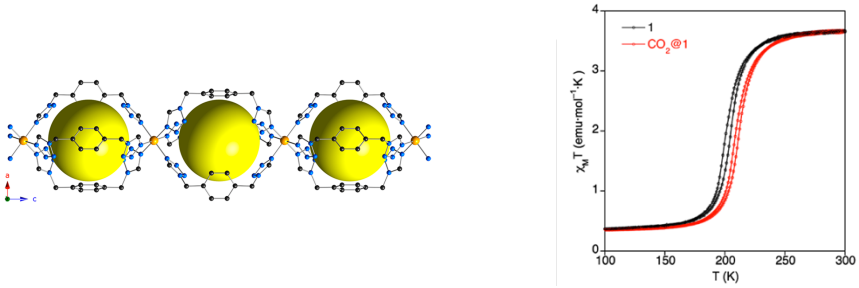

Figure 1.39. Crystal structure of $[Fe(btzx)_3](ClO_4)_2$, yellow spheres represent voids (left) and spin transition modification upon CO_2 sorption (right).

A related and extended study of the approach of using discrete compartments for gas sorption/separation and spin-crossover modification is the main goal of this thesis.

1.6 References

1. Kitagawa, S., Kitaura, R. & Noro, S. Functional Porous Coordination Polymers. *Angew. Chem. Int. Ed.* **43**, 2334–2375 (2004).
2. Furukawa, H., Cordova, K. E., O'Keeffe, M. & Yaghi, O. M. The Chemistry and Applications of Metal-Organic Frameworks. *Science* **341**, 1230444–1230444 (2013).
3. Cavka, J. H. *et al.* A New Zirconium Inorganic Building Brick Forming Metal Organic Frameworks with Exceptional Stability. *J. Am. Chem. Soc.* **130**, 13850–13851 (2008).
4. Kandiah, M. *et al.* Synthesis and Stability of Tagged UiO-66 Zr-MOFs. *Chem. Mater.* **22**, 6632–6640 (2010).
5. Park, K. S. *et al.* Exceptional chemical and thermal stability of zeolitic imidazolate frameworks. *Proc. Natl. Acad. Sci.* **103**, 10186–10191 (2006).
6. Fujita, M., Kwon, Y. J., Washizu, S. & Ogura, K. Preparation, Clathration Ability, and Catalysis of a Two-Dimensional Square Network Material Composed of Cadmium(II) and 4,4'-Bipyridine. *J. Am. Chem. Soc.* **116**, 1151–1152 (1994).

7. Nagao, Y., Ikeda, R., Kanda, S., Kubozono, Y. & Kitagawa, H. Complex-Plane Impedance Study on a Hydrogen-Doped Copper Coordination Polymer: N,N ′-bis-(2-hydroxyethyl)dithiooxamidato-copper(II). *Mol. Cryst. Liq. Cryst.* **379**, 89–94 (2002).
8. Li, H., Eddaoudi, M., Groy, T. L. & Yaghi, O. M. Establishing Microporosity in Open Metal−Organic Frameworks: Gas Sorption Isotherms for Zn(BDC) (BDC = 1,4-Benzenedicarboxylate). *J. Am. Chem. Soc.* **120**, 8571–8572 (1998).
9. Li, H., Eddaoudi, M., O'Keeffe, M. & Yaghi, O. M. Design and synthesis of an exceptionally stable and highly porous metal-organic framework. *Nature* **402**, 276–279 (1999).
10. Chae, H. K. *et al.* A route to high surface area, porosity and inclusion of large molecules in crystals. *Nature* **427**, 523–527 (2004).
11. Furukawa, H. *et al.* Ultrahigh Porosity in Metal-Organic Frameworks. *Science* **329**, 424–428 (2010).
12. Adil, K. *et al.* Gas/vapour separation using ultra-microporous metal–organic frameworks: insights into the structure/separation relationship. *Chem. Soc. Rev.* **46**, 3402–3430 (2017).
13. Matsuda, R. *et al.* Highly controlled acetylene accommodation in a metal–organic microporous material. *Nature* **436**, 238–241 (2005).

14. Li, D. & Kaneko, K. Molecular Geometry-Sensitive Filling in Semi-Rectangular Micropores of Organic−Inorganic Hybrid Crystals. *J. Phys. Chem. B* **104**, 8940–8945 (2000).

15. Kitaura, R. Formation of a One-Dimensional Array of Oxygen in a Microporous Metal-Organic Solid. *Science* **298**, 2358–2361 (2002).

16. Foo, M. L. *et al.* An Adsorbate Discriminatory Gate Effect in a Flexible Porous Coordination Polymer for Selective Adsorption of CO_2 over C_2H_2. *J. Am. Chem. Soc.* **138**, 3022–3030 (2016).

17. Hu, T.-L. *et al.* Microporous metal–organic framework with dual functionalities for highly efficient removal of acetylene from ethylene/acetylene mixtures. *Nat. Commun.* **6**, (2015).

18. Xue, D.-X. *et al.* Tunable Rare-Earth fcu-MOFs: A Platform for Systematic Enhancement of CO_2 Adsorption Energetics and Uptake. *J. Am. Chem. Soc.* **135**, 7660–7667 (2013).

19. Xue, D.-X. *et al.* Tunable Rare Earth **fcu** -MOF Platform: Access to Adsorption Kinetics Driven Gas/Vapor Separations via Pore Size Contraction. *J. Am. Chem. Soc.* **137**, 5034–5040 (2015).

20. Mínguez Espallargas, G. & Coronado, E. Magnetic functionalities in MOFs: from the framework to the pore. *Chem. Soc. Rev.* **47**, 533–557 (2018).

21. Beauvais, L. G. & Long, J. R. $Co_3[Co(CN)_5]_2$: A Microporous Magnet with an Ordering Temperature of 38 K. *J. Am. Chem. Soc.* **124**, 12096–12097 (2002).

22. Kaye, S. S., Choi, H. J. & Long, J. R. Generation and O_2 Adsorption Studies of the Microporous Magnets $CsNi[Cr(CN)_6]$ (T_C = 75 K) and $Cr_3[Cr(CN)_6]_2 \cdot 6H_2O$ (T_N = 219 K). *J. Am. Chem. Soc.* **130**, 16921–16925 (2008).

23. Navarro, J. A. R. *et al.* Guest-Induced Modification of a Magnetically Active Ultramicroporous, Gismondine-like, Copper(II) Coordination Network. *J. Am. Chem. Soc.* **130**, 3978–3984 (2008).

24. Rosi, N. L. *et al.* Rod Packings and Metal−Organic Frameworks Constructed from Rod-Shaped Secondary Building Units. *J. Am. Chem. Soc.* **127**, 1504–1518 (2005).

25. Dietzel, P. D. C., Morita, Y., Blom, R. & Fjellvåg, H. An In Situ High-Temperature Single-Crystal Investigation of a Dehydrated Metal-Organic Framework Compound and Field-Induced Magnetization of One-Dimensional Metal-Oxygen Chains. *Angew. Chem. Int. Ed.* **44**, 6354–6358 (2005).

26. Dietzel, P. D. C., Panella, B., Hirscher, M., Blom, R. & Fjellvåg, H. Hydrogen adsorption in a nickel based coordination polymer with open

metal sites in the cylindrical cavities of the desolvated framework. *Chem. Commun.* 959-961 (2006).

27. Caskey, S. R., Wong-Foy, A. G. & Matzger, A. J. Dramatic Tuning of Carbon Dioxide Uptake via Metal Substitution in a Coordination Polymer with Cylindrical Pores. *J. Am. Chem. Soc.* **130**, 10870–10871 (2008).
28. Zhou, W., Wu, H. & Yildirim, T. Enhanced H_2 Adsorption in Isostructural Metal−Organic Frameworks with Open Metal Sites: Strong Dependence of the Binding Strength on Metal Ions. *J. Am. Chem. Soc.* **130**, 15268–15269 (2008).
29. Sanz, R., Martínez, F., Orcajo, G., Wojtas, L. & Briones, D. Synthesis of a honeycomb-like Cu-based metal–organic framework and its carbon dioxide adsorption behaviour. *Dalton Trans* **42**, 2392–2398 (2013).
30. Bloch, E. D. *et al.* Hydrocarbon Separations in a Metal-Organic Framework with Open Iron(II) Coordination Sites. *Science* **335**, 1606–1610 (2012).
31. Ferrando-Soria, J. *et al.* Selective Gas and Vapor Sorption and Magnetic Sensing by an Isoreticular Mixed-Metal–Organic Framework. *J. Am. Chem. Soc.* **134**, 15301–15304 (2012).

32. Grancha, T. *et al.* Oxamato-based coordination polymers: recent advances in multifunctional magnetic materials. *Chem Commun* **50**, 7569–7585 (2014).

33. Faust, T. B. & D'Alessandro, D. M. Radicals in metal–organic frameworks. *RSC Adv* **4**, 17498–17512 (2014).

34. Maspoch, D. *et al.* A nanoporous molecular magnet with reversible solvent-induced mechanical and magnetic properties. *Nat. Mater.* **2**, 190–195 (2003).

35. Miyasaka, H., Nakata, K., Sugiura, K., Yamashita, M. & Clérac, R. A Three-Dimensional Ferrimagnet Composed of Mixed-Valence Mn_4 Clusters Linked by a$\{Mn[N(CN)_2]_6\}^{4-}$ Unit. *Angew. Chem. Int. Ed.* **43**, 707–711 (2004).

36. Jiang, X., Liu, C.-M. & Kou, H.-Z. Porous Coordination Polymers Based on $\{Mn_6\}$ Single-Molecule Magnets. *Inorg. Chem.* **55**, 5880–5885 (2016).

37. Ishikawa, N., Sugita, M., Ishikawa, T., Koshihara, S. & Kaizu, Y. Lanthanide Double-Decker Complexes Functioning as Magnets at the Single-Molecular Level. *J. Am. Chem. Soc.* **125**, 8694–8695 (2003).

38. Cardona-Serra, S. *et al.* Lanthanoid Single-Ion Magnets Based on Polyoxometalates with a 5-fold Symmetry: The Series $[LnP_5W_{30}O_{110}]^{12-}$

(Ln $^{3+}$ = Tb, Dy, Ho, Er, Tm, and Yb). *J. Am. Chem. Soc.* **134**, 14982–14990 (2012).

39. Baldoví, J. J. *et al.* A SIM-MOF: Three-Dimensional Organisation of Single-Ion Magnets with Anion-Exchange Capabilities. *Chem. - Eur. J.* **20**, 10695–10702 (2014).
40. López-Cabrelles, J., Mínguez Espallargas, G. & Coronado, E. Single-Crystal-to-Single-Crystal Anion Exchange in a Gadolinium MOF: Incorporation of POMs and $[AuCl_4]^-$. *Polymers* **8**, 171 (2016).
41. Real, J. A. *et al.* Spin Crossover in a Catenane Supramolecular System. *Science* **268**, 265–267 (1995).
42. Rayner, J. H. & Powell, H. M. Crystal Structure of the Compound of Benzene with an Ammonia-Nickel Cyanide Complex. *J. Chem. Soc. Resumed* 319–328 (1952).
43. Rayner, J. H. & Powell, H. M. Crystal structure of a hydrated nickel cyanide ammoniate. *J. Chem. Soc. Resumed* 3412 (1958).
44. Iwamoto, T. Inclusion compounds. in **1**, 29 (1984).
45. Iwamoto, T. Inclusion compounds. in **5**, 177 (1991).
46. Kitazawa, T. *et al.* Spin-crossover behaviour of the coordination polymer $Fe^{II}(C_5H_5N)_2Ni^{II}(CN)_4$. *J. Mater. Chem.* **6**, 119-121 (1996).

47. Niel, V., Martinez-Agudo, J. M., Muñoz, M. C., Gaspar, A. B. & Real, J. A. Cooperative Spin Crossover Behavior in Cyanide-Bridged Fe(II)−M(II) Bimetallic 3D Hofmann-like Networks (M = Ni, Pd, and Pt). *Inorg. Chem.* **40**, 3838–3839 (2001).

48. Gütlich, P. & Hauser, A. Thermal and Light-induced Spin Crossover in Iron (II) Complexes. *Coord. Chem. Rev.* **97**, 1–22 (1990).

49. Gütlich, P., Hauser, A. & Spiering, H. Thermisch und optisch schaltbare Eisen(II)-Komplexe. *Angew. Chem.* **106**, 2109–2141 (1994).

50. Gütlich, P. Spin Crossover, Liesst, and Niesst-Fascinating Electronic Games in Iron Complexes. *Mol. Cryst. Liq. Cryst. Sci. Technol. Sect. Mol. Cryst. Liq. Cryst.* **305**, 17–40 (1997).

51. Franke, P. L., Haasnoot, J. G. & Zuur, A. P. Tetrazoles as Ligands. Part IV. Iron(II) Complexes of Monofunctional Tetrazole Ligands, Showing High-Spin * Low-Spin Transitions. *Inorganica Chim. Acta* **59**, 5–9 (1982).

52. Mueller, E. W., Ensling, J., Spiering, H. & Guetlich, P. High-spin low-spin transition in hexacoordinate complexes of iron(II) with monodentate 1-alkyltetrazole ligands: a variable-temperature Mössbauer, magnetic susceptibility, and far-infrared study. *Inorg. Chem.* **22**, 2074–2078 (1983).

53. Poganiuch, P. & Gütlich, P. Light-induced formation of metastable high-spin states in $[Fe(mtz)_6](ClO_4)_2$. *Hyperfine Interact.* **40**, 331–334 (1988).

54. Adler, P. & Poganiuch, P. Mössbauer relaxation spectra in arbitrarily ordered absorbers – line shape analysis for an Iron (II) spin-crossover complex in the presence of texture– *Hyperfine Interact.* **52**, 47-63 (1989).

55. Poganiuch, P., Decurtins, S. & Guetlich, P. Thermal- and light-induced spin transition in $[Fe(mtz)_6](BF_4)_2$: first successful formation of a metastable low-spin state by irradiation with light at low temperatures. *J. Am. Chem. Soc.* **112**, 3270–3278 (1990).

56. Gütlich, P. & Poganiuch, P. Thermal and Light-Induced Spin Crossover to a Metastable Low-Spin State in $[Fe(mtz)_6](CF_3SO_3)_2$. *Angew. Chem. Int. Ed. Engl.* **30**, 975–977 (1991).

57. Buchen, T. & Gütlich, P. Thermal and light-induced spin crossover in iron (II) complexes with monodentate tetrazole ligands carrying long alkyl chains in the 1-position. *Chem. Phys. Lett.* **220**, 262–266 (1994).

58. Buchen, T., Poganiuch, P. & Gutlich, P. Effect of Metal Dilution on the Thermal and Light-induced Spin Transition in $[Fe_xZn_{1-x}(mtz)_6][ClO_4]_2$ (mtz = I -methyl-IH- tetrazoIe). *J. Chem. Soc. Dalton Trans.* **4**, 2285-2288 (1994).

59. Hauser, A., Gütlich, P., Hinek, R., Spiering, H. & Schollmeyer, D. The $[Fe(etz)_6](BF_4)_2$ Spin-Crossover System—Part One: High-Spin ⇌ Low-Spin Transition in Two Lattice Sites. *Chem. - Eur. J.* **2**, 1427–1434 (1996).

60. Koningsbruggen, P. J. van *et al.* Synthesis, Crystal Structure, EXAFS, and Magnetic Properties of Catena [μ-Tris(1,2-bis(tetrazol-1-yl)propane-N1,N1‘)iron(II)] Bis(perchlorate). First Crystal Structure of an Iron(II) Spin-Crossover Chain Compound. *Inorg. Chem.* **39**, 1891–1900 (2000).

61. Koningsbruggen, P. J. van *et al.* A new 3-D polymeric spin transition compound: [tris(1,4-bis(tetrazol-1-yl)butane-N1,N1′)iron(II)] bis(perchlorate). *J. Chem. Soc. Dalton Trans.* **0**, 466–471 (2001).

62. Schweifer, J. *et al.* catena-[μ-Tris(1,2-bis(tetrazol-1-yl)ethane-N4,N4′)iron(II)] bis(tetrafluoroborate): synthesis, structure, spectroscopic and magnetic characterization of a chain-type coordination polymer spin-crossover compound. *Inorganica Chim. Acta* **339**, 297–306 (2002).

63. Müller, D. *et al.* A Modified Synthetic Pathway for the Synthesis of so far Inaccessible N1-Functionalized Tetrazole Ligands - Synthesis and

Characterization of the 1D Chain-Type Spin Crossover Compound $[Fe(3ditz)_3](BF_4)_2$. *Eur. J. Inorg. Chem.* **2013**, 984–991 (2013).

64. Grunert, C. M. *et al.* Structure and Physical Properties of [μ-Tris(1,4-bis(tetrazol-1-yl)butane-N4,N4‘)iron(II)] Bis(hexafluorophosphate), a New Fe(II) Spin-Crossover Compound with a Three-Dimensional Threefold Interlocked Crystal Lattice. *Inorg. Chem.* **43**, 155–165 (2004).
65. Absmeier, A. *et al.* Both Spacer Length and Parity Influence the Thermal and Light-Induced Properties of Iron(II) α,ω-Bis(tetrazole-1-yl)alkane Coordination Polymers. *Chem. – Eur. J.* **12**, 2235–2243 (2006).
66. Quesada, M. *et al.* $[Fe(\mu\text{-btzmp})_2(btzmp)_2](ClO_4)_2$: a doubly-bridged 1D spin-transition bistetrazole-based polymer showing thermal hysteresis behaviour. *Dalton Trans.* **0**, 5434–5440 (2007).
67. Knoll, C. *et al.* Cooperativity in spin crossover materials as ligand’s responsibility – investigations of the Fe(II) – 1,3-bis((1 *H* -tetrazol-1-yl)methyl)bicyclo[1.1.1]pentane system. *Dalton Trans.* **47**, 5553–5557 (2018).
68. Quesada, M. *et al.* A 2D [FeII-bistetrazole] coordination polymer exhibiting spin-crossover properties. *Inorganica Chim. Acta* **360**, 3787–3796 (2007).

69. Quesada, M. *et al.* Counterion Effect on the Spin-Transition Properties of the Cation $[Fe(btzx)_3]^{2+}$ (btzx= *m* -Xylylenebis(tetrazole)). *Chem. - Eur. J.* **14**, 8486–8499 (2008).

70. Southon, P. D. *et al.* Dynamic Interplay between Spin-Crossover and Host−Guest Function in a Nanoporous Metal−Organic Framework Material. *J. Am. Chem. Soc.* **131**, 10998–11009 (2009).

71. Ohba, M. *et al.* Bidirectional Chemo-Switching of Spin State in a Microporous Framework. *Angew. Chem. Int. Ed.* **48**, 4767–4771 (2009).

72. Arcís-Castillo, Z. *et al.* Reversible Chemisorption of Sulfur Dioxide in a Spin Crossover Porous Coordination Polymer. *Inorg. Chem.* **52**, 12777–12783 (2013).

73. Coronado, E., Giménez-Marqués, M., Mínguez Espallargas, G., Rey, F. & Vitórica-Yrezábal, I. J. Spin-Crossover Modification through Selective CO_2 Sorption. *J. Am. Chem. Soc.* **135**, 15986–15989 (2013).

Chapter 2:
Gas confinement in SCO CCPs

2.1 INTRODUCTION

The interest in the study of materials for controlling gas emissions has been increasing in the last decades. That control is important from energetic, biological and environmental points of view and it can be applied in two different manners: on one hand, the capture of harmful gases like C_2H_2, SO_2, CO, Cl_2, H_2S, CNCl, NH_3, NO_2 and in the other hand, separation of light gases, waste gases from industrial processes like CO_2, N_2, O_2, CO, NO, H_2 and CH_4.[1] Specially interesting to the industry is the separation of some binary mixtures, like acetylene/ethylene (reagents used in the synthesis of diverse chemical products and materials), CO/H_2 (in fuel cells), CO_2/N_2 (to control the atmospheric CO_2 level), ethylene/ethane (especially important in the petrochemical industry) and CO_2/CH_4 (biogas and natural gas), among others.

In this *chapter* we have focused in the selective CO_2 capture. Usually, amine compounds have been used traditionally for gas sorption, being among the most commonly used materials for CO_2 removal.[2] Nowadays, these materials are being displaced by high surface area and large porosity compounds like zeolites and MOFs.[3–5] However, the enormous porosity characteristic of these materials is sometimes accompanied by problems in terms of selectivity, which can be overcome with restrictions in the accessibility of the pores. In these particular materials, the pores are interconnected by small apertures, providing an enhancement on the selectivity properties.[6,7] Interpenetrated frameworks have also been used for this purpose,[8,9] but the improvement in the gas selectivity typically causes also a decrease in gas capacity.

Normally, the selective sorption in MOFs is based on the different size of the gases for discriminating between them and modification of the pore size is a useful tool to tune that selectivity.[10] The major disadvantage of these ultramicroporous solids appears when the difference between molecules is small, so other approaches need to be considered to effectively separate the gas mixtures. In these cases, electronic properties like quadrupole moment and polarizability can be exploited to discriminate between gas species. This can be implemented through the insertion of cations[11,12] or ligand functionalization,[13,14] although the most used approach of tuning the interaction between the gas molecule and the framework. In fact, different techniques for introducing stronger bindings between the gas molecules and the framework have been typically used, including functionalization of the pores with Lewis basic sites[15,16] and generation of exposed metal sites.[17–20]

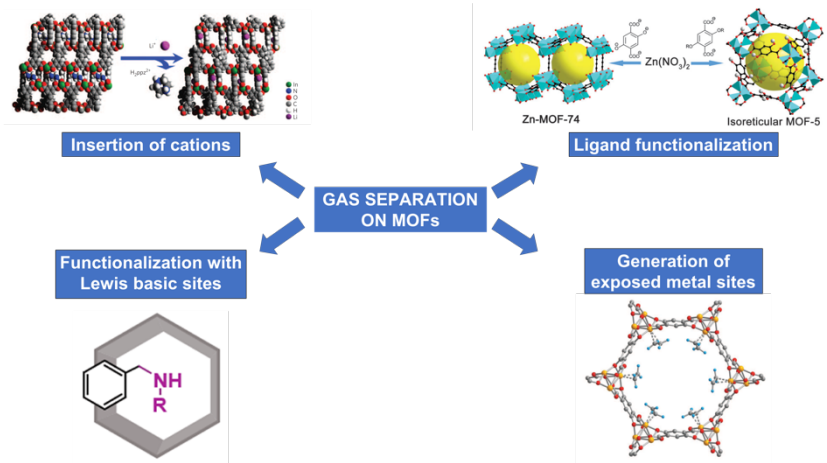

Figure 2.1. Different strategies for gas separation on MOFs.

Despite the high selectivity that can be achieved with these materials, the problem appears with their regeneration, due to the high-cost of that

procedure. This has been palliated recently with the study and use of supramolecular interactions,[21,22] provoking weaker binding of the gases, which consequently causes a lower energy cost in the regeneration of the solid.

In this *chapter*, a completely different approach for gas selective separation of gas mixtures has been studied, that is the use of coordination polymers with discrete and isolated compartments that allow a stronger interaction between the gas molecule and the framework. As has been reported before, gas sorption can be achieved in these types of materials[23,24] and, despite the absence of permanent channels or pores, these compounds are capable of absorbing and possibly discriminating between gases. With the discrete compartments present in the structure, the interaction between the gas and the frameworks is enhanced. Therefore, in order to achieve a selective discrimination in the gas mixtures, we could exploit not only thermodynamic equilibrium (due to an enhanced interaction between the gas and the framework), but also a kinetic trapping (due to the restricted accessibility of the solids). Two previously reported compartmentalized coordination polymers have been used, $[Fe(btzx)_3](ClO_4)_2$ (**CCP-1**) and $[Fe(btzx)_3](BF_4)_2$ (**CCP-2**) (btzx = 1,4-bis(tetrazol-1-ylmethyl)benzene), which are iron (II) coordination polymers with SCO behaviour and latent porosity with internal voids (figure 2.2). Previously, it was demonstrated that CO_2 can be located inside the cavities, modifying the magnetic behaviour of the coordination polymer.[23]

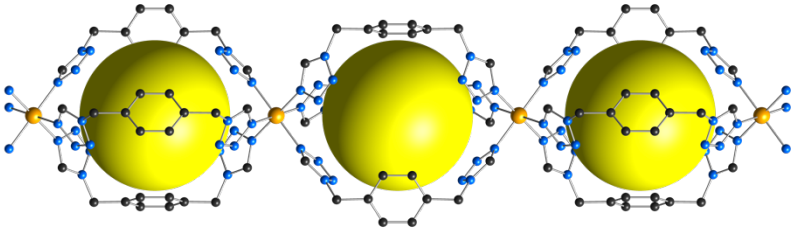

Figure 2.2. Crystal structure of compounds **CCP-1** and **CCP-2**. The counteranions and hydrogen atoms have been removed for clarity. Key: Fe, orange; C, gray; N, blue. Yellow spheres represent empty space in the voids.

2.2 RESULTS AND DISCUSSION

2.2.1 Structural description

The previously reported **CCP-1** and the isostructural **CCP-2** derivative crystallize in the $P6_3/m$ space group and are composed of $[Fe(btzx)_3]^{2+}$ units that form linear cationic chains running parallel to the crystallographic *c*-axis (figure 2.2). The different chains are forming a hexagonal packing, with the counterions occupying the positions between chains. In fact, SEM microparticles of the material adopts a perfect hexagonal shape (figure 2.3). In these chains, internal cavities can be found with void volumes of 11.8 % (**CCP-1**) and 12.4 % (**CCP-2**) of the unit cell (discrete voids of 132 $Å^3$ and 140 $Å^3$, respectively). These are potential voids for the accommodation of external molecules. Interestingly, no solvent molecules are found inside as synthesized, as demonstrated by thermogravimetric (TGA), NMR, and IR analyses.

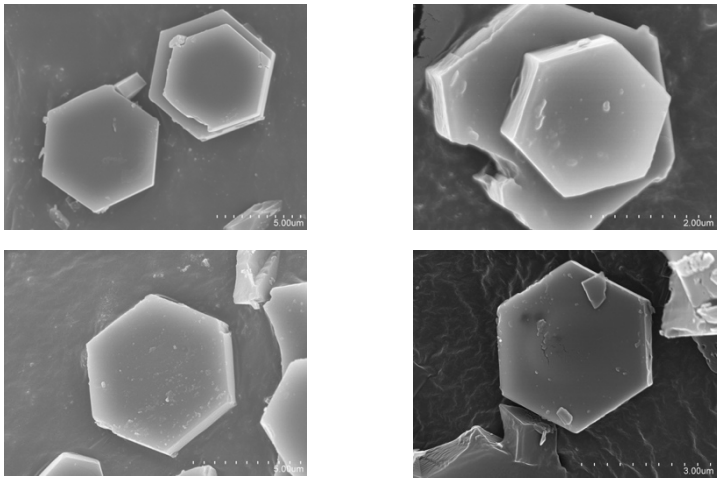

Figure 2.3. Different SEM images of **CCP-1**.

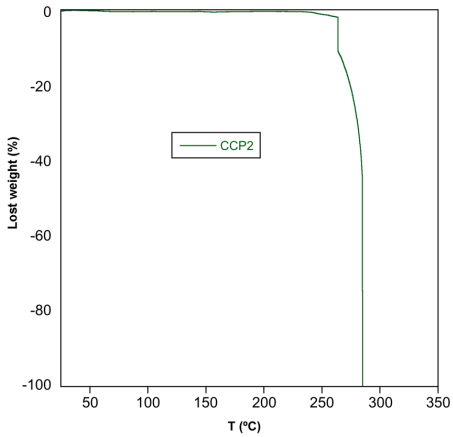

Figure 2.4. TGA analysis for **CCP-2**.

Any loss of solvent is observed in the thermogravimetric analysis (figure 2.4) until the decomposition of the material. The NMR of a digested sample of **CCP-2** can be observed in figure 2.5 and only the peaks corresponding to the ligand btzx, the deuterated solvent and the water related to the solvent are observed.

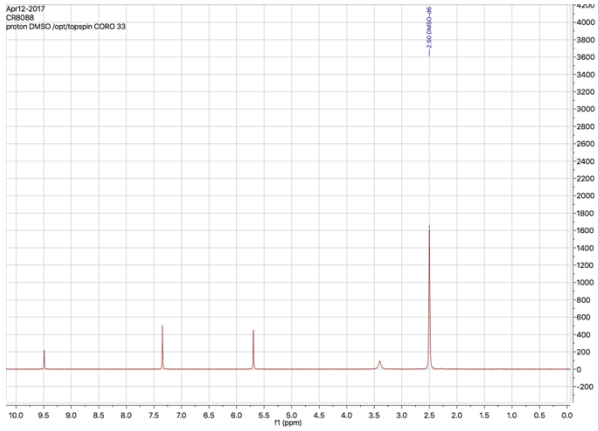

Figure 2.5. NMR analysis for digested **CCP-2**.

Finally, on figure 2.6 it can be seen the IR spectra of **CCP-2** and the signal corresponding to the -CN at 2250 cm^{-1} is not observed.

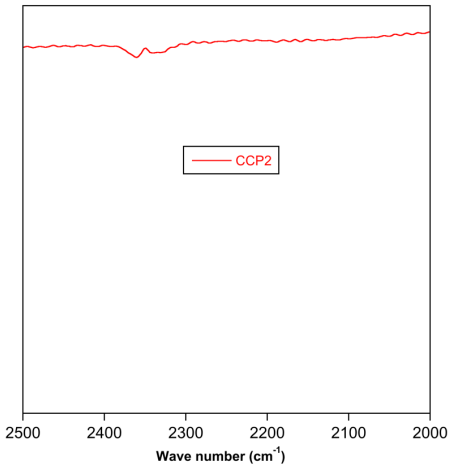

Figure 2.6. IR analysis for **CCP-2**.

Returning to the structural analysis and looking on only one chain, three rectangular pore windows with dimensions of 6.6 x 6.2 $Å^2$ can be observed, but a closer look of the crystal structure and the crystal packing reveals the

presence of a window-to-arene arrangement with three adjacent chains blocking the three windows (figure 2.7). Consequently, this blockage causes the absence of permanent channels in solids **CCP-1** and **CCP-2**, named as compartmentalized coordination polymer, that is, coordination polymers with internal voids accessible for host molecules.

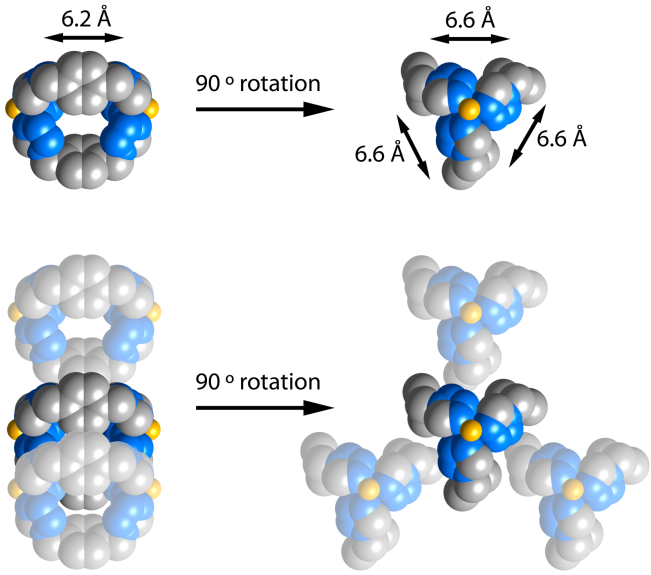

Figure 2.7. Observed blockage of the voids due to the adjacent chains.

2.2.2 Gas sorption studies

Gas sorption studies with N_2 and CO_2 were previously reported for **CCP-1**[23] and now the study has been extended with more gases performed in collaboration with Prof. F. Rey from the Instituto de Tecnología Química of the UPV. Single-component gas sorption isotherms are a useful technique to study the gas sorption capacities in coordination polymers in thermodynamic equilibrium and detect some preferences to specific gases. In this *chapter*, **CCP-1** is analyzed with CO_2, CO, N_2, CH_4, ethane (C_2H_6), ethylene (C_2H_4)

and acetylene (C_2H_2) and **CCP-2** only with CO_2, assuming the same behaviour due to the isostructural nature. Gas sorption isotherms are performed at different temperatures, that is 273, 283, 298, 313, 323 and 333 K, although not all temperatures have been performed on all gases. Virial equation has been used for fitting the experimental data points, finding that it can be properly fitted to a fourth-grade polynomial.

$$\ln\left(\frac{P}{Q}\right) = A_0 + A_1 \cdot Q + A_2 \cdot Q^2 + A_3 \cdot Q^3 + A_4 \cdot Q^4$$

Equation 2.1. Virial equation used during the data analysis of the gas sorption isotherms.

Figure 2.8 shows the gas sorption isotherms in $mol \cdot g^{-1}$ units at different temperatures for **CCP-1**. As can be seen, some diffusion problems occur for certain gases, not observing the normal behaviour of decreasing sorption capacity when the temperature raises. This will be discussed thoroughly in this *chapter*.

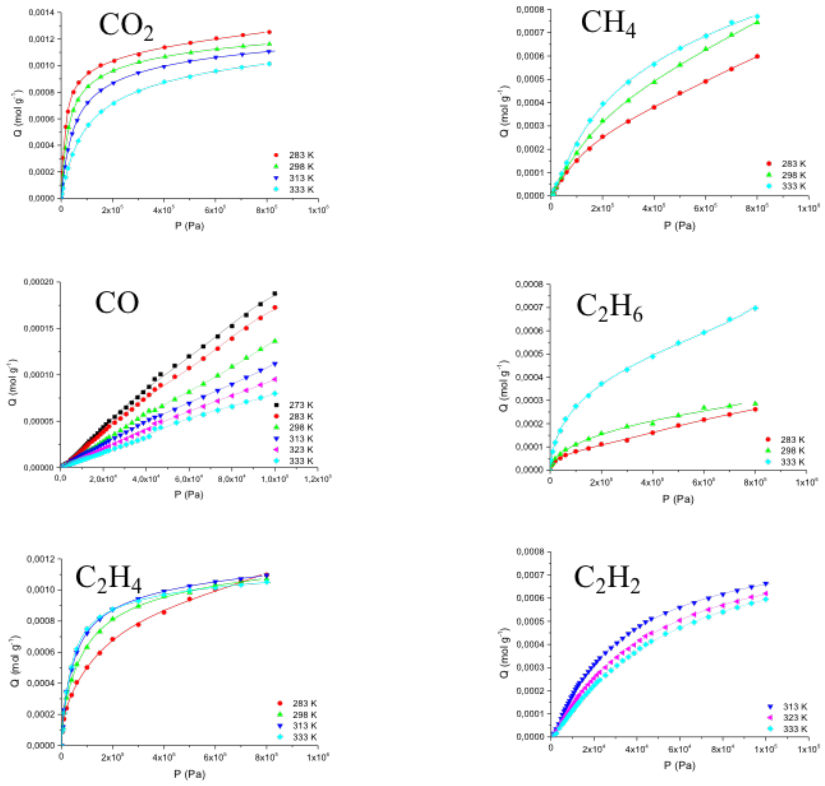

Figure 2.8. Gas adsorption isotherms (mol g^{-1}) for different gases at different temperatures for **CCP-1**. Lines correspond to virial fits.

To do a properly comparation of the adsorption for different gases, all the isotherms at 298 K have been compared (figure 2.9) and the gas capacity has been represented with two different units: molecules per void and volumetric units (cm^3 of CO_2 per cm^3 of compound).

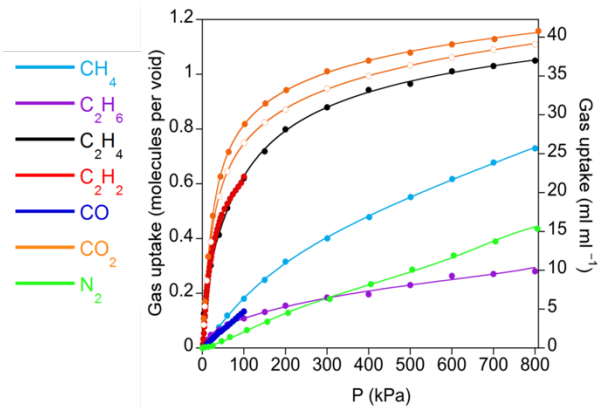

Figure 2.9. Gas adsorption isotherms at 298 K of **CCP-1** (closed symbols) and **CCP-2** (open symbols).

As can be observed, about one molecule of CO_2, CH_4, C_2H_2 and C_2H_4 can be located in each void; on the contrary, CO, N_2 and C_2H_6 remains almost unabsorbed. That observation could suggest a preferential sorption of some gases among others, a good starting point to use this compartmentalized coordination polymer for gas discrimination. Specially interesting is the fact that **CCP-1** and **CCP-2** present higher absorption capacity for CO_2 than C_2H_2 at ambient conditions, contrary to the inverse behaviour observed in typical MOFs that can absorb both gases.[25] In fact, only one example has been reported with this opposed behaviour, a MOF that combines gate opening effect and different electronic properties of the gases to perform preferential adsorption of CO_2 over C_2H_2.[26] **CCP-1** and **CCP-2** present a dense nature due to the absence of permanent channels. For this reason the volumetric sorption of CO_2 (volume of CO_2 absorbed/volume of material), presents very good results, with values of 29 and 27 $cm^3 \cdot cm^{-3}$ for **CCP-1** and **CCP-2** respectively, which are competitive results compared with other known and typically used MOFs in gas sorption (28 and 11 $cm^3 \cdot cm^{-3}$ for MIL-100[27] and

MOF-5[28] respectively) at 1 bar and 298 K. Another advantage in the use of these isolated compartments is the strong interaction of the gas with the framework, causing the trapping of the gas molecules with no need of using the approaches commented in the introduction of this *chapter*, that is no modification of the original framework to enhance the gas-framework interaction. Related to this, the isosteric enthalpy of adsorption at zero surface coverage of some gases in **CCP-1** and **CCP-2** have been studied. It was calculated from the isotherms taken at different temperatures applying the Clausius-Clapeyron equation:

$$q_{st} = -R \cdot \left[\frac{\partial(\ln P)}{\partial(1/T)} \right]_{Q=cte}$$

Equation 2.2. Clausius-Clapeyron equation used to calculate the heats of adsorption for different gases.

As can be observed in figure 2.10, low values of these enthalpies have been found whatever the gas observed (Q_{st} (CO_2) = 20 kJ·mol^{-1}; Q_{st} (C_2H_2) = 23 kJ·mol^{-1}; Q_{st} (CO) = 11 kJ·mol^{-1}) compared to typical values found on other archetypal materials used for gas storage like functionalized MOFs with alkylamines that present enthalpies of adsorption near 100 kJ·mol^{-1}.[29]

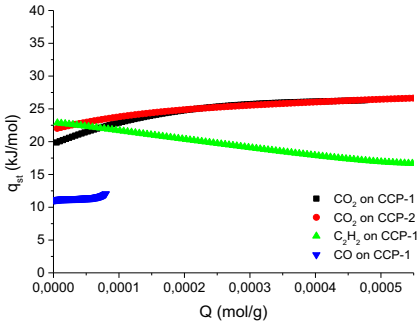

Figure 2.10. Isosteric heats of adsorption for different gases.

These low values affect directly the cost of regeneration of the material, due to that it is needed less energy to fully regenerate it and then, high working capacities for adsorption-desorption cycles could be achieved.

2.2.3 Location and binding of the gas molecules

2.2.3.1 Rietveld analysis using X-ray powder Synchrotron diffraction

This study was performed in collaboration with Dr. I. J. Vitórica-Yrezábal, from the University of Manchester (UK), on beamline BL04-MSPD at ALBA Synchrotron, Spain (proposal 2015091491). Typically, inclusion of guests in systems that can locate gas molecules in their pores result in disordered species inside these cavities[30] with difficulties to specific location determination. The use of compartmentalized coordination polymers take advantage of presenting ordered discrete voids that reduce the mobility of the gas molecules then allowing the exact determination of the guest inside the void. Structural determination of CO_2 inside **CCP-1** has been previously reported using Rietveld analysis and X-ray powder synchrotron diffraction

data. In this *chapter*, the gas location of CO_2 inside **CCP-1** and **CCP-2** has been repeated and extended with C_2H_4 and CH_4 using the same Rietveld analysis and synchrotron X-ray powder diffraction. Samples of **CCP-1** or **CCP-2** were pumped 30 minutes and then the pressure for each gas was increased to 6 bar. The corresponding Rietveld refinements can be seen on figure 2.11. The structures determined from single crystal data at 240 K for **CCP-1** and **CCP-2** have been used as starting points for the refinements and the occupancy of the gas molecules (CO_2, C_2H_2 and CH_4) have been refined introducing them as rigid bodies and their occupancies were freely refined with a constraint thermal parameter. The counterions (ClO_4^- for **CCP-1** and BF_4^- for **CCP-2)** were not being affected by the sorption process, remaining in the same position. As previously reported for CO_2, all three gases are disordered over six symmetry related positions with refined occupancies near to the calculated from the adsorption isotherms (figure 2.12). The gas-framework interactions found are different for two of the three gases studied despite all three species are located inside the same voids. For CO_2, the interaction observed is between the nucleophilic oxygen atom of the gas and two nitrogen atoms of one tetrazole in an end-on mode, with a O=C=O(δ^-)$\cdots\pi_{N-N}$ distances of 2.500 Å for **CO_2@CCP-1** and 2.778 Å in **CO_2@CCP-2**. The electrophilic carbon of CO_2 is not interacting with the framework, maybe due to the cationic nature of it, the constrained space of the void or a combination of both. C_2H_4 forms C–H$\cdots\pi_{N-N}$ hydrogen bonds with one nitrogen atom of one tetrazole, with C–H$\cdots\pi_{N-N}$ distances of 2.684 and 2.677 Å for **C_2H_4@CCP-1** and **C_2H_4@CCP-2**, respectively. CH_4 molecules form C–H$\cdots\pi_{N-N}$ distances of 2.661 and 2.781 Å for **CH_4@CCP-1** and **CH_4@CCP-2**, respectively.

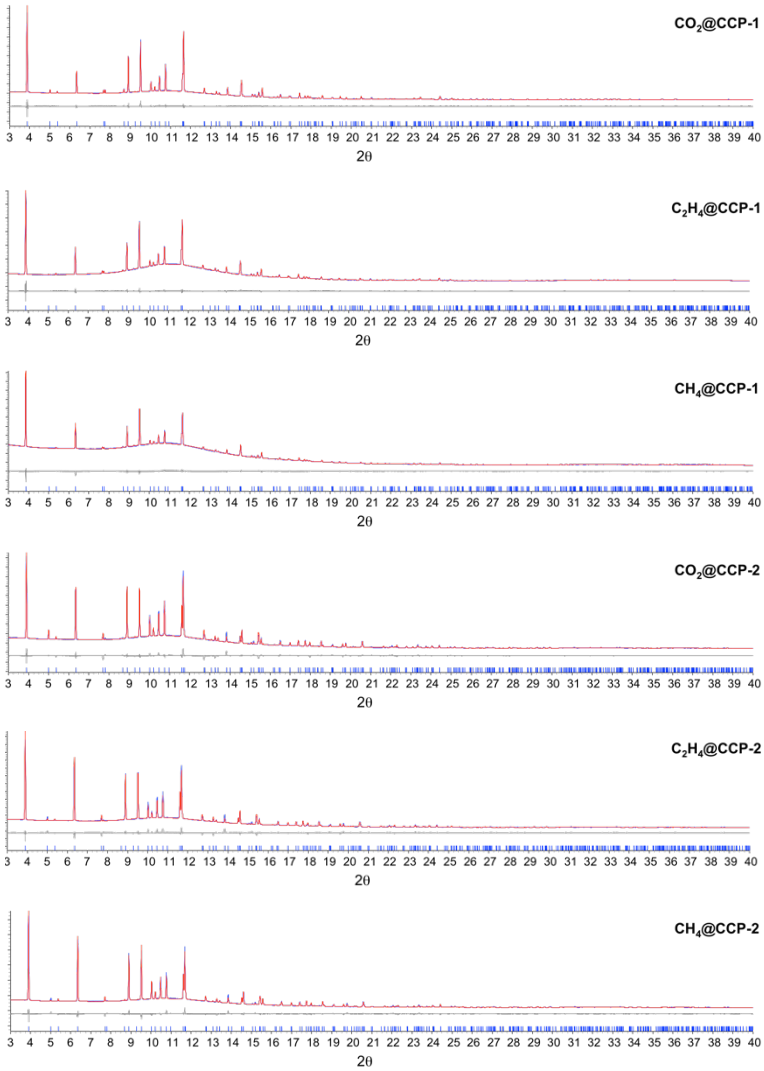

Figure 2.11. Observed (blue) and calculated (red) profiles and difference plot [(I_{obs} − I_{calcd})] (grey) of the Rietveld refinements for **CCP-1** and **CCP-2** after different gas loadings.

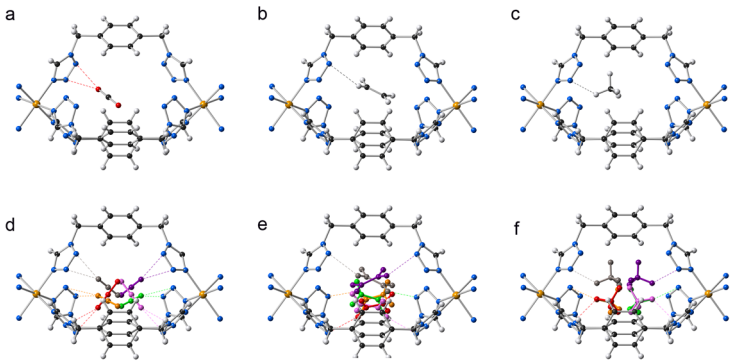

Figure 2.12. Crystal structures of **CCP-1/CCP-2** loaded with CO_2 (a), C_2H_4 (b) and CH_4 (c), showing the interactions between the gas molecules and the framework as dashed lines. The symmetry-related gas molecules are colored differently showing the positional disorder of the CO_2 (d), C_2H_4 (e) and CH_4 (f) molecules.

2.2.4. Magnetic response to gas sorption

It has been previously reported that **CCP-1** presents SCO and their $T_{1/2}$ can be modified with the inclusion of CO_2 inside its voids. That was the first example reported where the spin transition is affected by the inclusion of gas molecules adsorbed inside a coordination polymer. In this *chapter*, the magnetic measurements for bare **CCP-1** and **CCP-2** and with CO_2 located inside not only have been reproduced, but also the study has been extended with other gases adsorbed inside the voids: methane (CH_4), ethane (C_2H_6), propane (C_3H_8), ethylene (C_2H_4) and carbon monoxide (CO) and the magnetic response for each case can be observed in figure 2.13.

CCP-1 and **CCP-2** have been activated heating 150 ºC 3 hours under vacuum before loading the gases. Magnetic susceptibility measurements of the gas loaded systems were performed by sealing a glass tube with 10 mg of

CCP-1/**CCP-2** and 1 bar of the gas (CO_2, CH_4, C_2H_6, C_2H_4, CO, C_3H_8). CO_2 has been studied in both coordination polymers **CCP-1** and **CCP-2** but the other gases were studied only in **CCP-1**, assuming the same behaviour for both isostructural systems. As previously reported, the spin transition of **CCP-1** and **CCP-2**, centered at 200 K, is shifted to 209 K with the inclusion of one molecule of CO_2 inside the voids, thus stabilizing the low-spin (LS) state (figures 2.13a and 2.13b). For CH_4, C_2H_6 and CO (figures 2.13c, 2.13d and 2.13g) no modification of the magnetic behaviour is observed. Surprisingly, an inverse behaviour than that observed for CO_2 can be seen for ethylene (figure 2.13f), shifting the spin transition temperature to lower temperatures, thus stabilizing the high-spin (HS) state. In the case of propane (figure 2.13e), an enhance of the cooperativity between the metal centers is observed, that is, an increase in the thermal hysteresis. Unfortunately, that interesting behaviour cannot be discussed in detail, as the slow diffusion of this gas makes the study of the adsorption isotherm unachievable.

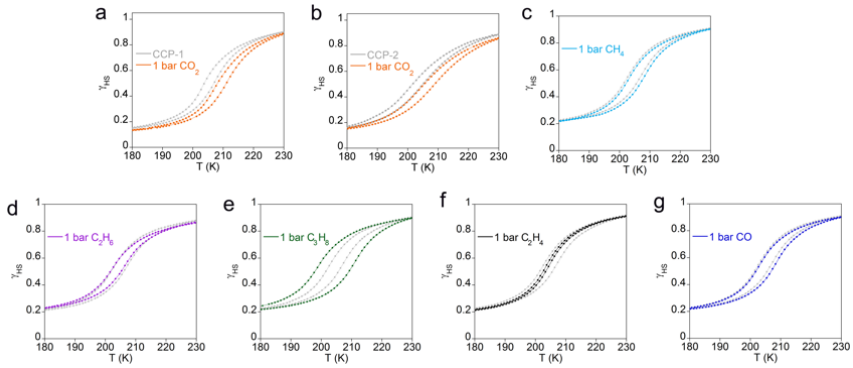

Figure 2.13. Temperature dependence of the high spin fraction (γ_{HS}) for **CCP-1** and **CCP-2** with different gases. The spin transition of the activated material is shown in grey in each case for comparison.

The explanation of these magnetic behaviours has different origins. On one hand, the lack at modification for C_2H_6 and CO is related to the gas adsorption isotherms in figure 2.8, as stated in the part 2.2.2 of this *chapter*: ethane and carbon monoxide remains almost unabsorbed. For that reason, despite putting 1 bar of the gas in the samples, no inclusion of the gas inside the voids occurs, thus retaining the original spin transition centered at 200 K of **CCP-1**. For the other gases, a list of their physical properties can be seen on table 2.1. In these cases, the three gases are interacting with the tetrazole ring, therefore changing the ligand field of the iron (II) center.

	CO_2	CH_4	Ethylene
Kinetic diameter [Å]	3.30	3.758	4.163
Quadrupolar moment x 10^{26} [esu·cm^2]	-4.30	0	1.50
Polarizability x 10^{25} [cm^3]	29.11	25.93	42.52
Dipole moment x 10^{18} [esu·cm]	0	0	0

Table 2.1. Physical properties of some gases studied.

The most plausible way is that the quadrupole moment of the different gases changes the electronic density of the tetrazole ring, thus causing a subtle modification of the spin transition temperature. In the case of methane, the absence of quadrupolar moment in the gas molecule imply that the spin transition suffers no modification in its value, as observed in figure 2.13c. For CO_2 and C_2H_4 it can be seen opposite behaviour: whereas for CO_2 the low-spin state is stabilized with a shifting of the spin transition to higher temperatures, C_2H_4 presents the stabilization of the high-spin state with a shifting of the spin transition to lower temperatures. In addition, with CO_2 the

change in temperature is more pronounced than for C_2H_4, an observation related to the value on the quadrupolar moment. The quadrupolar moment of CO_2 is larger in module than for C_2H_4 provoking that the change in the spin transition is larger for the first gas and in addition, both quadrupolar moment are opposite in sign, causing the opposite modification of the spin transition temperature. That hypothesis has been proved with the synthesis of **CCP-2** with CS_2 inside the voids [as can be related to the mass lost in the TGA analysis (figure 2.14 left)]. CS_2 presents a value of quadrupolar moment equal in module than for CO_2 but opposite in sign and is therefore the ideal candidate to test this hypothesis. The synthesis was analogous that the original one and was carried out replacing the original CH_3CN solvent for CS_2. XRPD data reveals a perfect fit for the original **CCP-2** synthesized with CH_3CN. As can be seen on the magnetic behavior of **CCP-2** with CS_2 in the voids (figure 2.14 right), the spin transition is modified in the same value than for CO_2 but to lower temperatures like C_2H_4 provokes, so demonstrating that the quadrupole moment of the gas located in the compartments is the cause of the modification in the spin transition temperature.

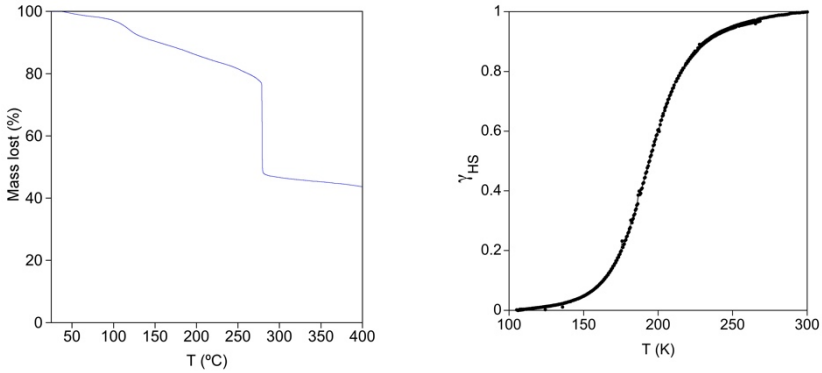

Figure 2.14. TGA analysis (left) of **CCP-2** loaded with CS_2 and its temperature dependence of the high spin fraction (right).

2.2.5 Selectivity in CCPs: Kinetic study

Thermodynamic sorption is typically used for the selective gas sorption, but not only thermodynamics can be used to study the potential gas discrimination of these materials, but also kinetics.[31,32] As commented before, in the gas sorption isotherms of figure 2.8, some diffusion problems can be observed in some gases. The presence of isolated voids, with no permanent channels in the material, is a challenge for the gas adsorption. Transport diffusion has been studied for CO_2, C_2H_4 and C_2H_6, not being studied for C_2H_2 due to incompatibilities in the thermogravimetric instrument but expecting an analogous behaviour than CO_2 due to the similar values in different properties. In figure 2.15, gravimetric evolution of the gases listed before is shown. 50 mg of **CCP-1** was kept under a constant pressure of 300 mbar and 298 K for each gas, showing that CO_2 is easily adsorbed and expecting the same behaviour for acetylene as stated before. But ethylene is

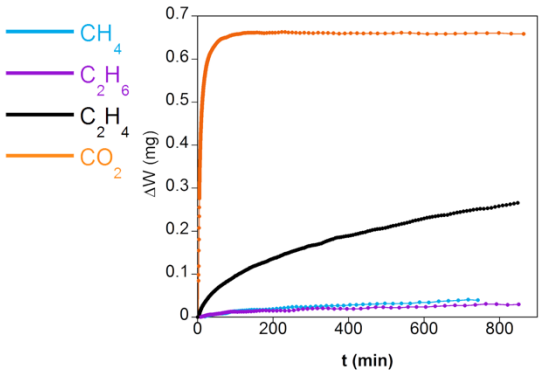

Figure 2.15. Kinetic sorption evolution of **CCP-1**.

adsorbed in a more difficult way, resulting even slower for ethane and methane. This observation is a good starting point to think about using these

compartmentalized coordination polymers to separate gas mixtures of acetylene/ethyelene/methane by kinetic trapping.

2.2.6 Selectivity in CCPs: binary breakthrough measurements

As has been exposed before, **CCP-1** and **CCP-2** present low heat of adsorption but separation of gases needs also good selectivities for some species. Typical materials for this purpose are MOFs that present breathing[33] or gate opening[34] processes which pores only being opened by certain gases. However, that opening of the pores sometimes imply the entrance of others gases or species presented in the mixtures, reducing the selectivity of these materials for the target gases. Different works presented in the literature about gas discrimination are based on the study of the isolated isotherms or computing simulations using an Ideal Absorbed Solution Theory (IAST). These methods are used due to difficulties to carry out real gas mixture experiments but sometimes the results obtained by these methods are far away from the real values. That is provoked for not considering kinetic and thermodynamic mechanisms of the gas mixtures. To avoid these problems, in this *chapter*, gas breakthrough experiments have been performed under kinetic gas-flow conditions for **CCP-1**, pelletizing it to avoid high-pressure drop and filling and packing a column with the material. Two different gas mixtures (CO_2/N_2 and CO_2/CH_4) at four different ratios (5:95, 10:90, 20:80 and 50:50) have been analyzed and can be seen on figures 2.16 and 2.17.

The composition of the exhausted gas was monitored with a mass spectrometer and the total flow together with its composition could be calculated by combining the calibrated Coriolis flow meter and the mass

spectrometer. The selectivity α_{ij} of **CCP-1** can be calculated defining it as the ratio of the two adsorbed gases under specific conditions of temperature and pressure, following the equation 2.3:

$$\alpha_{ij} = \frac{x_i}{x_j} \cdot \frac{y_j}{y_i}$$

Equation 2.3. Gas selectivity of two components.

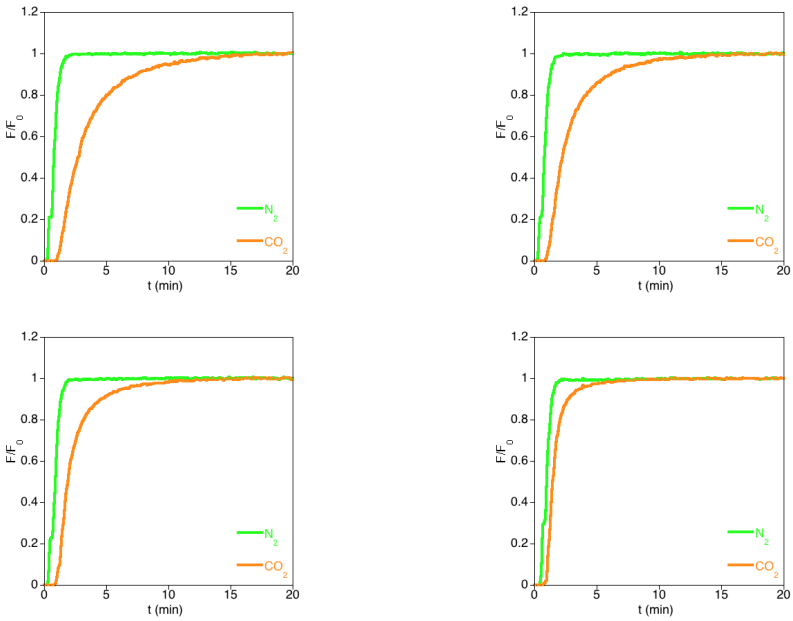

Figure 2.16. Binary breakthrough experiments for different mixtures of CO_2 and N_2 at 298 K and 2 bar for **CCP-1**. 5:95 (top left), 10:90 (top right), 20:80 (bottom left) and 50:50 (bottom right).

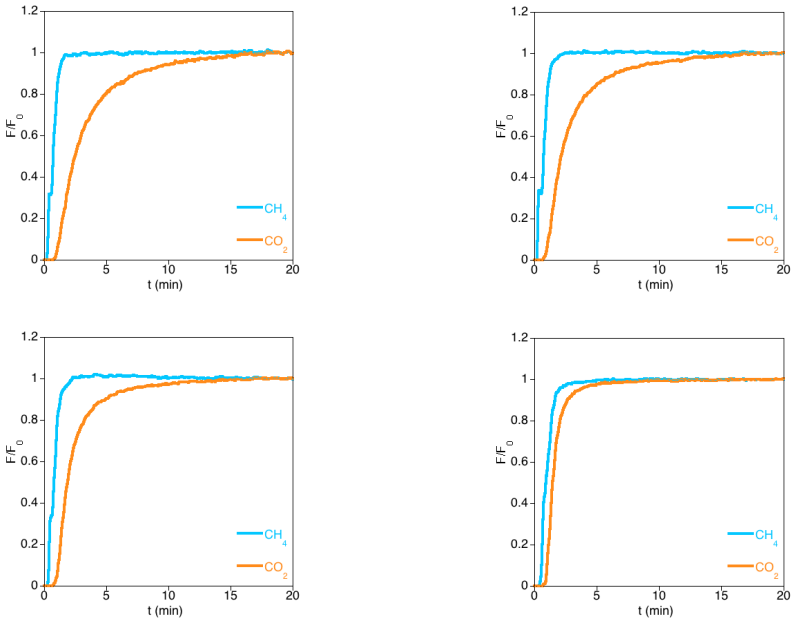

Figure 2.17. Binary breakthrough experiments for different mixtures of CO_2 and CH_4 at 298 K and 2 bar for **CCP-1**. 5:95 (top left), 10:90 (top right), 20:80 (bottom left) and 50:50 (bottom right).

Where $x_{i/j}$ are the adsorbed amounts of gases i and j at equilibrium from a gas mixture defined by the molar fractions $y_{i/j}$. This equation of selectivity can be expressed in terms of molar flow of the adsorbed gases according to the equation 2.4:

$$\alpha_{ij} = \frac{F_{i,0}\int_0^{t\infty}\left(1-\frac{F_i}{F_{i,0}}\right)dt}{F_{j,0}\int_0^{t\infty}\left(1-\frac{F_j}{F_{j,0}}\right)dt}\cdot\frac{y_j}{y_i}$$

Equation 2.4. Gas selectivity of two components in terms of the molar fluxes.

With F_i and F_j as the molar fluxes of gases i and j respectively during the breakthrough experiment, and $F_{i,0}$ and $F_{j,0}$ the molar fluxes of gases i and j in the feed stream. The dead volume was determined by flowing helium though the saturated column and subtracted for the calculation of the adsorbed amount of each specie. The calculated selectivities for the two mixtures and the four ratios between gases are listened in table 2.2:

Flow composition	**Selectivity (α)**	
CO_2:other gas	**CO_2:N_2**	**CO_2:CH_4**
5:95	85	89
10:90	33	42
20:80	11	15
50:50	2	2

Table 2.2. CCP-1 Selectivities in the gas breakthrough experiments

As can be observed, very good selectivities of 85 for CO_2/N_2 and 89 for CO_2/CH_4 have been obtained for low CO_2 concentration (ratio CO_2/N_2 or CH_4 5:95). This observation coincides with a separation process driven by kinetic mechanism, due to lower CO_2 flux implies longer mass transfer in the column.

There are not too many works in the literature in which the gas selectivity in MOFs is calculated from real gas breakthrough experiments, but some of them performed in similar conditions can be seen on table 2.3. As can be observed, the high values obtained at lower CO_2 concentrations for **CCP-1** are better than the reported ones for other similar systems, with exceptions

such as FCTF-1-600 but with the advantage that **CCP-1** is highly selective for two different mixtures of gases.

Compound	Selectivity (α)		Flow composition		Ref.
	CO_2/N_2	CO_2/CH_4	CO_2:N_2	CO_2:CH_4	
CTF-1	18	–	10:90	–	[35]
CTF-1-600	21	–	10:90	–	[35]
FCTF-1	77	–	10:90	–	[35]
FCTF-1-600	152	–	10:90	–	[35]
SIFSIX-2-Cu-i	72	51	10:90	50:50	[8]
MOF508b	5	3	50:50	50:50	[36]
MOF-5	22	–	20:80	–	[37]
NH_2-MIL-53	–	45	–	50:50	[38]
CPO-27-Ni	–	15	–	50:50	[39]
CPO-27-Co	–	12	–	50:50	[39]
CPO-27-Zn	–	9	–	50:50	[39]
STA-12-Ni	–	6	–	50:50	[39]
NH_2-MIL-101 (Al)	–	65	–	15:85	[40]
MIL-53 (Cr)	–	13	–	25:75	[41]
MIL-53 (Al)	–	7	–	30:70	[42]
MIL-101 (Cr)	–	7.5	–	30:70	[40]

Table 2.3. Gas breakthrough selectivities in the literature

Another interesting experiment carried out was the calculation of the adsorbed gas phase in **CCP-1** through mass spectrometry. The partition coefficient (P) after sorption was defined with the equation 2.5 as:

$$P = (X_{CO_2}/Y_{CO_2})/(X_{gas}/Y_{gas})$$

Equation 2.5. Partition coefficient of the gas mixtures

X_{CO_2} and X_{gas} represent the molar fractions of CO_2 and the other gas (N_2 or CH_4) in the adsorbed phase and Y_{CO_2} and Y_{gas} represent the molar fractions of CO_2 and the other gas (N_2 or CH_4) in the bulk phase. The results obtained are exhibited in table 2.4 together with another partition coefficients reported in the literature for the gas mixtures studied in other materials. As can be seen, **CCP-1** performed great results compared with other well-known materials used for gas mixtures separation. The results obtained can be more easily understood in the figure 2.18, comparing the ratio of both gases before and after the gas separation process by **CCP-1**. As can be observed, the adsorbed gas phase presents a higher CO_2/N_2 or CH_4 ratio than the injected phase, corroborating the preferential adsorption of CO_2 over the other two gases.

Compound	Partition coefficient (P)		Flow composition		Ref.
	CO_2/N_2	CO_2/CH_4	CO_2:N_2	CO_2:CH_4	
CCP-1	35	47	5:95	5:95	[43]
CCP-1	38	41	10:90	10:90	[43]
CCP-1	36	36	20:80	20:80	[43]
CCP-1	49	32	50:50	50:50	[43]
Cu-BTC	–	6	–	25:75	[44]
Ni-MOF-74	38	–	15:85	–	[45]
UiO-66(Zr)-$(COOH)_2$	56	–	15:85	–	[46]
CID-3	39	–	1:99	–	[47]

Table 2.4. Partition coefficients for different gas mixtures

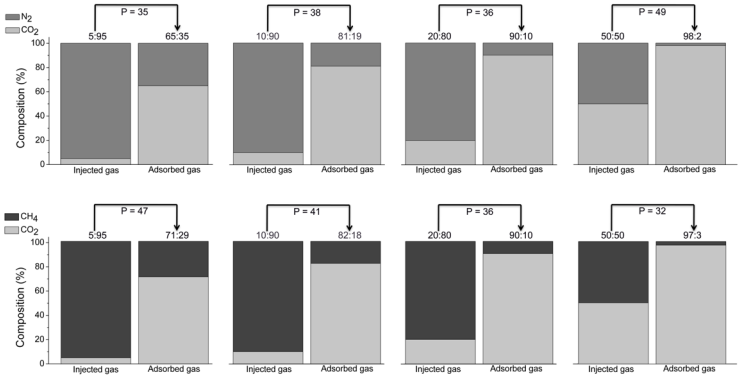

Figure 2.18. Enrichment of the CO_2 gas component after the breakthrough experiment for CO_2/N_2 (top) and CO_2/CH_4 (bottom).

2.3 CONCLUSIONS

In this *chapter*, new materials have been widely studied presenting a new concept for coordination polymers: the compartmentalized coordination polymers, that is, coordination polymers with discrete and isolated compartments with potential capacity to locate gas molecules inside the voids. The response of two previously reported compartmentalized coordination polymers, **CCP-1** and **CCP-2**, to different gases has been studied. It has been observed that the materials can adsorb certain gases, revealing potential capacity to be used as discriminators for gas mixtures. The gas selectivity studies revealed a high selectivity sorption for CO_2 in the presence of N_2 or CH_4 with high selectivity and partition coefficients compared with others in the literature for equivalent materials and conditions. In addition, Rietveld analysis using X-ray synchrotron data has been used to

determine the location and the interaction of the gas molecules inside the framework, revealing vital information to explain the magnetic behaviour of these materials with the gas molecules located inside. It has been revealed that the quadrupolar moment of the gas provokes changes in the tetrazole ring of the ligand, thus modifying the ligand field of the iron (II) centers then changing the spin transition temperature. A stabilization of the low-spin or the high-spin state occurs, depending on the sign of this quadrupolar moment. Additional experiments have been performed in different collaborations. Dr. Mónica Jiménez-Ruiz from the Institut Laue-Langevin of Grenoble performed DFT and molecular dynamics calculations to obtain the H partial density of states of **CCP-1**. Dr. Mónica Jiménez-Ruiz, Dr. J. Alberto Rodríguez-Velamazán and Dr. Miguel A. González from the Institut Laue-Langevin of Grenoble performed Inelastic Neutron Scattering (INS) experiments of bare **CCP-1** and **CCP-1** loaded with CO_2. Both techniques have been combined, observing a weak interaction of the gas with the H corresponding to the tetrazole group which was confirmed with DFT calculations. In addition, the scattering of the absorbed CO_2 molecules in the voids has been observed studying the difference between the INS spectra of **CCP-1** upon CO_2 sorption and bare **CCP-1**, remaining a band at 650 cm^{-1}, corresponding to the bending of the CO_2 molecule.

Germán Sastre from the Instituto de Tecnología Química of Valencia performed atomistic molecular dynamics helped to understand the mechanism of entrance of CO_2 inside the isolated cavities. It has been revealed that when low CO_2 pressure is applied to **CCP-1**, the gas starts to fill the voids. When the pressure increases, eventually two molecules of CO_2

are located inside the same void, increasing the energy of the system, forcing the migration of one of these molecules to the adjacent void via a gate-opening mechanism of the phenyl ring, only taking place to allow the transition of the CO_2 molecules.

No additional information is provided about these techniques as they have served to complement this study, but are not part of this *thesis*.

2.4. METHODS

2.4.1. Synthesis

All reagents were commercially available and used without further purification. Solvents were dried and purified before use, according to standard procedures. The ligand btzx, (1,4-bis(tetrazol-1-ylmethyl)benzene), was prepared as previously reported.[23]

Caution. Perchlorate salts are explosive (especially if they are dry) and should be handled with extreme caution.

Synthesis of 1,4-bis(tetrazol-1-ylmethyl)benzene (btzx). p-Xylylenediamine (5 g, 0.037 mol), triethylortoformate (54 g, 0.363 mol) and sodium azide (4.79 g, 0.074 mol) were dissolved in acetic acid (90 mL) and heated at 90 ºC for 2 days. After cooling down to room temperature, the solvent was evaporated at reduced pressure. The remaining yellow solid was washed with methanol and water yielding the ligand as a white powder. Yield = 68 %; 1H NMR (300 MHz, [D6]DMSO): d=5.7 (s, 4H; ttz-CH_2-ph), 7.4 (s, 4H; ph), 9.5 ppm (s, 2H; ttz); IR: = 3118 cm^{-1} (n Cttz-H).

Synthesis of $[Fe(btzx)_3](ClO_4)_2$ (CCP-1). A solution of $Fe(ClO_4)_2 \cdot xH_2O$ (112 mg) in 5 mL of MeCN was added into a suspension of btzx (152 mg, 0.63 mmol) in 40 mL of MeCN containing ascorbic acid (*ca*. 10 mg). The resulting milky suspension was refluxed and stirred for 4 h. A white crystalline precipitate appeared during the reaction. After cooling down to room temperature, the white powder was filtered and washed with MeCN. Alternative synthesis by microwaves was carried out in a CEM Focused Microwave Synthesis System. $Fe(ClO_4)_2 \cdot xH_2O$ (16.4 mg), btzx (22.8 mg, 0.09 mmol) and 6 mL of MeCN were introduced in a microwave vial and the reaction was carried out with 200 MHz and 82 ºC during 5 minutes. The reaction was cooled down and a white precipitate appeared after few hours. Phase purity was established by X-ray powder diffraction (vide infra). Yield = 71 %. Anal. calc. $C_{30}H_{30}FeN_{24}Cl_2O_8$ (981.47): C, 36.71; H, 3.08; N, 34.25 %. Found: C, 36.98; H, 3.16; N, 34.03 %.

Synthesis of $[Fe(btzx)_3](BF_4)_2$ (CCP-2). **CCP-2** was synthesized in a procedure analogous to that of **CCP-1** except that $Fe(BF_4)_2 \cdot 6H_2O$ (152 mg, 0.45 mmol) was used instead. A white crystalline precipitate was collected and washed with MeCN. Alternative synthesis by microwaves was carried out in a CEM Focused Microwave Synthesis System. $Fe(BF_4)_2 \cdot 6H_2O$ (21.7 mg, 0.06 mmol), btzx (22.8 mg, 0.09 mmol) and 6 mL of MeCN were introduced in a microwave vial and the reaction was carried out with 200 MHz and 82 ºC during 5 minutes. The reaction was cooled down and a white precipitate appeared after few hours. Phase purity was established by X-ray powder diffraction (vide infra). Yield = 62 %. Anal. calc. $C_{30}H_{30}FeN_{24}B_2F_8$ (956.18): C, 37.68; H, 3.16; N, 35.16 %. Found: C, 38.81; H, 3.37; N, 35.34 %.

2.4.2. Structural characterization

2.4.2.1. X-ray powder diffraction measurements under gas pressure

Polycrystalline samples of **CCP-1** and **CCP-2** were lightly ground in an agate mortar and pestle and filled into a 0.7 mm borosilicate capillary. Data was collected for each sample in the 2θ range 0 – 40 º on beamline BL04-MSPD at ALBA Synchrotron, Spain, using λ = 0.799332 Å and a Mythen detector comprising 6 modules. The samples were pumped for *ca*. 30 minutes, after which the gas pressure was increased to 6 bar. The capillaries were allowed for stabilization for 30 minutes before data collection at 295 K. A Rietveld refinement[48] was undertaken with the program TOPAS,[49] using as the starting point the structures determined from single crystal data at 240 K for **CCP-1** and **CCP-2** respectively. One gas molecule (CO_2, C_2H_4 or CH_4) was included in the refinement, and refined as a rigid body with rotational and translational freedom. In addition, the occupancies of the gas molecules were also refined, but the displacement parameter was kept fixed. Atomic positions and displacement parameters of the non-hydrogen atoms of the framework were refined subject to a series of restraints on bond lengths, bond angles and planarity of the aromatic rings. The perchlorate and tetrafluoroborate anions were modelled as disorder over two positions, as in the single-crystal experiments. A March-Dollase correction of the intensities for preferred orientation was applied in the final stage of refinement. Rietveld refinements converged to R_{wp} = 0.0214, gof = 2.183 in **CO_2@CCP-1**, R_{wp} = 0.0162, gof = 1.919 in **C_2H_4@CCP-1**, R_{wp} = 0.0107, gof = 1.285 in **CH_4@CCP-1**, R_{wp} = 0.0313, gof = 3.271 in **CO_2@CCP-2**, R_{wp} = 0.0357, gof = 3.738 in **C_2H_4@CCP-2**, and R_{wp} = 0.0329, gof = 3.442 in **CH_4@CCP-2**.

2.4.2.2. Scanning electron microscopy

Crystallite morphologies and dimensions of **CCP-1** were studied with a Hitachi S-4800 field emission scanning electron microscope at an accelerating voltage of 10 kV with metallization (Au-Pd) of the samples.

2.4.3. Gas sorption studies

All gas sorption studies were performed by Dr. Miguel Palomino in collaboration with Prof. F. Rey from the Instituto de Tecnología Química of Valencia.

2.4.3.1. Gas sorption isotherms

High-resolution isotherms of CO and C_2H_2 were measured at a series of temperatures in a Micromeritics ASAP 2010 volumetric instrument using approximately 150 mg of sample as a powder. The sample was placed in a sample holder that was immersed into a liquid recirculating thermostatic bath (Julabo FP40-HL) able to control the adsorption temperature from 273 to 333 K with accuracy better than 0.05 K. Prior to adsorption experiments, the sample was outgassed at 423 K for 6 hours under turbomolecular high vacuum. To avoid He adsorption after free space volume determination the sample was outgassed for 1 hour at 423 K prior to gas adsorption.

High pressure CO_2, CH_4, C_2H_6, and C_2H_4 adsorption isotherms were performed in an IGA-3 gravimetric analyser (Hiden Isochema). Approximately, 50 mg of sample were placed in the balance. Before each adsorption experiment, the sample was outgassed at 423 K under a final

pressure of 10^{-5} Pa during four hours. The temperature of the sample was subsequently reduced under high vacuum until the target temperature (from 283 to 333 K) for each adsorption experiment. Adsorption measurements were performed by introducing gas up to reach the desired pressures. Typically, 16 equilibrium data points up to 800 kPa were recorded for each gas and adsorption temperature in order to build the isotherms. The equilibrium conditions were fixed at the 98 % of the calculated uptake using the Avrami's model or a maximum equilibration time of 120 minutes for each point of the isotherms.

2.4.3.2. Kinetic study

The kinetic experiments were performed in an IGA-3 gravimetric analyser (Hiden Isochema). Approximately 50 mg of the adsorbant were outgassed in the balance at 423 K under high vacuum prior the kinetic study. Next, the sample was cooled down to the analysis temperature, 298 K. Then, the pressure was raised up to 30 kPa and the weight gain was recorded as a function of time for 12 hours.

2.4.3.3. Breakthrough experiments

Breakthrough curves of binary gaseous mixtures were carried out on a homemade instrument, illustrated in Scheme 2.1. In all cases, the sample was pelletized and sieved between 0.2 and 0.4 mm. The solid adsorbent was loaded into a stainless-steel tubular column of 6.0 mm internal diameter, with quartz wool as filler. The weight of adsorbent was 1.2375 g, with a length of 13.5 cm inside of the aforementioned column. The gaseous flows were adjusted by using calibrated mass-flow controllers (Iberfluid Instruments) so,

different feed compositions could be studied. The total feed flow was maintained at 40 ml/min in all cases. The gaseous mixture could be sent into the packed column of adsorbent, or by-passed by using a 6 port valve (Valco). The same valve was also used for feeding helium to the column during the degasification process at high temperature. The column was heated by means of an electric mantle, and the temperature was controlled during the experiments with a thermostatic bath (Julabo F25) connected to the double-jacketed column. Prior to the breakthrough experiments, the adsorbent was activated at 353 K in 40 ml/min of helium for two hours. The reactor was then cooled down to 298 K before switching to the gas mixture. Both the by-pass and the stream from the column can be sent to vent or to analyze through two different 4 port valves (Valco). The pressure in the column and the by-pass line was regulated by two different electronic pressure gage controllers (Bronkhorst). One particularity of the setup is the use of a mass flow meter based in the Coriolis effect (Bronkhorst) connected downstream the column. The Coriolis flow meter provide with a value of the mass flow in g/h. Also, the composition of the exhausted gas was monitored with a mass spectrometer. The total flow together with its composition could be calculated by combining the calibrated Coriolis flow meter and the mass spectrometer.

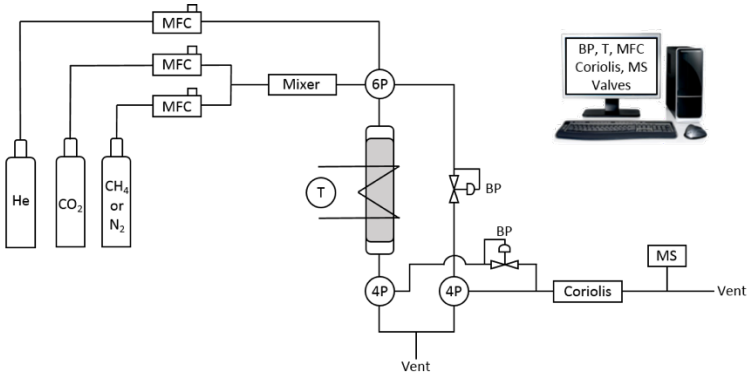

Scheme 2.1. Schematic diagram of the breakthrough apparatus used for binary adsorption. MFC, mass flow controller; 6P, 6 port valve; 4P, 4 port valve; BP, pressure controller; T, temperature control (heating mantle or recirculated bath); MS, mass spectrometer.

2.5 Physical measurements

Thermogravimetric analysis of **CCP-2** with CS_2 was carried out with a TA instruments TGA 550 apparatus in the 25-400 ºC temperature range under a 10 ºC·min^{-1} scan rate and a nitrogen flow of 40 mL·min^{-1}.

2.5.1 Magnetic measurements. Magnetic susceptibility measurements were carried out on single-phased polycrystalline samples with a Quantum Design MPMS-XL-5 SQUID susceptometer. The susceptibility data were all collected at 1 K·min^{-1}, with an applied field of 0.1 T for **CCP-1** and **CCP-2** and the gas loaded systems. Magnetic susceptibility measurements of the gas loaded systems were performed by sealing a glass tube with 10 mg of **CCP-1** and **CCP-2** and a known amount of the gas (CO_2, CH_4, C_2H_6, C_2H_4, CO, propane, N_2, N_2/CO_2) or after heating a loaded sample to remove the CO_2 molecules. Prior to the gas loading, the samples were activated by heating in situ at 150 °C for 3 h under vacuum.

2.6 REFERENCES

1. Keller, G. E., Marcinkowsky, A. E., Verma, S. K. & Williamson, K. D. *Separation and purification technology*. (Marcel Dekker, 1992).
2. McDonald, T. M. *et al.* Cooperative insertion of CO_2 in diamine-appended metal-organic frameworks. *Nature* **519**, 303–308 (2015).
3. Morris, R. E. & Wheatley, P. S. Gas Storage in Nanoporous Materials. *Angew. Chem. Int. Ed.* **47**, 4966–4981 (2008).
4. DeCoste, J. B. & Peterson, G. W. Metal–Organic Frameworks for Air Purification of Toxic Chemicals. *Chem. Rev.* **114**, 5695–5727 (2014).
5. Li, J.-R., Sculley, J. & Zhou, H.-C. Metal–Organic Frameworks for Separations. *Chem. Rev.* **112**, 869–932 (2012).
6. Xue, D.-X. *et al.* Tunable Rare Earth **fcu** -MOF Platform: Access to Adsorption Kinetics Driven Gas/Vapor Separations via Pore Size Contraction. *J. Am. Chem. Soc.* **137**, 5034–5040 (2015).
7. Xiang, S.-C. *et al.* Rationally tuned micropores within enantiopure metal-organic frameworks for highly selective separation of acetylene and ethylene. *Nat. Commun.* **2**, (2011).

8. Nugent, P. *et al.* Porous materials with optimal adsorption thermodynamics and kinetics for CO_2 separation. *Nature* **495**, 80–84 (2013).
9. Yang, S. *et al.* A partially interpenetrated metal–organic framework for selective hysteretic sorption of carbon dioxide. *Nat. Mater.* **11**, 710–716 (2012).
10. Southon, P. D. *et al.* Dynamic Interplay between Spin-Crossover and Host−Guest Function in a Nanoporous Metal−Organic Framework Material. *J. Am. Chem. Soc.* **131**, 10998–11009 (2009).
11. An, J. & Rosi, N. L. Tuning MOF CO_2 Adsorption Properties via Cation Exchange. *J. Am. Chem. Soc.* **132**, 5578–5579 (2010).
12. Yang, S. *et al.* Cation-induced kinetic trapping and enhanced hydrogen adsorption in a modulated anionic metal–organic framework. *Nat. Chem.* **1**, 487–493 (2009).
13. Lu, W. *et al.* Tuning the structure and function of metal–organic frameworks via linker design. *Chem Soc Rev* **43**, 5561–5593 (2014).
14. Couck, S. *et al.* An Amine-Functionalized MIL-53 Metal−Organic Framework with Large Separation Power for CO_2 and CH_4. *J. Am. Chem. Soc.* **131**, 6326–6327 (2009).

15. Fracaroli, A. M. *et al.* Metal–Organic Frameworks with Precisely Designed Interior for Carbon Dioxide Capture in the Presence of Water. *J. Am. Chem. Soc.* **136**, 8863–8866 (2014).

16. An, J., Geib, S. J. & Rosi, N. L. High and Selective CO_2 Uptake in a Cobalt Adeninate Metal−Organic Framework Exhibiting Pyrimidine- and Amino-Decorated Pores. *J. Am. Chem. Soc.* **132**, 38–39 (2010).

17. Bloch, E. D. *et al.* Hydrocarbon Separations in a Metal-Organic Framework with Open Iron(II) Coordination Sites. *Science* **335**, 1606–1610 (2012).

18. Caskey, S. R., Wong-Foy, A. G. & Matzger, A. J. Dramatic Tuning of Carbon Dioxide Uptake via Metal Substitution in a Coordination Polymer with Cylindrical Pores. *J. Am. Chem. Soc.* **130**, 10870–10871 (2008).

19. Bae, Y.-S. *et al.* High Propene/Propane Selectivity in Isostructural Metal-Organic Frameworks with High Densities of Open Metal Sites. *Angew. Chem. Int. Ed.* **51**, 1857–1860 (2012).

20. Quartapelle Procopio, E. *et al.* A Soft Copper(II) Porous Coordination Polymer with Unprecedented Aqua Bridge and Selective Adsorption Properties. *Chem. - Eur. J.* **18**, 13117–13125 (2012).

21. Yang, S. *et al.* Supramolecular binding and separation of hydrocarbons within a functionalized porous metal–organic framework. *Nat. Chem.* **7**, 121–129 (2015).

22. Xiang, S. *et al.* Microporous metal-organic framework with potential for carbon dioxide capture at ambient conditions. *Nat. Commun.* **3**, (2012).

23. Coronado, E., Giménez-Marqués, M., Mínguez Espallargas, G., Rey, F. & Vitórica-Yrezábal, I. J. Spin-Crossover Modification through Selective CO_2 Sorption. *J. Am. Chem. Soc.* **135**, 15986–15989 (2013).

24. Thesis of Mónica Giménez-Marqués. (2013).

25. Matsuda, R. *et al.* Highly controlled acetylene accommodation in a metal–organic microporous material. *Nature* **436**, 238–241 (2005).

26. Foo, M. L. *et al.* An Adsorbate Discriminatory Gate Effect in a Flexible Porous Coordination Polymer for Selective Adsorption of CO_2 over C_2H_2. *J. Am. Chem. Soc.* **138**, 3022–3030 (2016).

27. Yazaydın, A. Ö. *et al.* Screening of Metal−Organic Frameworks for Carbon Dioxide Capture from Flue Gas Using a Combined Experimental and Modeling Approach. *J. Am. Chem. Soc.* **131**, 18198–18199 (2009).

28. Mason, J. A. *et al.* Application of a High-Throughput Analyzer in Evaluating Solid Adsorbents for Post-Combustion Carbon Capture via

Multicomponent Adsorption of CO_2 , N_2 , and H_2O. *J. Am. Chem. Soc.* **137**, 4787–4803 (2015).

29. McDonald, T. M., D'Alessandro, D. M., Krishna, R. & Long, J. R. Enhanced carbon dioxide capture upon incorporation of N,N′-dimethylethylenediamine in the metal–organic framework CuBTTri. *Chem. Sci.* **2**, 2022 (2011).
30. Carrington, E. J., Vitórica-Yrezábal, I. J. & Brammer, L. Crystallographic studies of gas sorption in metal–organic frameworks. *Acta Crystallogr. Sect. B Struct. Sci. Cryst. Eng. Mater.* **70**, 404–422 (2014).
31. Herm, Z. R. *et al.* Separation of Hexane Isomers in a Metal-Organic Framework with Triangular Channels. *Science* **340**, 960–964 (2013).
32. Krishna, R. Diffusion in porous crystalline materials. *Chem. Soc. Rev.* **41**, 3099–3118 (2012).
33. Férey, G. & Serre, C. Large breathing effects in three-dimensional porous hybrid matter: facts, analyses, rules and consequences. *Chem. Soc. Rev.* **38**, 1380 (2009).
34. Horike, S., Shimomura, S. & Kitagawa, S. Soft porous crystals. *Nat. Chem.* **1**, 695–704 (2009).

35. Zhao, Y., Yao, K. X., Teng, B., Zhang, T. & Han, Y. A perfluorinated covalent triazine-based framework for highly selective and water–tolerant CO_2 capture. *Energy Environ. Sci.* **6**, 3684 (2013).

36. Bastin, L. *et al.* A Microporous Metal−Organic Framework for Separation of CO_2 /N_2 and CO_2 /CH_4 by Fixed-Bed Adsorption. *J. Phys. Chem. C* **112**, 1575–1581 (2008).

37. Jiang, N., Deng, Z., Liu, S., Tang, C. & Wang, G. Synthesis of metal organic framework (MOF-5) with high selectivity for CO_2/N_2 separation in flue gas by maximum water concentration approach. *Korean J. Chem. Eng.* **33**, 2747–2755 (2016).

38. Couck, S. *et al.* Adsorption and Separation of Light Gases on an Amino-Functionalized Metal-Organic Framework: An Adsorption and In Situ XRD Study. *ChemSusChem* **5**, 740–750 (2012).

39. García, E. J. *et al.* Role of Structure and Chemistry in Controlling Separations of CO_2 /CH_4 and CO_2 /CH_4 /CO Mixtures over Honeycomb MOFs with Coordinatively Unsaturated Metal Sites. *J. Phys. Chem. C* **116**, 26636–26648 (2012).

40. Serra-Crespo, P., Ramos-Fernandez, E. V., Gascon, J. & Kapteijn, F. Synthesis and Characterization of an Amino Functionalized MIL-

101(Al): Separation and Catalytic Properties. *Chem. Mater.* **23**, 2565–2572 (2011).

41. Hamon, L. *et al.* Co-adsorption and Separation of CO_2−CH_4 Mixtures in the Highly Flexible MIL-53(Cr) MOF. *J. Am. Chem. Soc.* **131**, 17490–17499 (2009).
42. Finsy, V. *et al.* Separation of CO_2/CH_4 mixtures with the MIL-53(Al) metal–organic framework. *Microporous Mesoporous Mater.* **120**, 221–227 (2009).
43. Giménez-Marqués, M. *et al.* Gas confinement in compartmentalized coordination polymers for highly selective sorption. *Chem. Sci.* **8**, 3109–3120 (2017).
44. Hamon, L., Jolimaître, E. & Pirngruber, G. D. CO_2 and CH_4 Separation by Adsorption Using Cu-BTC Metal−Organic Framework. *Ind. Eng. Chem. Res.* **49**, 7497–7503 (2010).
45. Liu, J., Tian, J., Thallapally, P. K. & McGrail, B. P. Selective CO_2 Capture from Flue Gas Using Metal–Organic Frameworks—A Fixed Bed Study. *J. Phys. Chem. C* **116**, 9575–9581 (2012).
46. Yang, Q. *et al.* A Water Stable Metal-Organic Framework with Optimal Features for CO_2 Capture. *Angew. Chem. Int. Ed.* **52**, 10316–10320 (2013).

47. Nakagawa, K. *et al.* Enhanced selectivity of CO_2 from a ternary gas mixture in an interdigitated porous framework. *Chem. Commun.* **46**, 4258 (2010).

48. Rietveld, H. M. A profile refinement method for nuclear and magnetic structures. *J. Appl. Crystallogr.* **2**, 65–71 (1969).

49. Coelho, A. A. TOPAS-Academic, Version 4.1, 2007, see http://www.topas-academic.net.

Chapter 3:
A mixed-ligand approach to tune the transition temperature

3.1 INTRODUCTION

The aim of tuning the properties of multifunctional materials has attracted a lot of interest in the last decades. One of the most interesting property for modification is the spin transition temperature on spin crossover (SCO) compounds. [1–10] Still, this spin transition often occurs at temperatures that are not practical for applications. A subtle modification of the material could modify the spin transition temperature while the material maintains its remaining properties. Different approaches have been used for this purpose. Some of them consist on the modification of the chemical environment of the metal center, that is introducing modifications on the organic ligand (subtle modifications maintaining the main moiety),[11–13] changing the counterion (some examples have been reported on how the packing of different counterions affects the transition) ,[14,15] modifying the coordination sphere of the SCO metal center (the loss of coordinated solvent may modify the spin transition temperature),[16,17] or the inclusion/desolvation of solvent molecules in the crystal packing of the framework (similar to what is observed with counterions).[18–30] Another different approach involves the inclusion of different metallic centers, the so-called metal dilution. This approach consists on the gradual inclusion of non-SCO behavior metal centers on the lattice,[31–45] resulting on a decrease of the magnetic metal cooperativity, thus provoking a more gradual spin transition curve.

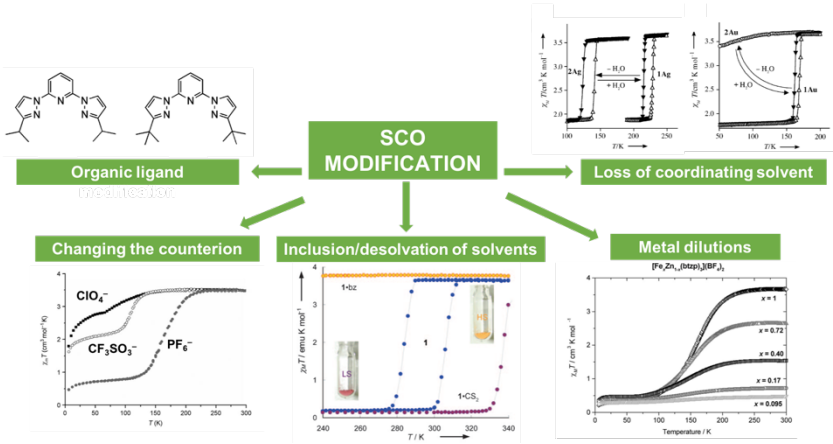

Figure 3.1. Different strategies for SCO modification.

The last approach uses mixtures of two (or more) organic ligands,[46,47] which are similar from the chemical point of view (size, coordination ability, functional groups) but that give rise to different ligand-strengths. This can subtle modify the magnetic behavior of the system designed only with one of these ligands. Very recently this approach have been used in the MOF field to synthesize multivariant MOFs whose pores are decorated by heterogeneous mixtures of functionalities.[48] However, the use of ligand mixtures is a challenge because of physical mixtures can be formed, instead of forming a single material combining the different ligands.

In this *chapter*, the problem described before has been successfully avoided, studying the effect of gradual ligand substitution in an Fe^{II} SCO coordination polymer. For that purpose, we have used two different types of azole ligands, only differing on a nitrogen atom in the five-membered ring. These azole derivatives are well-known in the design of Fe^{II} SCO coordination polymers[49]

due to their proper ligand field strength for obtaining the spin transition. Both ligands are represented in the figure 3.2.

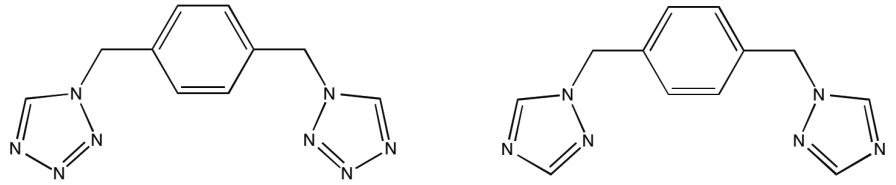

bis(tetrazol-yl)-p-xylene (btzx)

bis(triazol-yl)-p-xylene (btix)

Figure 3.2. Chemical structures of btzx and btix ligands.

The reaction of each ligand with $Fe(ClO_4)_2 \cdot x\ H_2O$ separately afforded two structurally related compounds: **CCP-1**, $[Fe(btzx)_3](ClO_4)_2$[50] and **CCP-1b**, $[Fe(btix)_3](ClO_4)_2$.[51] **CCP-1** and its properties have been described in detail in *chapter 2* of this thesis and **CCP-1b** was reported previously.[51] Both compounds are similar in terms of structural parameters: they are formed by 1D linear chains that run parallel to the crystallographic *c*-axis. However, they are completely different from the magnetic point of view: whereas **CCP-1** presents SCO behavior with a sharp spin transition centered at 200 K, **CCP-1b** remains at high-spin state over all temperatures. In this chapter a family of isostructural coordination polymers is presented based on the partial ligand substitution using different ligand mixtures of btzx and btix and the magnetic behavior of the family has been analyzed on detail.

3.2 RESULTS AND DISCUSSION

3.2.1 Structural description

As stated above, the ligands btzx and btix yield two coordination polymers of formula $[Fe(btzx)_3](ClO_4)_2$ and $[Fe(btix)_3](ClO_4)_2$ respectively. Both structures are isoreticular and are formed by 1D linear chains that run parallel to the crystallographic *c*-axis, with three ligands serving as bridges between the Fe^{II} centers, as is shown in figure 3.3.

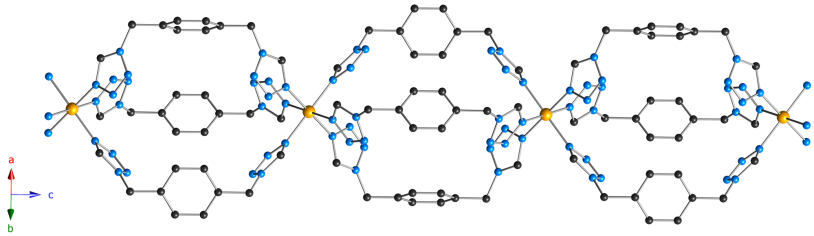

(a)

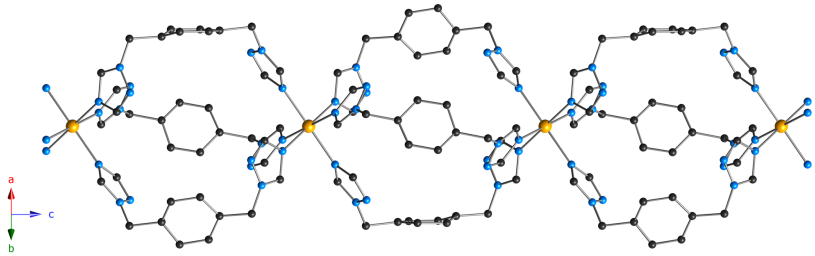

(b)

Figure 3.3. Crystal structures of compounds **CCP-1** (a) and **CCP-1b** (b). The ClO_4^- anions and hydrogen atoms have been removed for clarity. Key: Fe, orange; C, gray; N, blue.

The formation of **CCP-1** was reported by our group years ago, and was achieved by the reaction of $Fe(ClO_4)_2 \cdot x\ H_2O$ and btzx in refluxing acetonitrile, resulting in the formation of a white crystalline powder of

formula $[Fe(btzx)_3](ClO_4)_2$, **CCP-1**.[50] X-ray single crystal diffraction of one single crystal of **CCP-1** measured at 240 K reveals that it crystallizes in the $P6_3/m$ space group. Each Fe^{II} center lies on the 3-fold axis and is surrounded by six tetrazole rings coordinated through nitrogen atoms from six btzx ligands adopting a *syn-cis* conformation in an almost perfect octahedral environment. The different chains form a hexagonal packing, with the ClO_4^- counterions occupying the positions between chains (figure 3.4).

On the other hand, the reaction of $Fe(ClO_4)_2 \cdot x\ H_2O$ and btix in MeOH/water at room temperature results in the formation of crystalline powder of $[Fe(btix)_3](ClO_4)_2$, **CCP-1b**.[51] Similar to **CCP-1**, it is composed of $[Fe(btix)_3]^{2+}$ units that form linear chains that run parallel to the crystallographic *c*-axis, although **CCP-1b** crystallizes in a different space

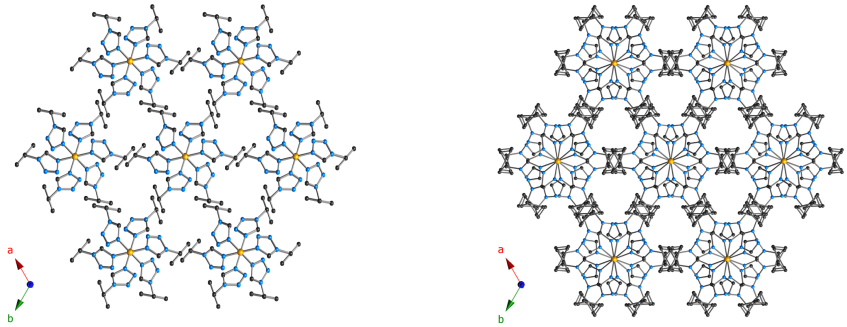

Figure 3.4. Hexagonal packing of **CCP-1** (left) and **CCP-1b** (right) viewed along the *c*-axis. Colour code as in figure 3.3. The ClO_4^- anions and hydrogen atoms have been removed for clarity.

group, $P\bar{3}c1$. Similar to **CCP-1**, each Fe^{II} center lies on the 3-fold axis and is surrounded by six triazole rings coordinated through nitrogen atoms from six different btix ligands in an almost perfect octahedral environment. In this

case, the different chains are packed forming a hexagonal array too, with the ClO_4^- counterions occupying the positions between chains and internal cavities of 145 $Å^3$.

The main difference observed between both structures is provoked by the conformation of the ligand: a *syn-cis* conformation for the btzx ligand and a *syn-trans* conformation for the btix one (figure 3.5). This is likely the cause for the reduction in symmetry from **CCP-1** to **CCP-1b**.

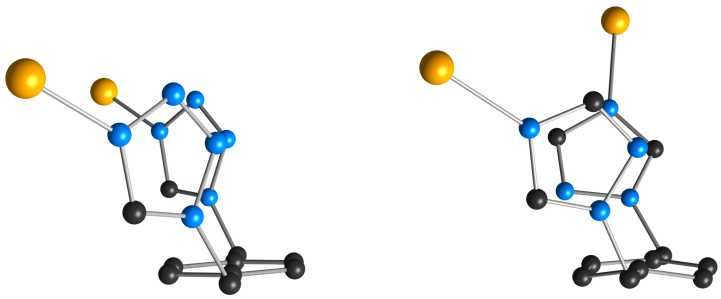

Figure 3.5. Representation of the *syn-cis* conformation of the btzx ligand (left) and *syn-trans* conformation of the btix ligand (right) adopted in compounds **CCP-1** and **CCP-1b**, respectively. Colour code as in figure 3.3.

Compound **CCP-1b** presents a twist in the ligand by its conformation, leading to the shortening in the intermetallic distances and changing the space group. That twist causes a slightly larger internal void too. This subtle difference leads to distinct Fe···Fe distances between the compounds due to the

alternation of the Fe centers: compound **CCP-1** presents Fe···Fe distances of 11.7881(12) Å at 240 K, meanwhile in compound **CCP-1b** we have significantly shorter Fe···Fe distances of 11.029(2) Å, remaining both compounds at high spin at this temperature (figure 3.6).

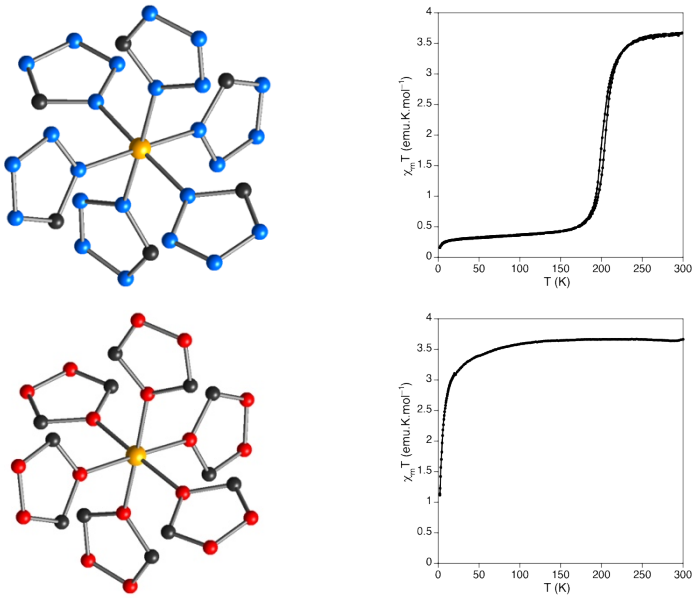

Figure 3.6. Top: octahedral environment of six tetrazole rings for the Fe (II) in **CCP-1** (left) and its magnetic behaviour (right). Bottom: octahedral environment of six triazole rings for the Fe (II) in **CCP-1b** (left) and its magnetic behaviour (right).

Given the similar chemical behaviour of both ligands, but their different physical properties, a detailed study has been done for synthesizing compounds with chemical ligand mixtures of both ligands. Different ratios of btzx:btix have been used resulting in the synthesis of seven mixed-ligand compounds. These compounds have been synthesized refluxing $Fe(ClO_4)_2 \cdot xH_2O$ and appropriate mixtures of the two ligands btzx and btix,

affording the different solid solutions as crystalline powders. For the nomenclature, **CCP-1(x)** has been used, being x the theoretical % of btzx ligand present in the structure, so **CCP-1(100)** corresponds to **CCP-1** and **CCP-1(0)** corresponds to **CCP-1b**. The different mixed-ligand compounds synthesized have the names **CCP-1(95)**, **CCP-1(90)**, **CCP-1(85)**, **CCP-1(80)**, **CCP-1(70)**, **CCP-1(60)** and **CCP-1(50)**. This new family of coordination polymers can be related to the general formula $[Fe(btzx)_{3x}(btix)_{3-3x}](ClO_4)_2$ with $0.95 \geq x \geq 0.5$.

3.2.2 Chemical *vs* physical mixture

For x = 0.95 to x = 0.80, only one crystalline phase is observed but interestingly, for x = 0.7 (*i.e.* compound **CCP-1(70)**), a decrease of the crystallinity of the material is observed, as perceived by the lower intensity of the diffraction peaks on the Pawley refinements (see figure 3.7), which is even more obvious for x = 0.6 (see figure 3.7). Besides, for x = 0.7 and x = 0.6 (*i.e.* samples **CCP-1(70)** and **CCP-1(60)**) some unreacted tetrazole is found in both crystalline solids. When the btix proportion is increased (x = 0.5), the crystallinity of the sample is recovered, although the system stops being a chemical mixture and becomes a mixed phase in which both the pure btix compound **CCP-1b** and the pure btzx compound **CCP-1** are present in the mixture. The amorphization of the sample observed for $0.7 \geq x \geq 0.5$ (samples **CCP-1(70)** – **CCP-1(50)**) is attributed to a competition between different conformations of the ligands. The gradual inclusion of btix in the chains provokes the insertion of a ligand which presents a twisted conformation, provoking a chemical pressure on the system. There comes a point where the system cannot resist the presence of too much btix ligands

combined with btzx ligands in the chains, resulting more stable the formation of both materials (**CCP-1** and **CCP-1b**) separately. Some examples of amorphous materials can be found on the literature based on the related ligand 1,4-bis(imidazol-1-ylmethyl)benzene.[52]

3.2.3 X-ray powder diffraction: Pawley refinements

Pawley refinements have been performed on X-ray diffraction patterns collected on crystalline samples for all the mixtures obtained, and their results are shown in figures 3.7 and 3.8. These can be divided in 3 categories: i) x = 0.95–0.8, ii) x = 0.7–0.6 and iii) x = 0.5–0.

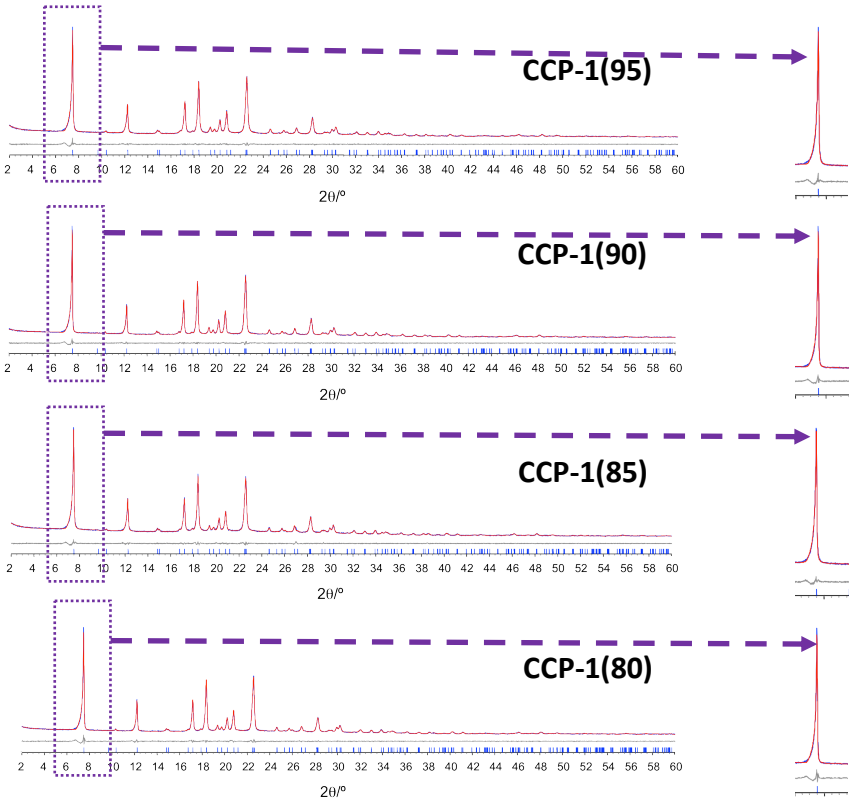

Figure 3.7. Observed (blue) and calculated (red) profiles and difference plot [(I_{obs} – I_{calcd})] (grey) of the Pawley refinements for compounds **CCP-1(95) - CCP-1(80)** and a zoom of the first peak (chemical mixtures, 2θ range 2.0–60.0 °; maximum resolution 1.54 Å).

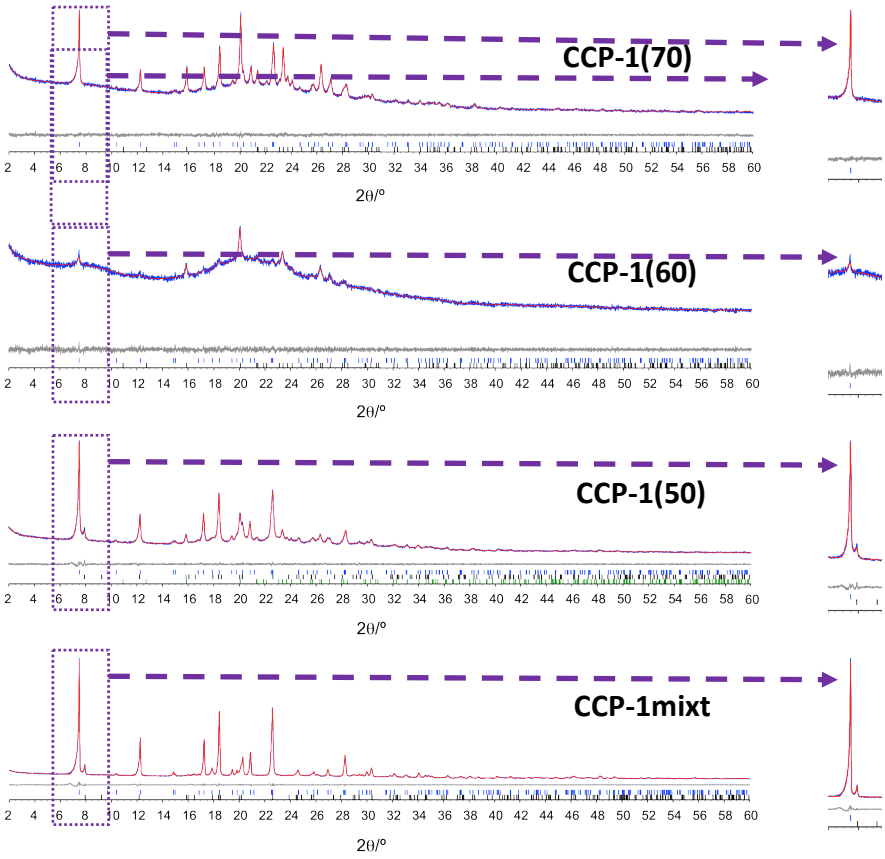

Figure 3.8. Observed (blue) and calculated (red) profiles and difference plot [(I_{obs} – I_{calcd})] (grey) of the Pawley refinements for compounds **CCP-1(70) - CCP-1(50)** and **CCP-1mixt** and a zoom of the first peak (2θ range 2.0–60.0 °; maximum resolution 1.54 Å) It can be clearly seen that **CCP-1(50)** has 2 peaks, each corresponding to a different phase.

For the chemical mixtures of compounds **CCP-1(95) - CCP-1(80)**, figure 3.7, only one phase can be observed from x = 0.95 to x = 0.8, confirming the presence of a mixed-ligand compound. For x = 0.7 and x = 0.6 (figure 3.8) only one phase of coordination polymer is observed too but some unreacted

tetrazole is presented in the sample. Indeed, a drastically decrease on the crystallinity of the samples is observed too, more evident for x = 0.6. As stated above, the sequential inclusion of the btix ligand inserts chemical pressure on the system, causing the decrease on the cristallinity and letting some tetrazole to stay unreacted for the instability of forming the mixed coordination polymer. When the limit of btix accepted is reached, x = 0.5, the mixed system cannot be formed and then a physical mixture of both pure-ligand separated compounds are formed, as can be observed in the figure 3.8, with the presence of the peaks corresponding to pure compound **CCP-1b**. The obtaining of chemical mixtures has been unequivocally confirmed preparing a mixed physical mixture of compounds **CCP-1** and **CCP-1b (CCP-1mixt)**, grinding them on a 80:20 proportion and observing a physical mixture of both compounds on figure 3.8.

A closer analysis of the crystallographic *c*-axis through the mixtures have been done performing the Pawley refinements on crystalline powder samples of each solid solution (figure 3.9), revealing a decrease of this axis (–5.7 % in the direction of the polymeric chain) upon increasing the amount of btix used, which can be ascribed to the insertion of btix ligands in the chains due to the different conformation of the triazole derivative ligand. The twisting on the btix ligand conformation causes this shortening. This decrease of the intrachain distance is also accompanied by an increase of the interchain distance (*a*-axis), which is of 5.5 %. Thus, for the chemical mixtures using small proportions of btix (x > 0.7), the insertion of btix in the chains occurs.

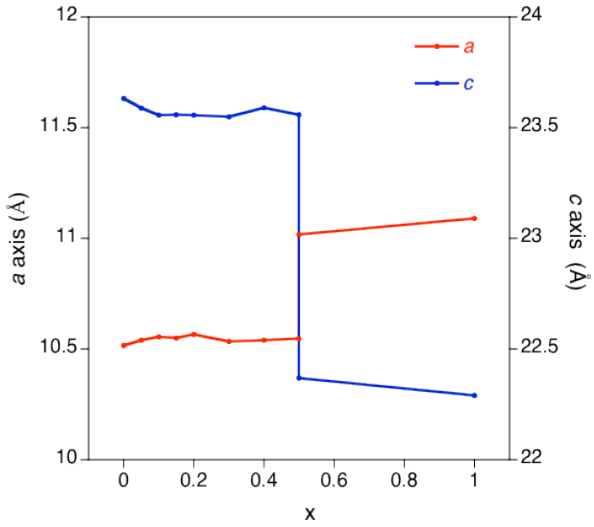

Figure 3.9. Variation of the *a* and *c* axes with x in compounds. The family of coordination polymers **CCP-1(95) - CCP-1(50)** respond to the general formula $[Fe(btzx)_{3x}(btix)_{3-3x}](ClO_4)_2$ with $0 \leq x \leq 1$.

3.2.4 Magnetic behaviour

As stated on the introduction of the chapter, both original compounds, **CCP-1** and **CCP-1b** are completely different from a magnetic point of view. **CCP-1** presents a spin transition with a spin transition temperature centered at 200 K but **CCP-1b** remains at high spin all over the temperatures.

It is well known that spin crossover is highly-sensitive to the coordination environment of the metal center and subtle changes can provoke a modification of the magnetism. The use of two different ligands in this work modifies the chemical environment of the Fe^{II} center. The spin transition centered at 200 K of compound **CCP-1** is originated by a coordination sphere

of six tetrazole ligands in an octahedral environment. This coordination environment will slowly be changed by the introduction of triazole ligands. With the combination of both ligands, starting with low quantities of btix, a gradual inclusion of btix in the polymeric chains occurs.

Two phenomena can be observed in the $\chi_M T$ plots with the gradual increase of the triazole ligand: on one hand, a subtle displacement of the 200 K transition to 190 K occurs and in the other hand, a new transition appears centered at 140 K with the subsequent decrease of the original one. The original octahedral environment of six tetrazole ligands of compound **CCP-1** is perturbed with the inclusion of the triazole ligand. When low quantities of btix ligands are used, some tetrazole moieties are substituted by the triazole ones. As discussed before, the triazole based ligand (btix) adopts a different conformation than the tetrazole one, with a twist that generates a tenser structure, shortening the chains. Thus, we hypothesize that the inclusion of

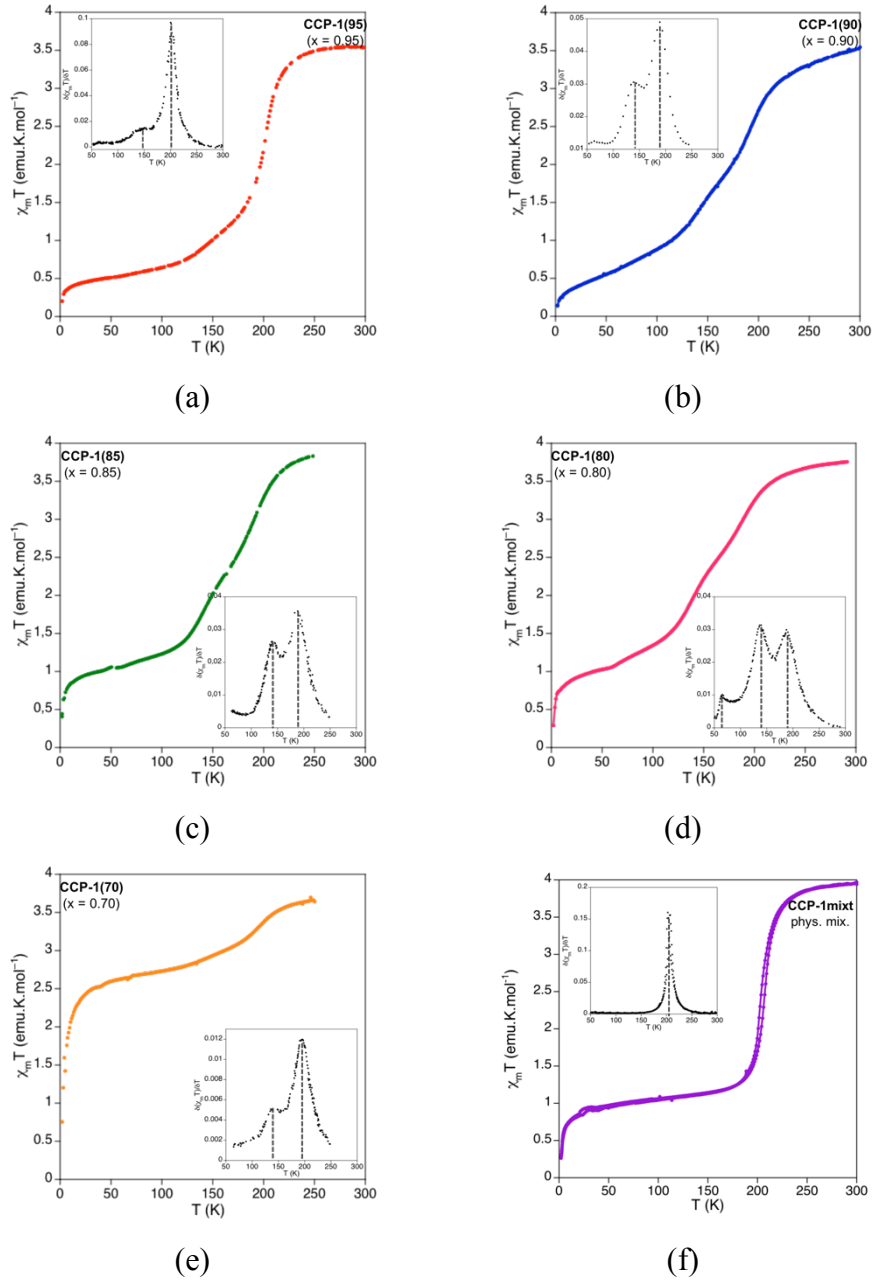

Figure 3.10. Temperature dependence of $\chi_M T$ for the solid solutions **CCP-1(95) - CCP-1(70)** (a–e) and **CCP-1mixt** (f).

some triazole-based ligands has two effects: change of crystal field environment and a chemical pressure. That appearance of some triazole ligands in the polymeric chains provoke an internal chemical pressure in the whole system, explaining the subtle displacement of the transition from 200 to 190 K. This reduction of the SCO $T_{1/2}$ is typically observed with the application of pressure.[53–57] Furthermore, that inclusion of the triazole ligand in the chains generates some new chemical environments. When a btix ligand substitutes one btzx ligand, a new coordination environment is generated, with the Fe^{II} center coordinated by five tetrazole and one triazole ring. That new environment, which possess a different ligand field, generates a new spin transition centered at 140 K as can be observed in the $\chi_M T$ plot (figure 3.10).

When the btix proportion is increased, more triazole ligands are inserted in the chains, so more coordination environments of five tetrazoles and one triazole ring are generated, resulting in the increase of the new spin transition centered at 140 K and the decrease of the original one. That effect can be observed in the insets of the $\chi_M T$ plots for x = 0.95, 0.90 and 0.85 (a, b and c of figure 3.10), that correspond to the derivative of that product. When the proportion of triazole used reaches x = 0.80, a new event can be observed in the magnetism. In addition to the previous observations, that is the displacement of the original transition to 190 K and the appearance of a new one at 140 K, an additional transition is observed at 60 K. Although this value is rather low for a spin-crossover, some examples of unusual low temperature spin transitions (< 80 K) have been found in the literature for monomeric complexes with 1-R-tetrazoles.[58–68] That new transition must be related to a new coordination environment of four tetrazole and two triazole rings.

For x = 0.70, some structural coherence is lost. It seems that the system is not progressing to a total substitution of the btzx ligands because the magnetic behaviour is similar to that for x = 0.90. Probably the pressure induced by the inclusion of btix ligands in the structure provokes a limit where no more btix is accepted, then breaking the structure and adopting a previous stage of only two different coordination environments and certain quantity of unreacted ligand in the mixture are present, demonstrated by the high residual spin fraction found in the sample. For the physical mixture, only the signal of the pure compound **CCP-1(100)** is observed, demonstrating that in the previous examples the chemical mixtures are formed generating the new transitions.

3.2.5 Structural discussion

The consecutive addition of triazole in the chains, until a btix proportion of 0.20 (x = 0.80), generates significant coordination environments with four tetrazoles and two triazoles, as can be observed in the magnetism. That possibility in which are present some bridges where two triazoles are added could be achieved in two different manners: two btix ligand located in the same bridge connecting two iron centers or two btix ligand located in consecutive bridges with an iron center situated between them. The first option possibly generates a tenser structure, due to the inclusion of two twisted btix ligands with a btzx ligand and might be the origin of the amorphization observed in the X-ray powder diffraction when the proportion of btix increase. As can be seen in the X-ray powder diffractogram for x = 0.70, some amorphization of the sample occurs and in the $\chi_M T$ plot, only an increase on the residual high spin fraction is observed, a clear signal that the

system reaches some limit of structural coherence where no more btix ligand can be included and then only the pure btix compound is formed.

Some ideal statistic distribution could be calculated. Our polymer could be defined as a system in which we have six different positions (corresponding to the ligands). The three possibilities observed experimentally in the magnetic behaviour are six tetrazoles, five tetrazoles and one triazole or four tetrazoles and two triazoles. The probability for obtaining each possibility depending on the proportion of ligands used at the beginning corresponds to the next formula:

$$prob\ (\%) = (\%\ \boldsymbol{btzx})^{n} \cdot\ (\%\ \boldsymbol{btix})^{6-n} \cdot \frac{6!}{(6-n)! \cdot n!}$$

Where "% btzx" and "% btix" are the percentage of ligands used in the synthesis and n is equal to the number of tetrazoles in each possibility. The results obtained can be seen in the table 3.1. For low proportions of btix used (x = 0.95, 0.90 and 0.85) the probability to observe the coordination environment of four tetrazoles and two triazoles, that is, the spin transition centered at 60 K, is low compared with the other two possibilities. That last transition is not so significative until x = 0.80, as observed in the $\chi_M T$ plot. It must be considered that these calculations are made as if all positions were equal, but as it can be observed in the X-ray powder diffractograms and applying a chemical sense, the inclusion of triazole ligands inserts a chemical pressure in the structure, resulting in the loss of crystallinity when the

proportion of btix further increase, with no observation of new coordination environments generated with for example three tetrazoles and three triazoles.

		% btzx : % btix				
Coordination environment	**n**	**95:5**	**90:10**	**85:15**	**80:20**	**70:30**
6 tetrazoles	6	73.5	53.1	37.7	26.2	11.8
5 tetrazoles + 1 triazole	5	23.2	35.4	39.9	39.3	30.3
4 tetrazoles + 2 triazoles	4	3.1	9.8	17.6	24.6	32.4

Table 3.1. Ideal statistical probability for the solid solutions.

A schematic representation of the evolution of the system through btix inclusion can be seen on figure 3.11. The use of only btzx affords the pure btzx spin-crossover compound (a), but upon inclusion of some btix on the synthesis, some btix ligands are included in the chains, creating a new coordination environment (b). Only a few positions with the use of small amounts of btix are substituted but upon further increase of the btix used in the synthesis, more coordination environments with five tetrazoles and one triazole are generated (c), in accordance with the magnetic data. A perfect inclusion of one triazole in all the bridges would produce a regular distribution of 1/6 of the positions of all the coordination polymer substituted by triazole ligands (d), but statistically this is not likely to happen and it is indeed not observed in the $\chi_M T$ plots.

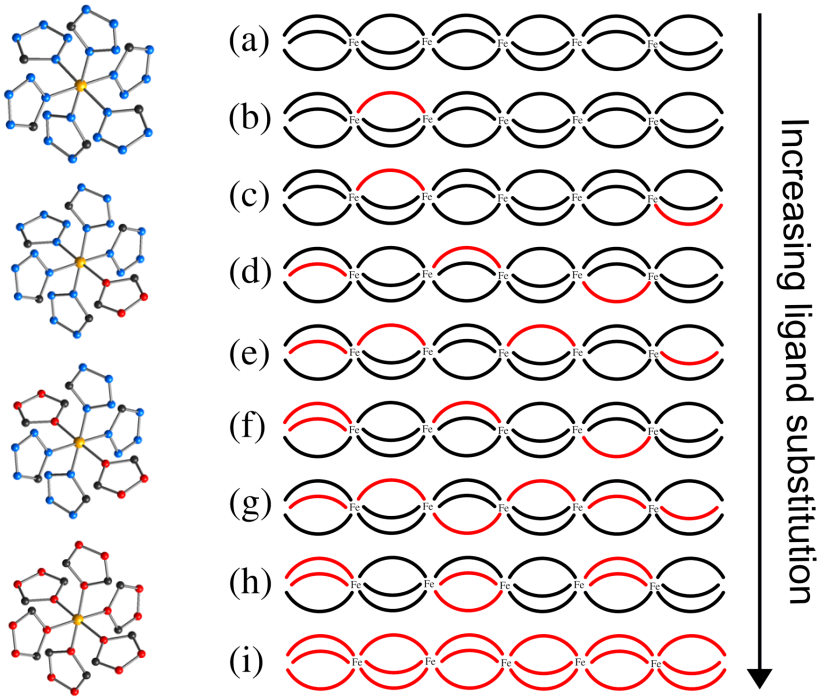

Figure 3.11. Schematic representation of the ligand substitution. Black lines represent btzx and red lines represent btix.

At some point, on consecutive bridges or even in the same bridge, two btix ligands could be inserted (chains e and f in figure 3.11), generating a new coordination environment of four tetrazole and two triazole rings. As stated before, these two possibilities can be present even at low proportions of btix used but are not representative over the total amount of centers. The inclusion of two triazoles in all positions would produce a regular distribution of 1/3 of the positions of all the coordination polymer substituted by triazole ligands (chains g and h in figure 3.11), but statistically this is not likely to happen and it is not observed in the $\chi_M T$ plots. Finally, no more inclusion of btix ligand

with new coordinations centers have been observed and only the pure btix coordination polymer is obtained (i).

3.3 CONCLUSIONS

In this *chapter*, a family of mixed-ligand Fe^{II} coordination polymers have been obtained. The use of two different but related ligands to obtain chemical mixtures has successfully modified the magnetic behaviour of the original system by two different manners: on one hand, the inclusion of twisted triazole ligands provokes some chemical pressure in the chains, shifting the original spin transition temperature from 200 to 190 K; on the other hand, the inclusion of triazoles generates new coordination environments with different ligand fields, creating new transitions at 140 K for an environment of five tetrazoles and one triazole and 60 K for an environment of four tetrazoles and two triazoles.

3.4 METHODS

3.4.1 Synthesis

All reagents and solvents were commercially available and used without further purification. The ligands 1,4-bis(tetrazol-1-ylmethyl)benzene (btzx) and 1,4-bis(triazol-1-ylmethyl)-benzene (btix) were prepared according to literature methods.[50,51]

Caution. Perchlorate salts are explosive (especially if they are dry) and should be handled in small quantities with caution.

Synthesis of $[Fe(btzx)_3](ClO_4)_2$ (CCP-1).[50] A solution of $Fe(ClO_4)_2 \cdot xH_2O$ (112 mg) in 5 mL of MeCN was added into a suspension of btzx (152 mg, 0.8 mmol) in 40 mL of MeCN containing ascorbic acid (*ca*. 10 mg). The resulting milky suspension was refluxed and stirred for 4 h under Ar atmosphere. A white crystalline precipitate appeared during the reaction. After cooling down to room temperature, the white powder was filtered and washed with MeCN. Phase purity was established by X-ray powder diffraction (*vide infra*). Yield = 52 %.

Synthesis of $[Fe(btix)_3](ClO_4)_2$ (CCP-1b).[22] A solution of $Fe(ClO_4)_2 \cdot xH_2O$ (63.7 mg) in 2.5 mL of EtOH was added slowly into an ethanolic solution of btix (120.0 mg, 0.5 mmol) without stirring. The mixture was left at RT for crystallization. After several days, colorless blocked-shaped crystals were filtered off and washed with EtOH. Phase purity was established by X-ray powder diffraction. Yield = 47 %.

Synthesis of $[Fe(btzx)_{3x}(btix)_{3-3x}](ClO_4)_2$ (x = 0.95 (**CCP-1(95)**); x = 0.90 (**CCP-1(90)**); x = 0.85 (**CCP-1(85)**); x = 0.80 (**CCP-1(80)**); x = 0.70 (**CCP-1(70)**); x = 0.60 (**CCP-1(60)**); x = 0.50 (**CCP-1(50)**). The chemical mixtures **CCP-1(95) - CCP-1(50)** were synthesized in a procedure analogous to that of **CCP-1** with the appropriate mixtures of the ligands 1,4-bis(tetrazol-1-ylmethyl)benzene (btzx) and 1,4-bis(triazol-1-ylmethyl)-benzene (btix). Phase purity was established by X-ray powder diffraction. The C/N ratio from elemental analyses was used to estimate the ligand composition of the final compounds, which were in good agreement with the starting values: x = 0.94 (**CCP-1(95)**); x = 0.96 (**CCP-1(90)**); x = 0.88 (**CCP-1(85)**); x = 0.78 (**CCP-1(80)**). Compound **CCP-1(70)** crystallizes with some unreacted tetrazole, as determined by powder diffraction, and thus its C/N ratio is unreliable. Typical

yields are about 50 % except for compounds **CCP-1(60)** and **CCP-1(50)**, which were obtained only as a few milligrams. Repetition of the synthesis in these two cases provided always the same results.

Synthesis of $[Fe(btzx)_3](ClO_4)_2$ and $[Fe(btix)_3](ClO_4)_2$ physical mixture (CCP-1mixt). A physical mixture was obtained by simply grinding **CCP-1** and **CCP-1b** in a ratio 80:20 (**CCP-1mixt**). Mixture of two phases was established by X-ray powder diffraction.

3.4.2 Structural characterization

3.4.2.1 X-ray powder diffraction measurements and Pawley refinements

Polycrystalline samples of **CCP-1, CCP-1b, CCP-1(95) - CCP-1(50)** and **CCP-1mixt** were lightly ground in an agate mortar and pestle and filled into 0.5 mm borosilicate capillaries prior to being mounted and aligned on an Empyrean PANalytical powder diffractometer, using Cu K_α radiation (λ = 1.54056 Å). For each sample, two repeated measurements were collected at room temperature (2θ = 2 – 60 º) and merged in a single diffractogram. Pawley refinements[69] were performed using the TOPAS computer program[70] and revealed an excellent fit to a one-phase model for compounds **CCP-1(95)** (R_{wp} = 0.0220; GOF = 1.301, figure 3.6), **CCP-1(90)** (R_{wp} = 0.0236; GOF = 1.283, figure 3.6), **CCP-1(85)** (R_{wp} = 0.0240; GOF = 1.274, figure 3.6), and **CCP-1(80)** (R_{wp} = 0.0229; GOF = 1.383, figure 3.6), indicating the absence of any other detectable crystalline phases. Unreacted btzx was also observed in the fit of compounds **CCP-1(70)** (R_{wp} = 0.0210; GOF = 1.080, figure 3.7), **CCP-1(60)** (R_{wp} = 0.0214; GOF = 1.096, figure 3.7) and **CCP-1(50)** (R_{wp} = 0.0224; GOF = 1.174, Figure 3.7). In the latter, compound **CCP-1b** was also

detected. Pawley refinement on the physical mixture **CCP-1mixt** revealed an excellent fit to a two-phase model of compounds **CCP-1** and **CCP-1b** (R_{wp} = 0.0225; GOF = 1.331, figure 3.7). Table 3.2 contains the refined structural parameters.

compound		x	ratio btzx:btix (3x : 3-3x)	a (Å)	c (Å)
CCP-1	100:0	1	3.00:0.00	10.51614	23.63192
CCP-1b	0:100	0	0.00:3.00	11.09054	22.29075
CCP-1(95)	95:5	0.95	2.85:0.15	10.5394(4)	23.589(2)
CCP-1(90)	90:10	0.90	2.70:0.30	10.5557(3)	23.557(2)
CCP-1(85)	85:15	0.85	2.55:0.45	10.5501(4)	23.559(2)
CCP-1(80)	80:20	0.80	2.40:0.60	10.5666(3)	23.557(2)
CCP-1(70)	70:30	0.70	2.10:0.90	10.5339(12)	23.549(9)
CCP-1(60)	60:40	0.60	1.80:1.20	10.54(3)	23.59(11)
CCP-1(50)	50:50	0.50	1.50:1.50	10.5473(10)	23.559(6)
				11.018(9)	22.369(12)
CCP-1mixt	80:20 (phys)	n.a.	n.a.	10.5183(2)	23.6197(10)
				11.0576(12)	22.308(3)

Table 3.2. Structural parameters of Pawley refinements.

3.4.3 Physical measurements

Thermogravimetric analysis of **CCP-1(95) - CCP-1(70)** and **CCP-1mixt** were carried out with a Mettler Toledo TGA/SDTA 851 apparatus in the 25–800 °C temperature range under a 10 °C·min^{-1} scan rate and an air flow of 30

$mL \cdot min^{-1}$. No solvent molecules are present in the voids. Due to the low amount of sample, TGA analysis on compounds **CCP-1(60)** and **CCP-1(50)** were not possible.

CCP-1(95)

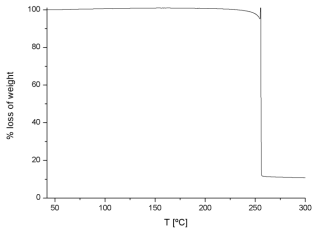

CCP-1(90)

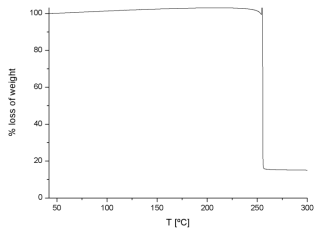

CCP-1(85)

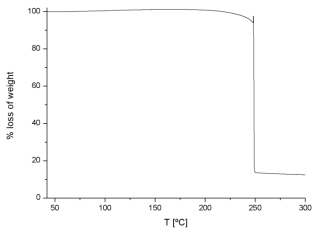

CCP-1(80)

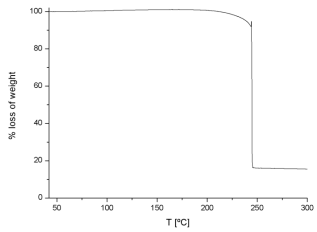

CCP-1(70)

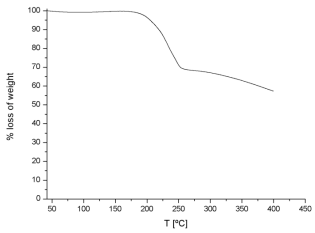

CCP-1mixt

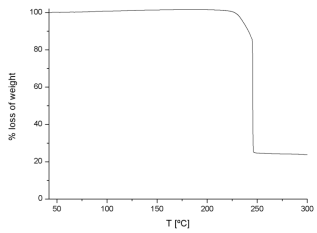

Figure 3.11. Thermogravimetric analysis (TGA) of compounds **CCP-1(95) - CCP-1(70)** and **CCP-1mixt**.

3.4.3.1 Magnetic measurements. Magnetic susceptibility measurements were performed with a Quantum Design SQUID magnetometer with an applied field of 1000 G. The susceptibility data were corrected from the diamagnetic contributions as deduced by using Pascal's constant tables.

3.5 REFERENCES

1. Gütlich, P. Spin crossover in iron(II)-complexes. in *Metal Complexes* (eds. Bau, R., Gütlich, P. & Teller, R. G.) 83–195 (Springer Berlin Heidelberg, 1981).
2. Beattie, J. K. Dynamics of Spin Equilibria in Metal Complexes. in *Advances in Inorganic Chemistry* **32**, 1–53 (Elsevier, 1988).
3. Khan, S. U. M. & Zhou, Z. Y. Force constant of transition metal ion–ligand bonds: molecular-orbital calculations. *J. Chem. Soc. Faraday Trans.* **87**, 535–538 (1991).
4. Gütlich, P., Hauser, A. & Spiering, H. Thermisch und optisch schaltbare Eisen(II)-Komplexe. *Angew. Chem.* **106**, 2109–2141 (1994).
5. Gütlich, P., Garcia, Y. & Goodwin, H. A. Spin crossover phenomena in Fe(II) complexes. *Chem. Soc. Rev.* **29**, 419–427 (2000).
6. Murray, K. S. & Kepert, C. J. Cooperativity in Spin Crossover Systems: Memory, Magnetism and Microporosity. in *Spin Crossover in Transition Metal Compounds I* (eds. Gütlich, P. & Goodwin, H. A.) **233**, 195–228 (Springer Berlin Heidelberg, 2004).
7. Real, J. A., Gaspar, A. B. & Muñoz, M. C. Thermal, pressure and light switchable spin-crossover materials. *Dalton Trans.* **0**, 2062–2079 (2005).

8. Gamez, P., Costa, J. S., Quesada, M. & Aromí, G. Iron Spin-Crossover compounds: from fundamental studies to practical applications. *Dalton Trans.* **0**, 7845–7853 (2009).
9. Bousseksou, A., Molnár, G., Salmon, L. & Nicolazzi, W. Molecular spin crossover phenomenon: recent achievements and prospects. *Chem. Soc. Rev.* **40**, 3313–3335 (2011).
10. Roubeau, O. Triazole-Based One-Dimensional Spin-Crossover Coordination Polymers. *Chem. – Eur. J.* **18**, 15230–15244 (2012).
11. Haasnoot, J. G. Mononuclear, oligonuclear and polynuclear metal coordination compounds with 1,2,4-triazole derivatives as ligands. *Coord. Chem. Rev.* **200–202**, 131–185 (2000).
12. Halcrow, M. A. The spin-states and spin-transitions of mononuclear iron(II) complexes of nitrogen-donor ligands. *Polyhedron* **26**, 3523–3576 (2007).
13. Halcrow, M. A. Iron(II) complexes of 2,6-di(pyrazol-1-yl)pyridines—A versatile system for spin-crossover research. *Coord. Chem. Rev.* **253**, 2493–2514 (2009).
14. Quesada, M. *et al.* Counterion Effect on the Spin-Transition Properties of the Cation $[Fe(btzx)_3]^{2+}$ (btzx= *m* -Xylylenebis(tetrazole)). *Chem. - Eur. J.* **14**, 8486–8499 (2008).

15. Jameson, G. N. L. *et al.* Anion, Solvent and Time Dependence of High-Spin–Low-Spin Interactions in a 3D Coordination Polymer. *Eur. J. Inorg. Chem.* **26**, 3948–3959 (2009).

16. Quesada, M. *et al.* A Molecule-Based Nanoporous Material Showing Tuneable Spin-Crossover Behavior near Room Temperature. *Adv. Mater.* **19**, 1397–1402 (2007).

17. Niel, V. *et al.* Crystalline-State Reaction with Allosteric Effect in Spin-Crossover, Interpenetrated Networks with Magnetic and Optical Bistability. *Angew. Chem. Int. Ed.* **42**, 3760–3763 (2003).

18. Halder, G. J., Kepert, C. J., Moubaraki, B., Murray, K. S. & Cashion, J. D. Guest-Dependent Spin Crossover in a Nanoporous Molecular Framework Material. *Science* **298**, 1762–1765 (2002).

19. Neville, S. M., Moubaraki, B., Murray, K. S. & Kepert, C. J. A Thermal Spin Transition in a Nanoporous Iron(II) Coordination Framework Material. *Angew. Chem. Int. Ed.* **46**, 2059–2062 (2007).

20. Neville, S. M. *et al.* Single-Crystal to Single-Crystal Structural Transformation and Photomagnetic Properties of a Porous Iron(II) Spin-Crossover Framework. *J. Am. Chem. Soc.* **130**, 2869–2876 (2008).

21. Halder, G. J. *et al.* Elucidating the Mechanism of a Two-Step Spin Transition in a Nanoporous Metal−Organic Framework. *J. Am. Chem. Soc.* **130**, 17552–17562 (2008).

22. Coronado, E., Giménez-López, M. C., Giménez-Saiz, C. & Romero, F. M. Spin crossover complexes as building units of hydrogen-bonded nanoporous structures. *CrystEngComm* **11**, 2198–2203 (2009).

23. Neville, S. M. *et al.* Guest Tunable Structure and Spin Crossover Properties in a Nanoporous Coordination Framework Material. *J. Am. Chem. Soc.* **131**, 12106–12108 (2009).

24. Southon, P. D. *et al.* Dynamic Interplay between Spin-Crossover and Host−Guest Function in a Nanoporous Metal−Organic Framework Material. *J. Am. Chem. Soc.* **131**, 10998–11009 (2009).

25. Ohba, M. *et al.* Bidirectional Chemo-Switching of Spin State in a Microporous Framework. *Angew. Chem. Int. Ed.* **48**, 4767–4771 (2009).

26. Clemente-León, M. *et al.* Multifunctional Magnetic Materials Obtained by Insertion of a Spin-Crossover FeIII Complex into Bimetallic Oxalate-Based Ferromagnets. *Chem. – Eur. J.* **16**, 2207–2219 (2010).

27. Muñoz-Lara, F. J. *et al.* Fast Detection of Water and Organic Molecules by a Change of Color in an Iron(II) Microporous Spin-Crossover Coordination Polymer. *Inorg. Chem.* **51**, 13078–13080 (2012).

28. Craig, G. A., Costa, J. S., Roubeau, O., Teat, S. J. & Aromí, G. Local Coordination Geometry and Spin State in Novel FeII Complexes with 2,6-Bis(pyrazol-3-yl)pyridine-Type Ligands as Controlled by Packing Forces: Structural Correlations. *Chem. – Eur. J.* **18**, 11703–11715 (2012).

29. Clemente-León, M. *et al.* Stimuli Responsive Hybrid Magnets: Tuning the Photoinduced Spin-Crossover in Fe(III) Complexes Inserted into Layered Magnets. *J. Am. Chem. Soc.* **135**, 8655–8667 (2013).

30. Costa, J. S. *et al.* Three-Way Crystal-to-Crystal Reversible Transformation and Controlled Spin Switching by a Nonporous Molecular Material. *J. Am. Chem. Soc.* **136**, 3869–3874 (2014).

31. Sorai, M., Ensling, J. & Gütlich, P. Mössbauer effect study on low-spin $^1A_1 \rightleftharpoons$ high-spin $^5T_2$ transition in tris(2-picolylamine) iron chloride I. Dilution effect in $[Fe_xZn_{1-x}(2\text{-pic})_3]Cl_2 \cdot C_2H_5OH$. *Chem. Phys.* **18**, 199–209 (1976).

32. Jakobi, R., Spiering, H., Wiehl, L., Gmelin, E. & Guetlich, P. Thermoanalytic investigations on mixed crystals of the spin-crossover

system $[Fe_xZn_{1-x}(2\text{-pic-}ND_2)_3]Cl_2.EtOD$. *Inorg. Chem.* **27**, 1823–1827 (1988).

33. Renz, F. *et al.* Strong Field Iron(II) Complex Converted by Light into a Long-Lived High-Spin State. *Angew. Chem. Int. Ed.* **39**, 3699–3700 (2000).
34. Baldé, C., Desplanches, C., Gütlich, P., Freysz, E. & Létard, J. F. Effect of the metal dilution on the thermal and light-induced spin transition in $[Fe_xMn_{1-x}(bpp)_2](NCSe)_2$: When T(LIESST) reaches $T_{1/2}$. *Inorganica Chim. Acta* **361**, 3529–3533 (2008).
35. Baldé, C. *et al.* Effect of metal dilution on the light-induced spin transition in $[Fe_xZn_{1-x}(phen)_2(NCS)_2]$ (phen = 1,10-phenanthroline). *Dalton Trans.* **0**, 2702–2707 (2008).
36. Zheng, S., Siegler, M. A., Costa, J. S., Fu, W.-T. & Bonnet, S. Effect of Metal Dilution on the Thermal Spin Transition of $[FexZn_{1-x}(bapbpy)(NCS)_2]$. *Eur. J. Inorg. Chem.* **5–6**, 1033–1042 (2013).
37. Ganguli, P., Guetlich, P. & Mueller, E. W. Effect of metal dilution on the spin-crossover behavior in $[Fe_xM_{1-x}(phen)2(NCS)_2]$ (M = Mn, Co, Ni, Zn). *Inorg. Chem.* **21**, 3429–3433 (1982).
38. Lavrenova, L. G., Ikorskii, V. N., Varnek, V. A., Oglezneva, I. M. & Larionov, S. V. Influence of magnetic dilution on the spin transition in

the complex of iron(II) nitrate with 4-amino-1,2,4-triazole. *J. Struct. Chem.* **34**, 960–965 (1993).

39. Martin, J.-P., Zarembowitch, J., Dworkin, A., Haasnoot, J. G. & Codjovi, E. Solid-State Effects in Spin Transitions: Influence of Iron(II) Dilution on the Magnetic and Calorimetric Properties of the Series $[Fe_xNi_{1-x}$(4,4'-bis(1,2,4-triazole))$_2(NCS)_2]$.cntdot.H_2O. *Inorg. Chem.* **33**, 2617–2623 (1994).
40. Martin, J.-P. *et al.* Solid State Effects on Spin Transitions: Magnetic, Calorimetric, and Mössbauer-Effect Properties of $[Fe_xCo_{1-x}$(4,4'-bis-1,2,4-triazole)$_2(NCS)_2]$.cntdot.H_2O Mixed-Crystal Compounds. *Inorg. Chem.* **33**, 6325–6333 (1994).
41. Varnek, V. A., Lavrenova, L. G. & Gromilov, S. A. Mössbauer study of the effect of iron substitution by nickel on the $^1A_1 – {}^5T_2$ spin transition in Fe(4-amino-1,2,4-triazole)$_3(NO_3)_2$. *J. Struct. Chem.* **38**, 585–592 (1997).
42. Tayagaki, T. *et al.* Metal Dilution Effects on the Spin-Crossover Properties of the Three-Dimensional Coordination Polymer Fe(pyrazine)$[Pt(CN)_4]$. *J. Phys. Chem. B* **109**, 14859–14867 (2005).
43. Baldé, C. *et al.* Influence of Metal Dilution on the Light-Induced Spin Transition in Two 1D Chain Compounds: $[Fe_xZn_{1-x}(btzp)_3](BF_4)_2$ and

$[Fe_xZn_{1-x}(endi)_3](BF_4)_2$ btzp = 1,2-Bis(tetrazol-1-yl)propane and endi = 1,2-Bis(tetrazol-1-yl)ethane. *Eur. J. Inorg. Chem.* **34**, 5382–5389 (2008).

44. Krivokapic, I., Chakraborty, P., Enachescu, C., Bronisz, R. & Hauser, A. Low-Spin→High-Spin Relaxation Dynamics in the Highly Diluted Spin-Crossover System $[Fe_xZn_{1-x}(bbtr)_3](ClO_4)_2$. *Inorg. Chem.* **50**, 1856–1861 (2011).
45. Chakraborty, P., Enachescu, C., Walder, C., Bronisz, R. & Hauser, A. Thermal and Light-Induced Spin Switching Dynamics in the 2D Coordination Network of $\{[Zn_{1-x}Fe_x(bbtr)_3](ClO_4)_2\}_\infty$: The Role of Cooperative Effects. *Inorg. Chem.* **51**, 9714–9722 (2012).
46. Krober, J., Codjovi, E., Kahn, O., Groliere, F. & Jay, C. A spin transition system with a thermal hysteresis at room temperature. *J. Am. Chem. Soc.* **115**, 9810–9811 (1993).
47. Kahn, O., Sommier, L. & Codjovi, E. Spin Transition Molecular Alloys: An Attempt of Fine Tuning of the Transition Temperatures. *Chem. Mater.* **9**, 3199–3205 (1997).
48. Deng, H. *et al.* Multiple Functional Groups of Varying Ratios in Metal-Organic Frameworks. *Science* **327**, 846–850 (2010).

49. Aromí, G., Barrios, L. A., Roubeau, O. & Gamez, P. Triazoles and tetrazoles: Prime ligands to generate remarkable coordination materials. *Coord. Chem. Rev.* **255**, 485–546 (2011).

50. Coronado, E., Giménez-Marqués, M., Mínguez Espallargas, G., Rey, F. & Vitórica-Yrezábal, I. J. Spin-Crossover Modification through Selective CO_2 Sorption. *J. Am. Chem. Soc.* **135**, 15986–15989 (2013).

51. Chen, Y. *et al.* Assembly of two ferrous coordination polymers with triazole derivative: Syntheses, structures and magnetic properties. *Inorg. Chem. Commun.* **13**, 699–702 (2010).

52. Imaz, I., Hernando, J., Ruiz-Molina, D. & Maspoch, D. Metal–Organic Spheres as Functional Systems for Guest Encapsulation. *Angew. Chem. Int. Ed.* **48**, 2325–2329 (2009).

53. Gütlich, P., Ksenofontov, V. & Gaspar, A. Pressure effect studies on spin crossover systems. *Coord. Chem. Rev.* **249**, 1811–1829 (2005).

54. Pinkowicz, D. *et al.* Enforcing Multifunctionality: A Pressure-Induced Spin-Crossover Photomagnet. *J. Am. Chem. Soc.* **137**, 8795–8802 (2015).

55. Paradis, N. *et al.* Effects of Internal and External Pressure on the [Fe(PM-PEA)$_2$(NCS)$_2$] Spin-Crossover Compound (with PM-PEA = N-(2′-

pyridylmethylene)-4-(phenylethynyl)aniline). *Magnetochemistry* **2**, 15 (2016).

56. Li, J., Chen, S., Jiang, L., Li, Y. & Li, B. External Pressure Effect on a Twofold Interpenetrated 3D *PtS* -Type Spin-Crossover Coordination Polymer. *Cryst. Growth Des.* **18**, 1931–1934 (2018).
57. Tailleur, E. *et al.* Pressure-Induced Spin-Crossover Features at Variable Temperature Revealed by In Situ Synchrotron Powder X-ray Diffraction. *Chem. - Eur. J.* **24**, 14495–14499 (2018).
58. Franke, P. L., Haasnoot, J. G. & Zuur, A. P. Tetrazoles as Ligands. Part IV. Iron(II) Complexes of Monofunctional Tetrazole Ligands, Showing High-Spin * Low-Spin Transitions. *Inorganica Chim. Acta* **59**, 5–9 (1982).
59. Mueller, E. W., Ensling, J., Spiering, H. & Guetlich, P. High-spin to low-spin transition in hexacoordinate complexes of iron(II) with monodentate 1-alkyltetrazole ligands: a variable-temperature Mössbauer, magnetic susceptibility, and far-infrared study. *Inorg. Chem.* **22**, 2074–2078 (1983).
60. Poganiuch, P. & Gütlich, P. Light-induced formation of metastable high-spin states in $[Fe(mtz)_6](ClO_4)_2$. *Hyperfine Interact.* **40**, 331–334 (1988).

61. Wiehl, L. Structures of hexakis(1-propyltetrazole)iron(II) bis(tetrafluoroborate), $[Fe(CHN_4C_3H_7)_6](BF_4)_2$, hexakis(1-methyltetrazole)iron(II) bis(tetrafluoroborate), $[Fe(CHN_4CH_3)_6](BF_4)_2$, and the analogous perchlorates. Their relation to spin crossover behaviour and comparison of Debye–Waller factors from structure determination and Mössbauer spectroscopy. *Acta Crystallogr. B* **49**, 289–303 (1993).

62. Hinek, R., Gutlich, P. & Hauser, A. Cooperative effects in the $[Fe(mtz)_6](BF_4)_2$ spin-crossover system: fine tuning the energy gap. *Inorg. Chem.* **33**, 567–572 (1994).

63. Jeftić, J., Hinek, R., Capelli, S. C. & Hauser, A. Cooperativity in the Iron(II) Spin-Crossover Compound $[Fe(ptz)_6](PF_6)_2$ under the Influence of External Pressure (ptz = 1-n-Propyltetrazole). *Inorg. Chem.* **36**, 3080–3087 (1997).

64. Vértes, A. *et al.* Effect of spin-crossover on the parameters of the lifetime spectra of positrons and positronium in crystalline materials. *J. Phys. Chem. Solids* **59**, 1235–1239 (1998).

65. Kusz, J., Spiering, H. & Gütlich, P. X-ray structure study of the light-induced metastable states of the spin-crossover compound $[Fe(mtz)_6](BF_4)_2$. *J. Appl. Crystallogr.* **34**, 229–238 (2001).

66. Roubeau, O. *et al.* Surprising features in old and new [Fe(alkyl-tetrazole)$_6$] spin-crossover systems. *Polyhedron* **20**, 1709–1716 (2001).

67. Marek, T. *et al.* Extended NMR Study of Spin-Crossover Compounds [Fe(1-alkyl-1*H* tetrazole)$_6$](BF$_4$)$_2$ and Their Zn^{II} Analogs. *Struct. Chem.* **14**, 349–368 (2003).

68. Weinberger, P. & Grunert, M. Variable temperature far and mid FT-IR as a valuable tool to determine the spin transition temperature of iron(II) spin-crossover coordination compounds. *Vib. Spectrosc.* **34**, 175–186 (2004).

69. Pawley, G. S. Unit-cell refinement from powder diffraction scans. *J. Appl. Crystallogr.* **14**, 357–361 (1981).

70. Coelho, A. A. TOPAS-Academic, Version 4.1, 2007, see http://www.topas-academic.net.

Chapter 4:
Chemical design of the ligand to enhance gas sorption capability

4.1 INTRODUCTION

As stated in previous *chapters* of this thesis, one of the most studied types of coordination polymers are those which can locate molecules inside their structures, presenting channels and large voids, the so-called MOFs. This type of materials presents wide advantages in the field of sensors,[1] magnetism,[2] separation[3] and storage of gases,[4] among others, due to the combination of porosity with another physical property. *Chapters* 2 and 3 of this thesis have presented the concept of compartmentalized coordination polymers (CCPs). This type of coordination polymers possesses internal isolated cavities, presenting latent porosity to the adsorption of gases despite the absence of permanent channels. Two compartmentalized coordination polymers composed of iron (II) centers have been previously reported, namely **CCP-1** and **CCP-2** (see *chapter* 2). These interesting materials present spin-crossover (hereafter SCO) behaviour, which can be easily tuned in different ways. For example, as stated in *chapter* 2 of this thesis, these materials can adsorb different gas molecules in their internal cavities, provoking changes in the magnetic response of the materials depending on the gas located inside. In this *chapter* we present the chemical design to extend the original bis-tetrazole ligand, btzx, adding an additional benzene ring, thus extending the total length to obtain the new 4,4′-bis((1*H*-tetrazol-1-yl)methyl)-1,1′-biphenyl ligand (btzbp). Our aim is to increase the sorption capacity of these CCPs, which is limited to one molecule per void. Figure 4.1 shows the comparison in length between btzx and btzbp.

This ligand has been used to prepare two isostructural CCPs, analogous to **CCP-1** and **CCP-2**, which have been denoted **CCP-3** and **CCP-4**, affording a larger capacity for gas sorption while maintaining the SCO properties. In addition, the surface deposition of this crystalline solids has been developed in order to implement these materials in gas separation.

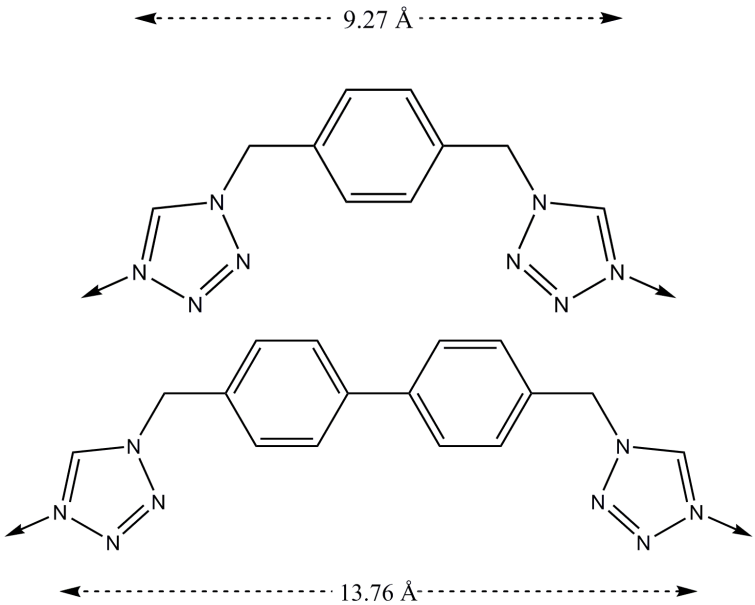

Figure 4.1. Chemical structures and lengths of btzx (top) and btzbp (bottom) ligands.

4.2 RESULTS AND DISCUSSION

4.2.1 Structural description

$Fe(btzbp)_3](ClO_4)_2$ (CCP-3) and $[Fe(btzbp)_3](BF_4)_2$ (CCP-4). The controlled reaction of 4,4′-bis((1*H*-tetrazol-1-yl)methyl)-1,1′-biphenyl (btzbp) and $Fe(ClO_4)_2 \cdot x\ H_2O$ (for **CCP-3**) or $Fe(BF_4)_2 \cdot 6\ H_2O$ (for **CCP-4**) afford white crystalline solids after several hours. Single-crystals have been obtained exclusively for **CCP-4,** but the isostructural nature of both compounds is demonstrated by X-ray powder diffraction, thus allowing to indirectly characterize the structure of **CCP-3**. The crystal structure of **CCP-4** was determined in both spin states (LS and HS) using the same crystal at 120 and 240 K respectively. In both states, **CCP-4** crystallizes in the space group $P6_3$, and is composed of $[Fe(btzbp)_3]^{2+}$ units that form one-dimensional chains that run parallel to the crystallographic *c*-axis with Fe···Fe distances of 16.145 Å at 240 K and 15.952 Å at 120 K (figure 4.2). This system is isoreticular to **CCP-1** and **CCP-2**, as shown in *chapter* 2.

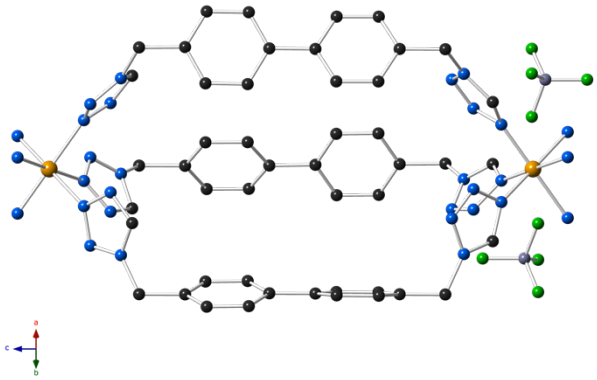

Figure 4.2. Crystal structure of **CCP-4**. The hydrogen atoms have been removed for clarity. Key: Fe, orange; C, black; N, blue; B, gray; F, green.

Each iron (II) center lies on the 3-fold axis and is surrounded by six crystallographically related tetrazole rings coordinated through nitrogen atoms from six btzbp ligands in an almost perfect octahedral environment. At 120 K, the Fe–N distances are 2.01(3) Å, while these are 2.16(3) Å at 240 K, which are in the expected range for Fe–N distances at LS and HS respectively in Fe-tetrazole systems.[5] This change in distance corresponds to a 7 % decrease of the bond length upon the transition in the spin of the iron (II) (lower Fe–N distances at LS), which is also accompanied by a colour change of the crystal from colourless (240 K) to pink (120 K). The ligands btzbp arrange in a *syn* conformation, triply bridging the iron (II) centers and the two phenyl rings in the ligands are not coplanar (30.69 º of torsion angle), causing a reduction in symmetry from $P6_3/m$ to $P6_3$ when compared with **CCP-1** and **CCP-2** that contain the shorter btzx ligand. These chains present internal cavities with no permanent porosity with void volumes of 257 $Å^3$ at 240 K and 235 $Å^3$ at 120 K (figure 4.3), which are practically double in size to those

found in **CCP-1** and **CCP-2** (135 $Å^3$ at 240 K and 117 $Å^3$ at 120 K). The BF_4^- counterions are located separating the different chains, which are closely packed affording a hexagonal arrangement (figure 4.4). Selected bond lengths and angles are shown in table 4.1.

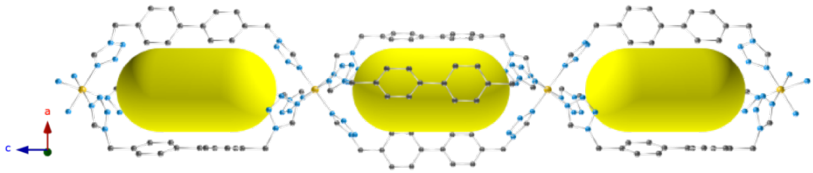

Figure 4.3. Crystal structure of **CCP-4** viewed along the *b*-axis. The BF_4^- anions and hydrogen atoms have been removed for clarity. Key: same as figure 4.2. The yellow ellipsoids are placed in the structure to represent the empty space of the internal voids.

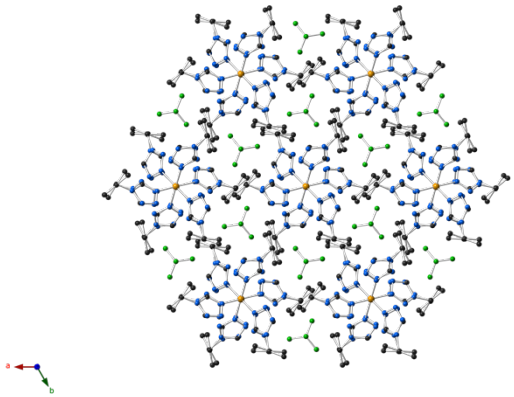

Figure 4.4. Hexagonal packing of **CCP-4** viewed along the *c*-axis. The hydrogen atoms have been removed for clarity. Key: same as figure 4.2.

	CCP-4-HS (240 K)	**CCP-4-LS** (120 K)
Fe–N	2.16(3)	2.01(3)
N–Fe–N	86.54	88.02
	90.50	89.23
	91.30	91.27
	91.75	91.49
	176.54	179.14

Table 4.1. Selected bond lengths (Å) and angles (°) for **CCP-4** in the HS (240 K) and LS (120 K).

4.2.2 X-ray powder diffraction: Pawley refinements

XRPD analysis have served to establish the phase purity of polycrystalline samples of **CCP-3** and **CCP-4**. Pawley refinements[6] have been applied to experimental powder patterns of both compounds. As expected, both materials present an isostructural nature, as can be seen on the powder diffractograms. The only remark is that **CCP-4** is more crystalline with more defined peaks. That may explain why only single-crystals of **CCP-4** have been obtained. The observed and calculated diffraction patterns for the refined crystal structures are shown in figure 4.5. Pawley refinement converged to R_{wp} = 0.0218 and GOF = 1.502 for **CCP-3** and R_{wp} = 0.0239 and GOF = 1.225 for **CCP-4**, indicating the absence of any other detectable crystalline phases.

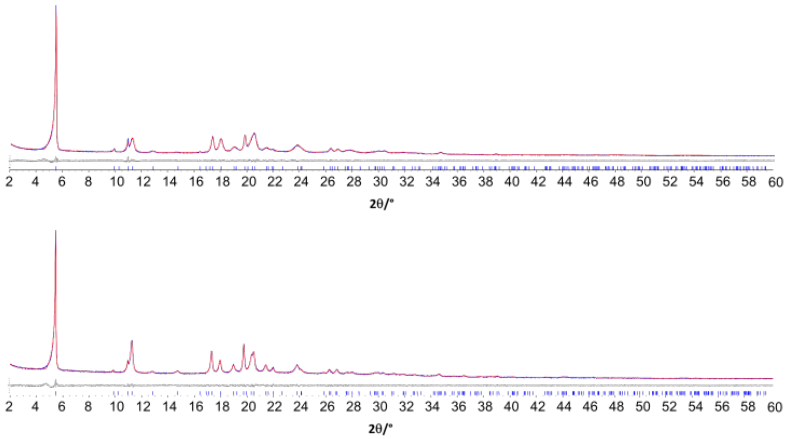

Figure 4.5. Observed (blue) and calculated (red) profiles and difference plot [(I_{obs} – I_{calcd})] (grey) of the Pawley refinements for compounds **CCP-3** (top) and **CCP-4** (bottom) (2θ range 2.0–60 °; maximum resolution 1.54 Å).

4.2.3 Gas sorption studies

As stated in *chapter* 2, compartmentalized coordination polymers present internal but non-connected cavities with potential for gas sorption. In that *chapter* it was demonstrated that compounds **CCP-1** and **CCP-2** can load gas molecules inside their internal voids. The two polymers studied in the present *chapter*, **CCP-3** and **CCP-4,** are isostructural to the previous materials shown, albeit with internal voids that are double in size. Due to the fact that the only structure analyzed is for **CCP-4**, only its gas sorption capacity has been studied, assuming a very similar behaviour for **CCP-3** in analogy to that observed for **CCP-1** and **CCP-2**. Gas sorption studies have been performed in collaboration with the group of Prof. F. Rey from the Instituto de

Tecnología Química of Valencia. The sorption capacity of **CCP-4** is analyzed towards CO_2, N_2 and CH_4.

Gas sorption isotherms are performed at different temperatures, that is 283, 298, 313 and 333 K for CO_2 and N_2; 283, 298 and 313 K for CH_4 as shown in figure 4.6. As can be seen, similar to what was observed for **CCP-1** and **CCP-2**, some diffusion problems occur for N_2 and CH_4 sorption, not observing the normal behaviour of decreasing sorption capacity when the temperature raises. This is not unexpected given the non-porous nature of this solid.

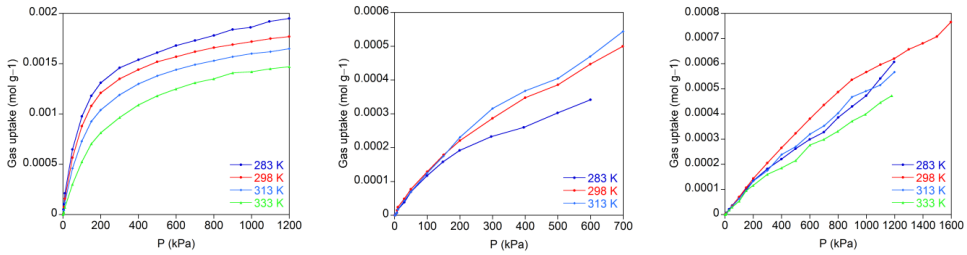

Figure 4.6. Adsorption isotherms for **CCP-4** collected at different temperatures for CO_2 (left), CH_4 (mid) and N_2 (right).

Virial equation has been used for fitting the experimental data points and they can be properly fitted to a fourth-grade polynomial.

$$\ln\left(\frac{P}{Q}\right) = A_0 + A_1 \cdot Q + A_2 \cdot Q^2 + A_3 \cdot Q^3 + A_4 \cdot Q^4$$

Equation 4.1. Virial equation used during the data analysis of the gas sorption isotherms.

The isosteric enthalpy of adsorption at zero surface coverage of CO_2 in **CCP-4** has been studied. It was calculated from the isotherms taken at different temperatures applying the Clausius-Clapeyron equation:

$$q_{st} = -R \cdot \left[\frac{\partial(\ln P)}{\partial(1/T)} \right]_{Q=cte}$$

Equation 4.2. Clausius-Clapeyron equation used to calculate the heats of adsorption for CO_2.

As can be observed in figure 4.7, a value of Q_{st} (CO_2) = 16 kJ·mol^{-1} has been found, a value lower compared with the observed for **CCP-1** and **CCP-2 (**20 kJ·mol^{-1}). Similar to the previous reported systems, this value is small if compared to typical values found on other archetypal materials used for gas storage like functionalized MOFs with alkylamines, which present enthalpies of adsorption near 100 kJ·mol^{-1}.

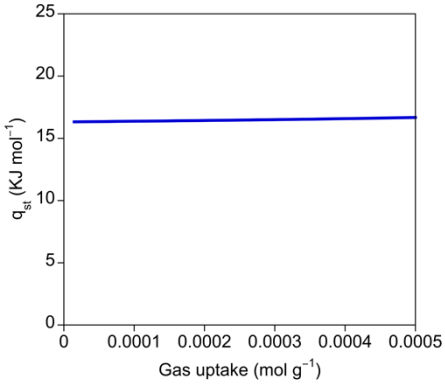

Figure 4.7. Isosteric heat of adsorption for CO_2.

Given the larger size of the void, a larger sorption capacity of **CCP-3** is expected. In fact, if we plot the number of molecules per void (figure 4.8), it can be observed that two molecules of CO_2 can be located in each void at 12 bar and 298 K; on the contrary, N_2 and CH_4 present a lower adsorption capacity. In *chapter* 3 of this thesis, an adsorption of one molecule per void has been demonstrated for the analogous **CCP-1** and **CCP-2**, thus demonstrating here that the gas capacity of the material has been doubled by simply chemical design of the ligand to obtain larger voids.

The volumetric sorption has been calculated too, obtaining a maximum value of 29 $cm^3 \cdot cm^{-3}$ at 1 bar and 298 K, very similar to the value showed in *chapter* 3 of this thesis of 29 and 27 $cm^3 \cdot cm^{-3}$ for **CCP-1** and **CCP-2** respectively. It has been demonstrated that the presence of larger voids is not in detriment of maintaining a good volumetric sorption due to the fact that the dense nature of the material is maintained, that is one of the advantages of using compartmentalized coordination polymers. The enhancing of the gas capacity of **CCP-4** cannot be only analyzed in terms of simply capacity, but also in terms of the working capacity[7] of the materials, defined as the difference of the uptake at 800 kPa minus the uptake at 50 kPa. Comparing the compartmentalized coordination polymers with the same counterion, as can be observed in figure 4.8, the CO_2 working capacity of **CCP-4** is more than twice than that of **CCP-2.** This could be related not only for the larger voids presented in the new material presented in this *chapter* but also for the lower isosteric heat of adsorption found.

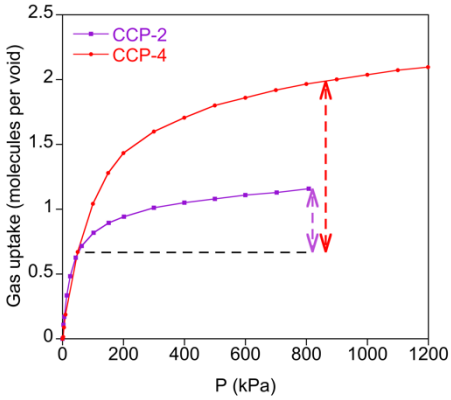

Figure 4.8. Comparison between the CO_2 sorption capacity of **CCP-2** and **CCP-4**. Dashed lines represent the working capacity.

4.2.4. Magnetic behaviour

In *chapters* 2 and 3 it has been shown that **CCP-1** and **CCP-2** present SCO behaviour due to the presence of iron (II) centers in an octahedral environment with tetrazole rings. The isostructural nature of **CCP-3** and **CCP-4** with respect to the previous materials, changing only the length of the ligand, allow us to think about maintaining the magnetic behaviour. The only problem that can occur is related to the larger distance between iron (II) centers, because as stated on the *introduction* of this thesis, SCO is a cooperative phenomenon.

Magnetic susceptibility measurements were performed on polycrystalline samples of **CCP-3** and **CCP-4** in the temperature range 2-300 K at 1 K·min^{-1} under an applied magnetic field of 0.1 T. Both compounds present a spin transition centered at 195 and 199 K (figure 4.9), which is similar to that obtained for **CCP-1** and **CCP-2** (200 K). The transition is less abrupt than in

the previous case, a behaviour that can be related to the progressive loss in cooperativity when the distance between the iron (II) centers increases. Nevertheless, the transition is still abrupt, given the long distance (16 Å) that separates the iron (II) centers. Possibly, the triple ligand bridge between the iron (II) centers provide a good way to propagate the spin transition along the polymeric chain, maintaining a good cooperativity between the metal centers. In addition, as can be seen on figure 4.9, a residual high spin fraction of *ca.* 20 % remains, possibly due a different size in the crystals or defects in the crystal structure.

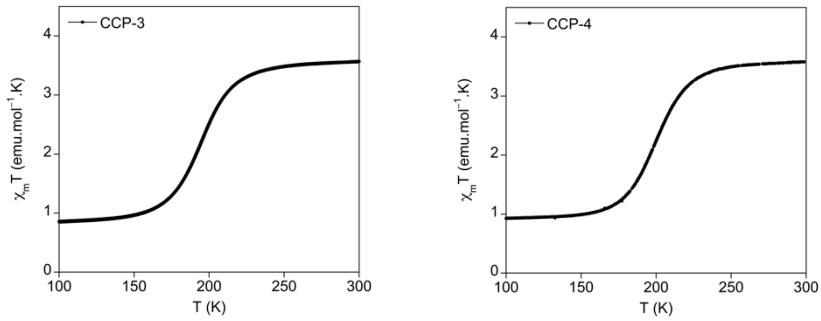

(a) (b)

Figure 4.9. Temperature dependence of $\chi_M T$ for **CCP-3** (a) and **CCP-4** (b).

4.2.5. Magnetic response to CO_2 sorption

As previously shown in this thesis, the use of compartmentalized coordination polymers for gas sorption provokes a stronger interaction between the gas and the framework, with the possibility of tuning the properties of the material. In this family of compounds, **CCP-1** to **CCP-4** studied in this thesis, the presence of iron (II) centers surrounded by tetrazole ligands causes a SCO behaviour of the material. As demonstrated in *chapter* 2, the inclusion of gas

molecules in **CCP-1** and **CCP-2** shifts the spin transition temperature, likely caused by the interaction of the quadrupole moment of the gas and the tetrazole ring. Despite the presence of larger voids, the interaction of the gas molecule and the framework in this larger material should be strong enough to modify the SCO behaviour. As **CCP-4** can load until two molecules of CO_2 per void, it has been studied the magnetic response with the partial inclusion of one molecule and with the full occupancy of the voids. Both situations can be seen on figure 4.10 and interesting responses have been obtained.

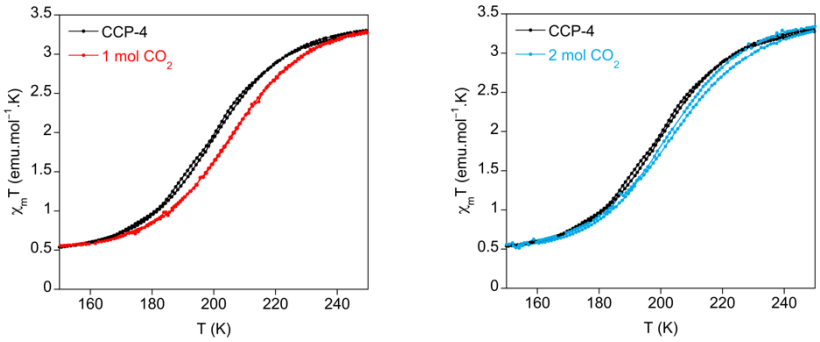

Figure 4.10. Temperature dependence of $\chi_M T$ for **CCP-4** loaded with one (left) and two (right) molecules of CO_2 in each void.

Upon the inclusion of one equivalent of CO_2 (figure 4.10 left), the spin transition temperature is shifted 7 K from 199 to 206 K. As related in the previous *chapter* of this thesis, the quadrupolar moment of the gas exerts a change in the ligand field of the tetrazole ligand causing the change in the magnetic behaviour. Very surprisingly, the inclusion of another equivalent in the voids to achieve the fully occupancy does not cause a further increase of the spin transition temperature; on the contrary, a reduction of this value occurs, reaching 202 K (figure 4.10 right). This event can be ascribed to a

competition between the quadrupolar moments of the two CO_2 molecules, with some gas-gas interaction that may provoke a decrease on the total quadrupolar moment that is affecting the tetrazole ring. Thus, a shift of only 3 K when the two molecules are located inside the voids is observed with respect to the bare **CCP-4**.

4.2.6 Surface deposition studies

One of the potential applications of materials capable of sorption and discrimination between gases, as stated for **CCP-1** and **CCP-2** in *chapter* 2, is the production of membranes of the material for using in gas separation.[8] For this purpose, it is first necessary to study the deposition of the material onto different substrates and analyze the effect on its properties. First of all, the bulk material has been analyzed by scanning-electron microscope (SEM) (figure 4.11).

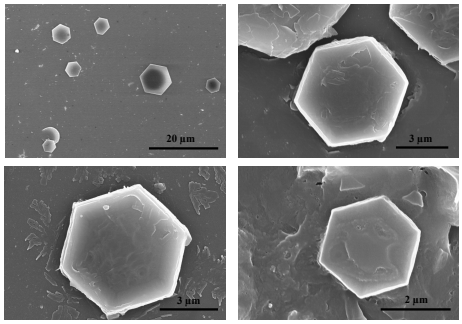

Figure 4.11. SEM images of **CCP-4** crystals.

As can be seen, the same morphology as **CCP-1** and **CCP-2** (figure 2.3 in *chapter* 2 of this thesis) is maintained, obtaining the same well-defined hexagonal microparticles but with larger sizes. For the surface deposition, two

different substrates have been used, selecting quartz and silicon. Both substrates were previously cleaned using acid piranha. The substrates were immersed on a solution of acetonitrile containing the btzbp ligand dissolved, then a solution with $Fe(BF_4)_2$ was added. After one day, both substrates were covered with powder of **CCP-4** and then retired from the solutions. The excess of powder was cleaned and the substrates were analyzed by SEM. As can be seen in figure 4.12, the selection of the substrate plays a crucial role. For quartz, only a few microcrystals of **CCP-4** are attached to the surface. Interestingly, the perfect hexagonal shape is maintained (figure 4.13). On the contrary, all the silicon substrate is covered by irregular micrometric particles. The analysis of this layer reveals a 400 μm thickness (figure 4.14). The confirmation that the powder deposited on top is **CCP-4** was achieved from grazing incidence X-ray diffraction (GIXRD) measurements.

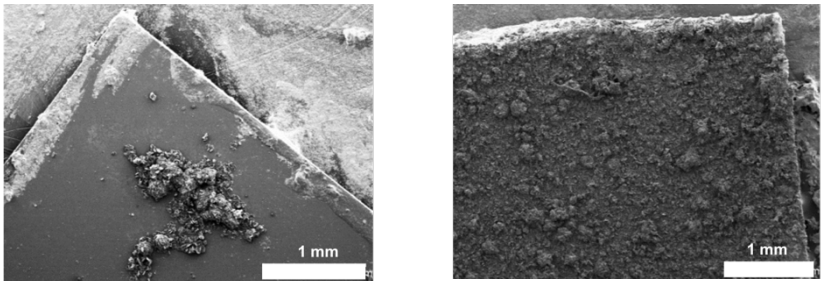

Figure 4.12. Partially coverage on a quartz substrate (left) and totally coverage on a silicon substrate (right) of **CCP-4**.

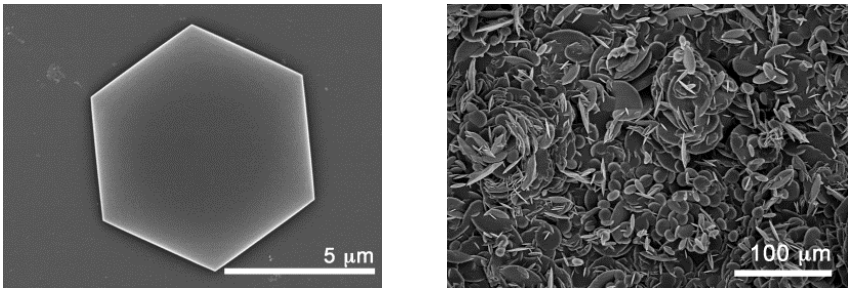

Figure 4.13. Hexagonal microcrystal of **CCP-4** on a quartz substrate (left) and irregular micrometric particles of **CCP-4** covering all the Silicon substrate (right).

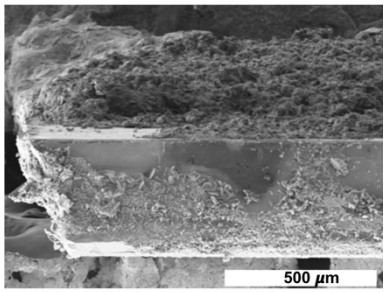

Figure 4.14. Lateral view of the silicon substrate with **CCP-4** deposited on top.

As can be seen on figure 4.15, the GIXRD and the magnetism obtained for the substrate matches perfectly with the XRPD and the magnetism of the bulk **CCP-4**, thus confirming that the crystallinity and nature of the material is maintained upon deposition.

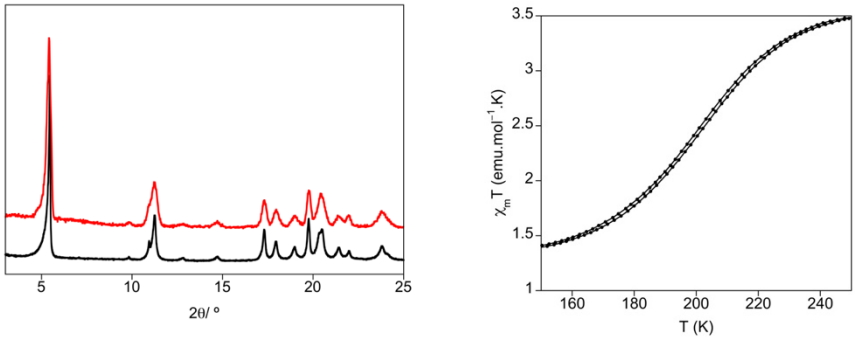

Figure 4.15. On left: XRPD of polycrystalline powder of **CCP-4** (black) and GIXRD of **CCP-4** deposited on a silicon substrate (red). On right: Temperature dependence of $\chi_M T$ for **CCP-4** deposited on a silicon substrate.

4.3 CONCLUSIONS

In this *chapter*, the family of compartmentalized coordination polymers presented in the previous *chapters* has been extended with the synthesis of two isostructural materials to the previous ones, **CCP-3** and **CCP-4**. By chemical design of the organic ligand, it has been extended, maintaining the same coordination moieties of tetrazole rings and obtaining isostructural 1D iron (II) chains that present SCO behaviour. It has been demonstrated that **CCP-4** can load up to two molecules of CO_2 in each void and in addition, the transition temperature ($T_{1/2}$) can be tuned with the partial inclusion of CO_2 molecules. When only one molecule of CO_2 is adsorbed, that is, 50% of occupancy for the internal voids, a shifting of 7 K for $T_{1/2}$ to higher temperatures occurs, related to the interaction of the quadrupole moment of the gas with the tetrazole ring. Furthermore, when two molecules of CO_2 are inserted, the interaction between them recover the transition 4 K to lower temperatures, still 3 K higher than the original one. That behaviour should be

related to different orientations of the CO_2 molecules inside the voids, where the presence of two molecules do not allow a strong interaction between the quadrupole moment of the CO_2 and the tetrazole ring, therefore provoking a soft modification of $T_{1/2}$. The deposition of **CCP-4** on a substrate for a future application on gas membranes has been studied, demonstrating that **CCP-4** can be deposited on a silicon substrate, maintaining its crystalline and magnetic nature.

4.4. METHODS

4.4.1. Synthesis

All reagents and solvents were commercially available and used without further purification.

Caution. Perchlorate salts are explosive (especially if they are dry) and should be handled with extreme caution.

Synthesis of the ligand (btzbp). The ligand ligand 4,4'-bis((1H-tetrazol-1-yl)methyl)-1,1'-biphenyl (btzbp) was synthesized following a three-step synthesis:

a) 4,4'-bis(azidomethyl)-1,1'-biphenyl. A mixture of sodium azide (1.0 g, 15 mmol) and 4,4'-bis(bromomethyl)-1,1'-biphenyl (3.4 g, 10 mmol) was dissolved in 15 mL of dry DMF and stirred at 60 °C for 10 hours. Then, 100 mL of water was added and the product was extracted with ether (3 x 10 mL). The organic layer was washed three times with water (3 x 10 mL). Yield 80

%. IR (KBr disk) ν 2109.5 cm^{-1} (N_3); ^{1}H-NMR (300 MHz, DMSO): δ 4.5 (4 H, CH_2-N_3), 7.5 (4 H, CH aromatic), 7.8 (4 H, CH aromatic).

b) [1,1'-biphenyl]-4,4'-diyldimethanamine. 4,4'-bis(azidomethyl)-1,1'-biphenyl (1.5 g, 5.7 mmol) was dissolved in 25 mL of dry THF and added dropwise to a stirring solution of $LiAlH_4$ (0.75 g) in 25 mL of dry THF cooled to 0 °C under Ar atmosphere. When the addition was complete, the solution was heated to reflux with stirring for 4h. Then, the excess of $LiAlH_4$ was quenched by slowly adding 0.75 mL of H_2O, followed by 0.75 mL of a 15 % aqueous NaOH solution and finally 2.25 mL of H_2O with the suspension kept at 0 °C under constant stirring. The crude product was filtered and washed with ethyl acetate and dried under reduced pressure to yield the pure product. Yield 82 %. IR (KBr disk) N_3 band was not observed.

c) 4,4'-bis((1H-tetrazol-1-yl)methyl)-1,1'-biphenyl (btzbp). A mixture of [1,1'-biphenyl]-4,4'-diyldimethanamine (1.5 g, 7.1 mmol), NaN_3 (0.92 g, 14.1 mmol) and $CH(OEt)_3$ (12 ml, 69.3 mmol) was dissolved in 20 mL of acetic acid under Ar atmosphere and heated 90 °C for 4 days. After cooling to room temperature, the solvent was evaporated and the solid was washed with methanol to yield the pure product. Yield 74 %. ^{1}H-NMR (300 MHz, DMSO): δ 5.8 (4 H, CH_2), 7.4 (4 H, CH aromatic), 7.7 (4 H, CH aromatic), 9.6 (2 H, CH tetrazole).

Synthesis of $[Fe(btzbp)_3](ClO_4)_2$ (CCP-3). A solution of $Fe(ClO_4)_2 \cdot xH_2O$ (28.0 mg) in 2 mL of MeCN was added into a solution of btzbp (63.6 mg, 0.2 mmol) in 24 mL of MeCN. A white crystalline precipitate appeared after a few days. The white powder was filtered and washed with MeCN. Phase purity was established by X-ray powder diffraction (*vide infra*). Yield 61 %.

Anal. calc. $C_{48}H_{42}FeN_{24}Cl_2O_8$ (1209.75): C, 47.66; H, 3.50; N, 27.79 %. Found: C, 47.50; H, 3.48; N, 26.94 %.

Synthesis of $[Fe(btzbp)_3](BF_4)_2$ (CCP-4). A solution of $Fe(BF_4)_2 \cdot xH_2O$ (33.8 mg) in 2 mL of MeCN was added into a solution of btzbp (63.6 mg, 0.2 mmol) in 24 mL of MeCN. A white crystalline precipitate appeared after a few days. The white powder was filtered and washed with MeCN. Phase purity was established by X-ray powder diffraction (*vide infra*). Yield 70 %. Anal. calc. $C_{48}H_{42}FeN_{24}B_2F_8$ (1184.46): C, 48.67; H, 3.57; N, 28.38 %. Found: C, 47.86; H, 3.54; N, 27.47 %.

4.4.2. Structural characterization

4.4.2.1. Single crystal X-ray diffraction for CCP-4

A single crystal of **CCP-4** was mounted on a glass fibre using a viscous hydrocarbon oil to coat the crystal and then transferred directly to the cold nitrogen stream for data collection. X-ray data was collected on the same crystal at 240 K (**CCP-4–HS**) and then at 120 K (**CCP-4–LS**) on a Supernova diffractometer equipped with a graphite-monochromated Enhance (Mo) X-ray Source (λ = 0.71073 Å). The program CrysAlisPro, Oxford Diffraction Ltd., was used for unit cell determinations and data reduction. Empirical absorption correction was performed using spherical harmonics, implemented in the SCALE3 ABSPACK scaling algorithm. Crystal structures were solved and refined against all F^2 values using the SHELXTL suite of programs.[9] Due to the tiny size of the crystal (and thus weak diffraction data, figure 4.17), restrains on all aromatic rings and on chemical

bonds have been applied to maintain chemical sense, and only the Fe atoms were refined anisotropically. The disordered anions were modelled over two orientations with fixed thermal parameters, with occupancies 50:50. Hydrogen atoms were placed in calculated positions that were refined using idealized geometries (riding model) and assigned fixed isotropic displacement parameters.

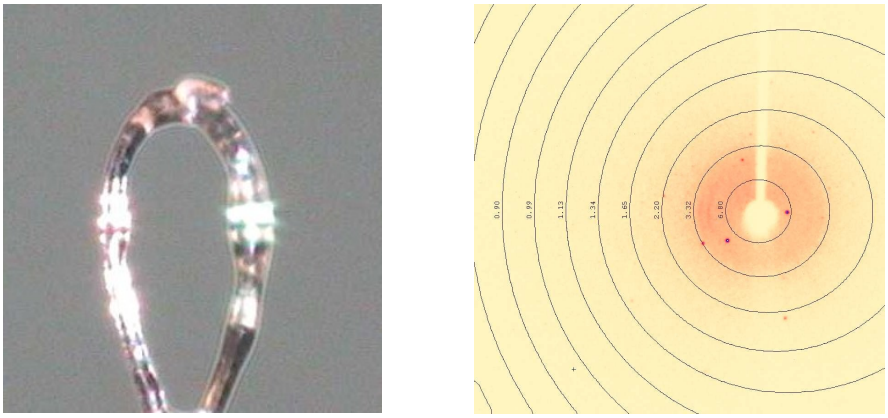

Figure 4.17. Measured single-crystal of **CCP-4** (left) at 120 K (characteristic pink color of Fe (II) LS) and the weak diffraction data of the crystal (right).

A summary of the data collection and structure refinements is provided in table 4.2.

Compound	**CCP–4–HS**	**CCP–4–LS**
Empirical formula	$C_{48}H_{42}N_{24}B_2F_8Fe$	$C_{48}H_{42}N_{24}B_2F_8Fe$
Formula weight	1184.53	1184.53
Crystal color	Colorless	Pink
Crystal size (mm^3)	0.06 × 0.06 × 0.01	0.05 × 0.05 × 0.02
Temperature (K)	240(2)	120(2)
Crystal system, Z	Hexagonal, 2	Hexagonal, 2
Space group	$P6_3$	$P6_3$
a (Å)	10.3650(10)	10.2235(14)
b (Å)	10.3650(10)	10.2235(14)
c (Å)	32.289(5)	31.903(8)
α (°)	90.00	90.00
β (°)	90.00	90.00
γ (°)	120.00	120.00
V ($Å^3$)	3004.2(6)	2887.8(11)
ρ_{calc} (Mg/m^3)	1.309	1.362
$\mu(Mo_K\alpha)$ (mm^{-1})	0.330	0.344
θ range (°)	3.39 – 25.02	2.99 – 25.03
Reflns collected	24825	11791
Independent reflns (R_{int})	3571 (0.4179)	3408 (0.2722)
Reflns used in refinement, *n*	3571	3408
L. S. parameters, *p*/ restraints, *r*	90/46	60/46
$R1(F)$,[a] $I>2\sigma(I)$	0.2271	0.2157
$wR2(F^2)$,[b] all data	0.5406	0.5271
$S(F^2)$,[c] all data	1.232	1.150

[a] $R1(F) = \Sigma(|Fo| - |Fc|)/\Sigma|Fo|$; [b] $wR2(F^2) = [\Sigma w(Fo^2 - Fc^2)^2/\Sigma wFo^4]^{½}$; [c] $S(F^2) = [\Sigma w(Fo^2 - Fc^2)^2/(n + r - p)]^{½}$

Table 4.2. Crystallographic data for **CCP-4**

4.4.2.2. X-ray powder diffraction, phase purity

Polycrystalline samples of **CCP-3** and **CCP-4** were lightly ground in an agate mortar and pestle and filled into 0.5 mm borosilicate capillaries prior to being mounted and aligned on an Empyrean PANalytical powder diffractometer, using Cu Kα radiation (λ = 1.54056 Å). For each sample, two repeated measurements were collected at room temperature (2θ = 2–60°) and merged in a single diffractogram. Pawley refinements were performed using the TOPAS[10] computer program and revealed an excellent fit to a one-phase model for compounds **CCP-3** (R_{wp} = 0.0218; GOF = 1.502) and **CCP-4** (R_{wp} = 0.0239; GOF = 1.225), indicating the absence of any other detectable crystalline phases.

4.4.2.3. Scanning electron microscopy

All SEM experiments were performed with a Hitachi S-4800 field emission scanning electron microscope at an accelerating voltage of 10 kV with metallization (Au-Pd) of the samples.

4.4.3. Surface deposition

Two different substrates were studied for this purpose: silicon and quartz substrates. The same procedure was carried out in the two cases. The substrates were washed by immersion in an acid piranha solution for three minutes and subsequent washing with water. Then, the clean substrates were introduced in a fresh solution containing both the ligand and the metal. After a few days the substrate was removed from the solution, washed with acetonitrile and dried over a nitrogen stream.

4.4.4. Gas sorption isotherms

All gas sorption studies were performed by Dr. Miguel Palomino in collaboration with Prof. F. Rey from the Instituto de Tecnología Química of Valencia.

High pressure adsorption isotherms of CO_2, CH_4 and N_2, were performed in an IGA-3 gravimetric analyser (Hiden Isochema). Approximately, 50 mg of sample were placed in the balance. Before each adsorption experiment, the sample was outgassed at 423 K under a final pressure of 10^{-5} Pa during four hours. The temperature of the sample was subsequently reduced under high vacuum until the target temperature (from 283 to 333 K) for each adsorption experiment. Adsorption measurements were performed by introducing gas up to reach the desired pressures.

4.4.5. Magnetic measurements

Magnetic susceptibility measurements were carried out on single-phased polycrystalline samples with a Quantum Design MPMS-XL-5 SQUID susceptometer. The susceptibility data were all collected at 1 $K \cdot min^{-1}$, with an applied field of 0.1 T for **CCP-3** and **CCP-4** and for **CCP-4** with CO_2 loaded. Magnetic susceptibility measurements of the gas loaded system were performed by sealing a glass tube with 10 mg of **CCP-4** and a known amount of the gas or after heating a loaded sample to remove the CO_2 molecules. Prior to the gas loading, the samples were activated by heating in situ at 150 °C for 3 h under vacuum.

4.5 REFERENCES

1. Hu, Z., Deibert, B. J. & Li, J. Luminescent metal–organic frameworks for chemical sensing and explosive detection. *Chem Soc Rev* **43**, 5815–5840 (2014).
2. Coronado, E. & Mínguez Espallargas, G. Dynamic magnetic MOFs. *Chem. Soc. Rev.* **42**, 1525–1539 (2013).
3. Li, J.-R., Kuppler, R. J. & Zhou, H.-C. Selective gas adsorption and separation in metal–organic frameworks. *Chem. Soc. Rev.* **38**, 1477 (2009).
4. Murray, L. J., Dincă, M. & Long, J. R. Hydrogen storage in metal–organic frameworks. *Chem. Soc. Rev.* **38**, 1294 (2009).
5. Aromí, G., Barrios, L. A., Roubeau, O. & Gamez, P. Triazoles and tetrazoles: Prime ligands to generate remarkable coordination materials. *Coord. Chem. Rev.* **255**, 485–546 (2011).
6. Pawley, G. S. Unit-cell refinement from powder diffraction scans. *J. Appl. Crystallogr.* **14**, 357–361 (1981).
7. Palomino, M., Corma, A., Rey, F. & Valencia, S. New Insights on CO_2 −Methane Separation Using LTA Zeolites with Different Si/Al Ratios and a First Comparison with MOFs. *Langmuir* **26**, 1910–1917 (2010).

8. Xiang, Z. & Cao, D. Porous covalent–organic materials: synthesis, clean energy application and design. *J Mater Chem A* **1**, 2691–2718 (2013).
9. Sheldrick, G. M. A short history of *SHELX*. *Acta Crystallogr. A* **64**, 112–122 (2008).
10. Coelho, A. A. TOPAS-Academic, Version 4.1, 2007, see http://www.topas-academic.net.

Chapter 5:
Unveiling pathway complexity in the crystal growing *via* microfluidics

5.1 INTRODUCTION

The chemical and physical properties of functional materials strongly depend on the nature and arrangement of their constituent units.[1] The vast current knowledge on molecular self-assembly allows for the preparation of materials with controllable physico-chemical properties, with the position and orientation of the constituent units being coordinated within the final structure as has been shown in previous chapters.[2] In this respect, crystals of organic-inorganic materials such as coordination polymers (CPs), including metal-organic frameworks (MOFs), have recently attracted much attention, due to their high versatility in terms of material structure and structure-property correlations.[3] Accordingly, by combining the rational design of the organic ligands with the directionality imparted by metal-ligand coordination bonds, specific structures and functions can be realized. In practice, artificial organic-inorganic crystals are commonly equilibrium structures obtained under thermodynamic control, and they display defined properties (or functions) depending on both the nature of the metal ions or molecular constituents, as well as on the final thermodynamic conditions (*e.g.* temperature, pH, solvent composition). Moreover, dynamic molecular crystals that exhibit adjustable functional properties have been successfully synthesized through changes in the final thermodynamic state (i.e. changes in the free energy landscape), upon application of external stimuli.[4,5,6,7,8,9,10] On the other hand, and in sharp contrast, crystallization processes in living systems (*i.e.* biomineralization), as well as biomimetic crystallizations, often occur under non-equilibrium conditions (*e.g.* chemical gradients, reaction-

diffusion control, hydrodynamic effects), which leads to kinetic growth pathways.[11]

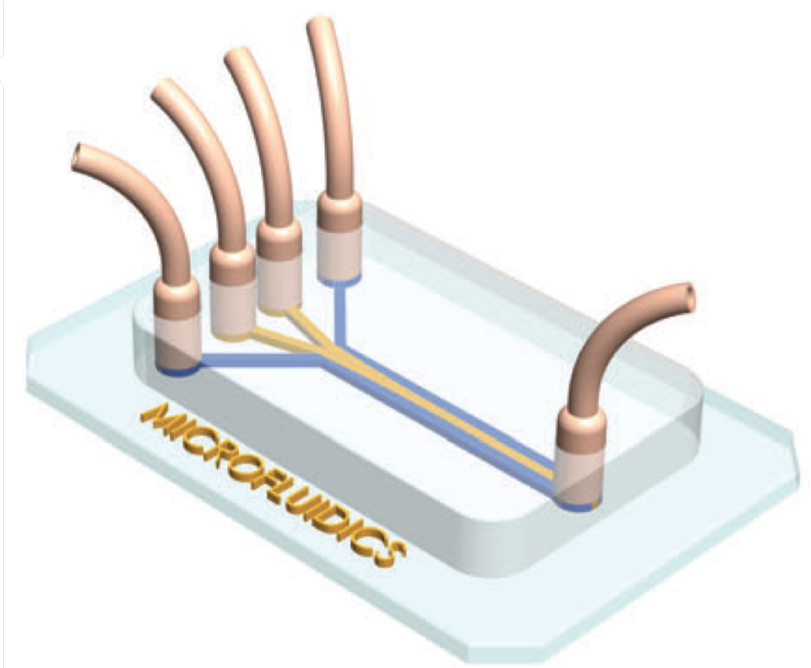

Figure 5.1. Schematic representation of the microfluidic synthesis performed in this *chapter*.

Kinetic effects may often dominate thermodynamic control and, as a result, self-assembly cannot be properly described by classical thermodynamic theories.[12] It is significant to note that, to date, any understanding of the mechanisms and dynamics underlying CP self-assembly is very limited, with their crystallization pathways being largely unknown and unresolved. This is despite the fact that properties and functions of CPs may be a direct consequence of the pathways followed during their assembly and development. Accordingly, there is a pressing need to elucidate pathway

complexity and, more importantly, to control the hiking of functional materials on the free energy landscape during the self-assembly process (very well pictured in nature but elusive with conventional synthetic methods).[13] Such an understanding and ultimate control will lead to new adaptable structures with unique properties and functions.[14]

In this *chapter*, microfluidics methods have been used for this purpose (figure 5.1). For studying crystallization processes, microfluidic devices are a useful tool using the liquid-liquid interfacial reactions present in continuous-flow, going from the thermodynamic (temperature-time dependent protocols) to the kinetic control (space-time strategies). In most microfluidic systems, mixing of reagents only occurs through molecular diffusion,[15] the so-called laminar flow conditions and is a useful way to control crystallization process in space (because the crystallization only happens in the reaction-diffusion (RD) area generated between the co-flowing reagent streams) and time (crystallization proceeds along the length of the microfluidic channel).[16]

Additionally, and in contrast to bulk synthetic approaches, microfluidic liquid-liquid interfacial reactions are characterized by a constant mass transport of reagent species to the RD area. As a result, no depletion of reagents occurs during self-assembly, which in turn favours a fine control over self-assembly dynamics and growth pathways (*vide infra*).[17] This *chapter* presents a detailed crystal growth of one compartmentalized coordination polymer. More specifically, this *chapter* shows the formation of **CCP-4**,[18] previously presented in *chapter* 4, under microfluidic conditions. As stated in the previous *chapter*, **CCP-4** crystallizes in the $P6_3$ space group, forming hexagonal microcrystals observed by SEM (figure 5.2).

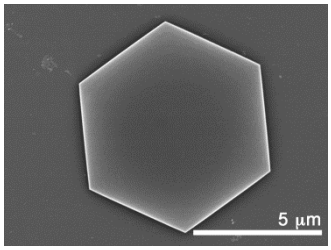

Figure 5.2. SEM image of **CCP-4** crystal.

These crystals have been obtained by a thermodynamic synthesis of the material, that is, the ambient temperature mixture of solutions of the ligand btzbp, 4,4′-bis((1H-tetrazol-1-yl)methyl)-1,1′-biphenyl and $Fe(BF_4)_2 \cdot 6\ H_2O$ in acetonitrile. Here, the same final material has been synthesized, using microfluidic methods.

5.2 RESULTS AND DISCUSSION

5.2.1 Microfluidic study

Microfluidic synthesis has been performed in collaboration with the group of Dr. Josep Puigmartí-Luís from the Institute of Chemical and Bioengineering, Department of Chemistry and Applied Biosciences, ETH Zurich. The microfluidic device used in this study for the kinetic control of the synthesis works on a continuous-flow and contains four inlets and one outlet made from poly(dimethylsiolaxane) (PDMS). This microfluidic configuration permits the establishment of a controlled RD area within the main microfluidic channel. In figure 5.3 a schematic representation of the device can be seen.

Figure 5.3. Schematic representation of the RD area generated within the main microfluidic channel (fuchsia color).

In the experiments performed, two pure acetonitrile sheath flows were introduced from inlets a and d (figure 5.3) while acetonitrile solutions of $Fe(BF_4)_2 \cdot 6\ H_2O$ (15.7 mM) and btzbp (31.4 mM) were separately injected into the two middle input channels b and c (figure 5.3). The flow rate ratio (FRR), defined as the ratio between the flow rates of the reagent-laden flows and that of the sheath flows, was fixed to 1. The compound synthesized by this method has been named as **MF-CCP-4** to differentiate the material obtained from the bulk mixing synthesis procedure and the microfluidic one. The evolution of the structures generated under controlled RD conditions was studied over time by transmission electron microscopy (TEM). The effluent from the microfluidic device was collected in a vial at different times (0, 1, 3, 6 and 12 hours) and analyzed.

For characterization of the particles and confirming that **MF-CCP-4** and **CCP-4** are the same material, energy dispersive X-ray (EDX) measurements (figure 5.4) indicate the presence of both N and Fe in the microparticles of **MF-CCP-4**, elements present in **CCP-4**. In addition, some powder of **MF-CCP-4** was isolated 12 hours after preparation and analyzed, confirming by X-ray powder diffraction that it has the same crystal structure that the material

synthesized in bulk, **CCP-4** (figure 5.5). In addition, SCO behaviour of the resulting microfluidic synthesis particles has been analyzed, to fully confirm that the material obtained maintain the same properties that the previously bulk. As can be seen on figure 5.6, the spin transition is present at the same temperature, 199 K.

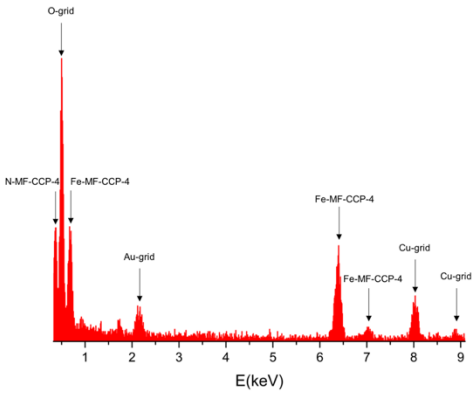

Figure 5.4. EDAX analysis of **MF-CCP-4**.

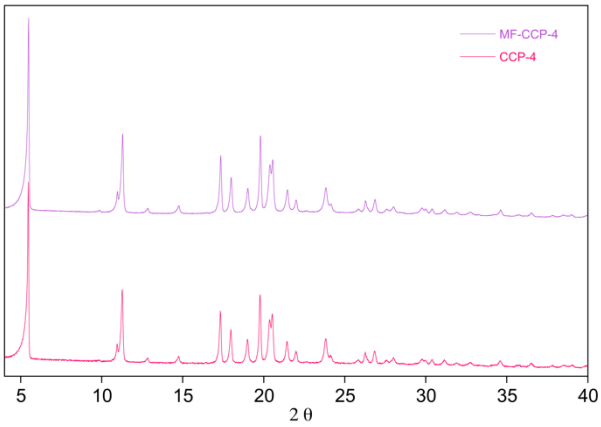

Figure 5.5. X-ray powder diffraction of **CCP-4** (pink) and **MF-CCP-4** (violet).

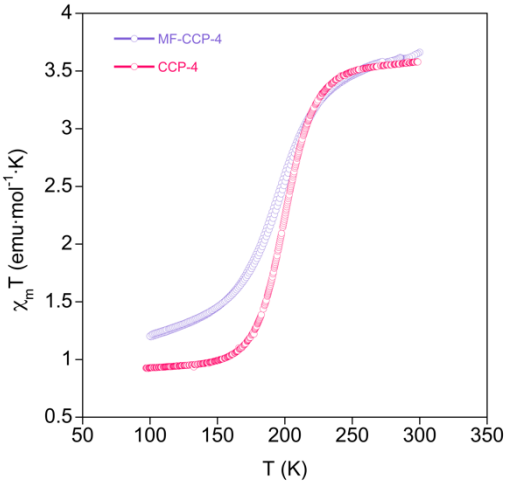

Figure 5.6. Temperature dependence of $\chi_M T$ product for **CCP-4** (pink) and **MF-CCP-4** (violet).

After fully confirmation of the purity of the microfluidic material, the analysis of the material synthesized at different times has been performed. For time zero, the solution exiting the microfluidic device was immediately drop-casted onto a TEM grid to ensure a rapid quenching of the reaction. The TEM images at different times spawn for the microfluidic synthesis have been represented in the next figures for further discussion of the results observed. Note that more than 850 particles have been observed in the TEM study but only two representative images for each time have been shown.

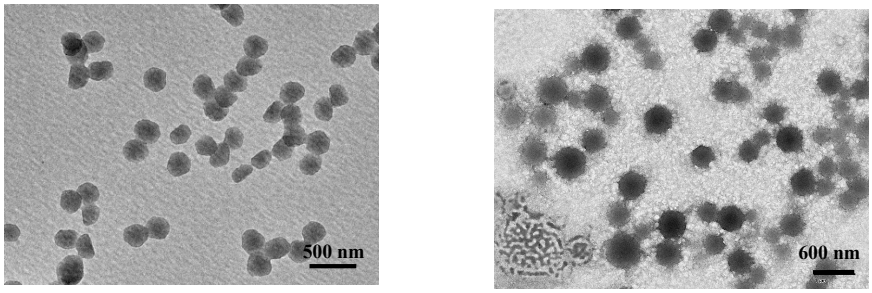

Figure 5.7. TEM images of **MF-CCP-4** samples prepared at time zero.

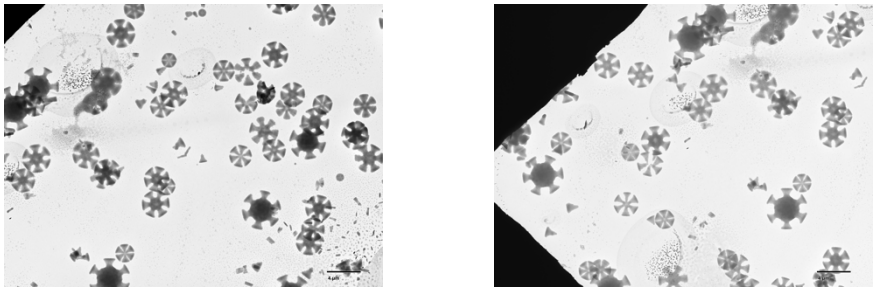

Figure 5.8. TEM images of **MF-CCP-4** samples prepared at 1 hour. Scalebars are 4 μm.

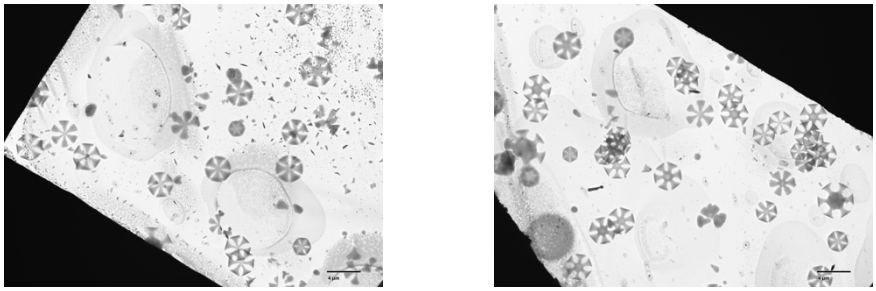

Figure 5.9. TEM images of **MF-CCP-4** samples prepared at 3 hours. Scalebars are 4 μm.

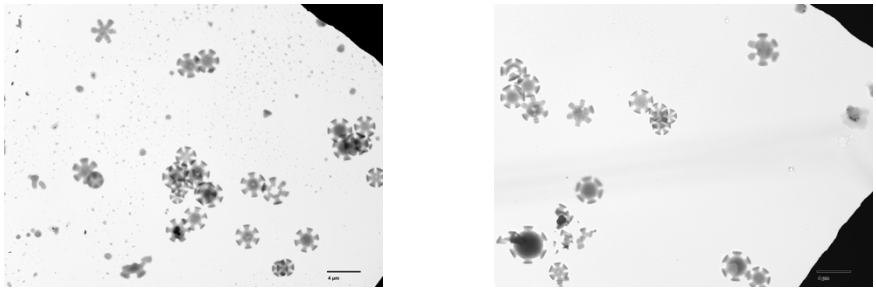

Figure 5.10. TEM images of **MF-CCP-4** samples prepared at 6 hours. Scalebars are 4 μm.

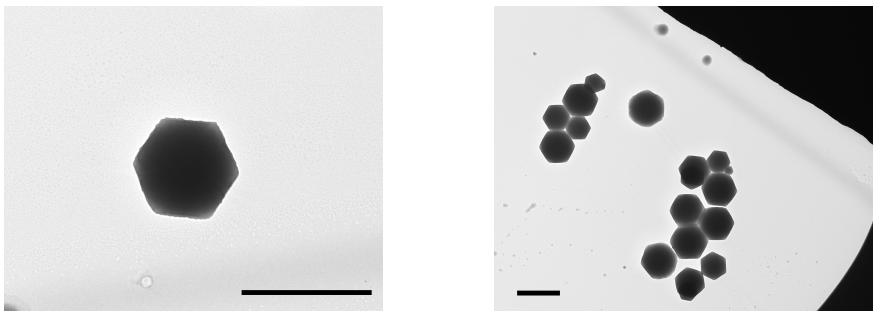

Figure 5.11. TEM images of **MF-CCP-4** samples prepared at 12 hours. Scalebars are 4 μm.

The analysis of the microfluidic products allows to some interesting observations that can be done on the images. First of all, at time zero, some "seeds" can be seen. The size of these particles is around 200-400 nm, and they are the initial step of the growing. At 1, 3 and 6 hours, very interesting observations could be done. In all images, intermediates of the final **MF-CCP-4** crystals have been observed. As can be seen with a closer inspection, all particles are uncompleted hexagons. Two different pathways of crystal growing can be observed in the images, hereafter named Path A and Path B

and both represent a systematic growth of the seed until hexagons, as can be observed in the next figure.

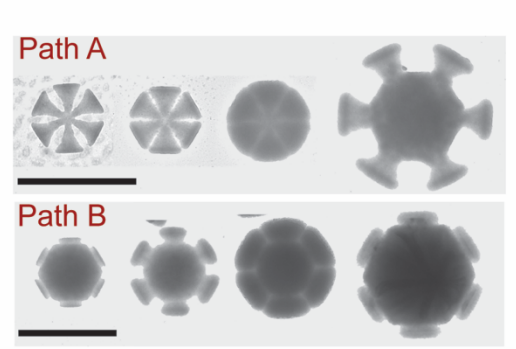

Figure 5.12. Schematic sequential growth along the two kinetic pathways. Scalebars are 4 μm.

In path A, the crystal growth happens in the vertices of a previously formed **MF-CCP-4** crystal. The crystal propagates from the vertices, and then the structure is filled with more material until the crystal evolves again from the vertices of a bigger hexagon. This gradual growing finally will lead to the final hexagon observed in the bulk SEM analysis. In Path B, the growth proceeds in the same manner, that is, the consecutive developing of a hexagon, but now the growing proceed from the lateral part of it. A hexagon propagates from the lateral part, then the crystal is filled with more material, forming a bigger hexagon until it grows again from the lateral part. The two different pathways of growing involves distinct intermediates (hexagons developing from the vertices, Path A, or hexagons developing from the lateral, Path B) and then represent two different competing routes along the free energy landscape undertaken simultaneously by the system in the

microfluidic synthesis. All structures arise and develop from nucleation events that occur under controlled diffusion conditions over a period of approximately 40 ms, the residence time of the reacting solution in the main microfluidic channel. As an additional observation, Pathway A involves a 30 º rotation in the process of growing, that is, when the original hexagon grows, it grows from the vertex of the smaller one to the lateral of the bigger one (figure 5.13 left). On the other hand, Pathway B retains the original orientation of the particle with a growing process from the lateral of the smaller hexagon to the lateral of the bigger one (figure 5.13 right). So, both pathways involve a process of growing from a seed that is the core of the material, with consecutive growing of hexagons, where the bigger hexagon is the core of the next step in the growing. In figure 5.11, corresponding to the images from the synthesis prepared at 12 hours, it can be seen perfect hexagons formed. Characterization of the particles obtained under microfluidic conditions by selected area electron diffraction (SAED) have been tried, with no success due to the damage of the particles under electron beam irradiation.

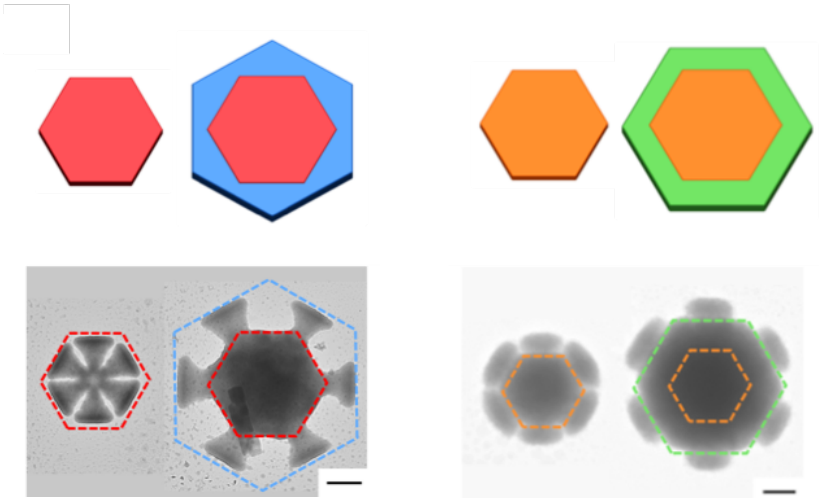

Figure 5.13. Schematic representation and real TEM images of the vertex growth (Path A) with a 30 º rotation in orientation (left) and the lateral growing (Path B) with retention of the orientation (right). Scalebars are 1 μm.

5.2.2 Comparison between Pathways A and B

To fully understand which is the origin of the two different pathways found in the microfluidic synthesis, a more detailed view to the TEM images has been performed. 876 microcrystals have been analyzed in the different grids at different times and a statistical analysis of the abundance of each type of intermediate at given time intervals reveals useful information (figure 5.14). 94 % of the **MF-CCP-4** observed after 1 hour of reaction present the vertex growth (Path A). On the other hand, lateral growth is not significantly observed until 6 hours of reaction. Both pathways lead to the same crystalline structure, so different intermolecular interactions in the crystal packing could explain the different pathways observed.

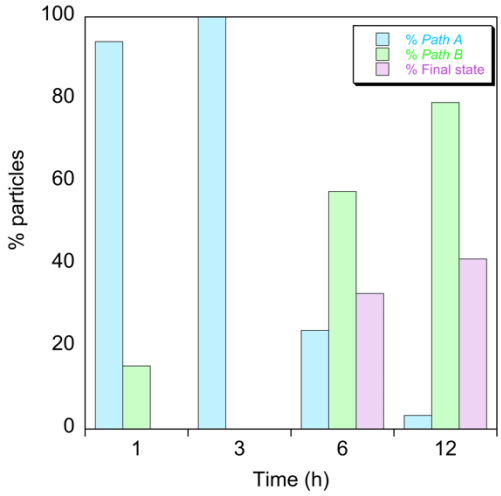

Figure 5.14. Percentage of particles observed at different times.

Figure 5.15 is a crystallographic representation and it shows the hexagonal crystal packing of **CCP-4** along the crystallographic *c*-axis, with A being the initial seed for Pathway A and D the initial seed for Pathway B. With a closer look, it can be seen that the vertexs of the hexagonal seed correspond to the location of the BF_4^- counter-ions, coloured as yellow in B and C (and also indicated with arrows) while the edge of the hexagon corresponds to the two phenyl groups of the btzbp organic ligand, coloured as yellow in E and F (and also indicated with arrows). So, with this information about the crystal structure, a hypothesis can be done about the driving force of each pathway, A and B: the growing in path A is dominated by the electrostatic interactions involving the BF_4^- anions in the vertex while in path B, weaker π–π interactions in the edges of the hexagon provoke the crystal growing. These two different driving forces could explain the faster growth through path A (almost all particles at low reaction times correspond to this pathway) because

the Coulombic interactions are energetically more favourable than Van der Waals forces in the crystallization processes.

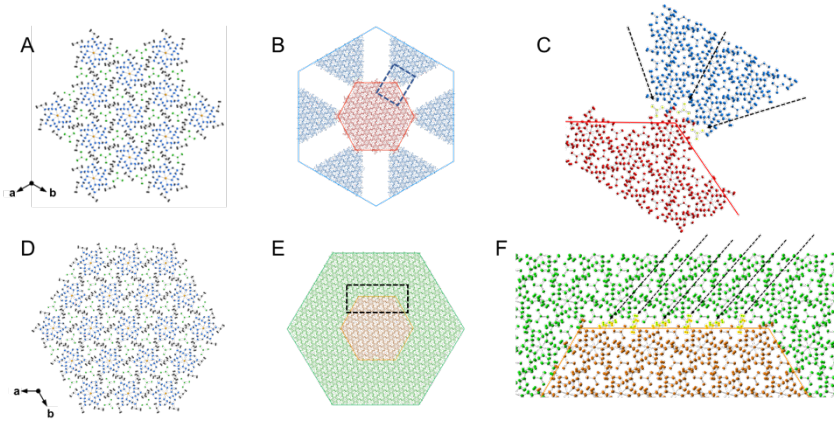

Figure 5.15. A, fragment of **CCP-4** of formula $[Fe(btzbp)_3]_{19}(BF_4)_{36}$; D, fragment of **CCP-4** of formula $[Fe(btzbp)_3]_{13}(BF_4)_{24}$; B and E are illustrations of the crystal growing for pathway A and B respectively; In (C) an image of the corner of a hexagon that follows the vertex growth, pathway A, triggered by electrostatic interactions involving negative BF_4^- anions. The yellow moieties correspond to BF_4^- anions. (F) Image of a crystal edge in a lateral growth where the phenyl groups of the organic ligands are represented with yellow moieties.

5.2.3 Bulk synthesis study

With the confirmation that microfluidics lead to two pathways of growing that finally yield the same hexagon microparticles observed by bulk synthesis, the crystal growing of this method has been studied. **CCP-4** synthesis was carried out with the same experimental conditions that **MF-CCP-4**, that is, room temperature, same concentration of the reactants (31.4 mM for btzbp and 15.7 mM for $Fe(BF_4)_2 \cdot 6\ H_2O$) and solvent composition (acetonitrile). Both solutions of the reactants were mixed and then, for TEM analysis, direct

drop casting of the reacting solution were carried out at the same time intervals than for the microfluidic synthesis (0, 1, 3, 6 and 12 hours). In contrast to the microfluidic synthesis, no particle is observed at time zero. For times higher than 1 hour, no particle is observed in the TEM grids. It is observed that in the bulk synthesis, after 3 hours the complete precipitation of the powder occurs from the reaction mixture, leaving a clear supernatant solution. Only particles have been observed for 1 hour of reaction, and two representative images can be seen on the figure 5.16.

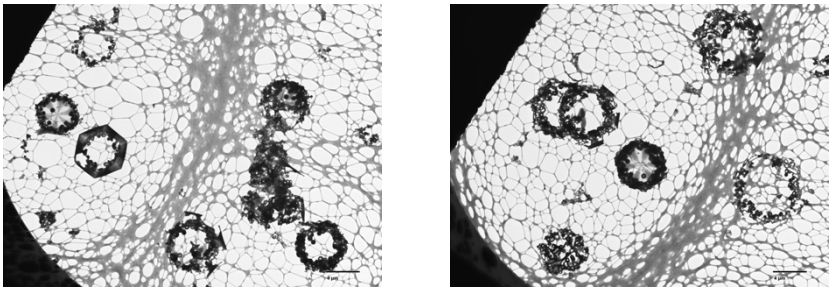

Figure 5.16. TEM images of **CCP-4** after 1 hour reaction. The scale bar is 4 μm.

Surprisingly, another different pathway than A or B is observed, named hereafter pathway C. Incomplete hexagonal crystals have been observed after 1 hour of reaction, and they are formed by self-assembly of smaller hexagonal crystallites (figure 5.17). All the smaller hexagons are well-oriented in the same direction, and form an incomplete but bigger hexagon microparticle.

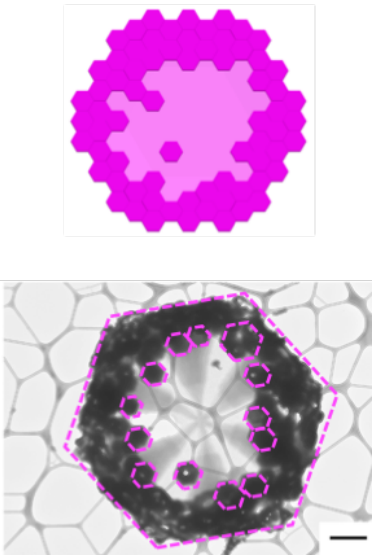

Figure 5.17. Schematic representation and real TEM image of the mesoscale assembling (Path C) found in the bulk synthesis. Scalebar is 1 μm.

The analysis of the precipitate fully confirm that the result obtained in this synthesis of **CCP-4** are complete crystal microparticles with a hexagonal shape (figure 5.18). This characterization confirms that the synthesis of **CCP-4** (bulk synthesis) and **MF-CCP-4** (microfluidic synthesis) move forward by different pathways along the free energy landscape, but the three pathways lead eventually to the thermodynamic product (the global minimum in the free energy landscape), that is, the same hexagonal microcrystals (figure 5.19).

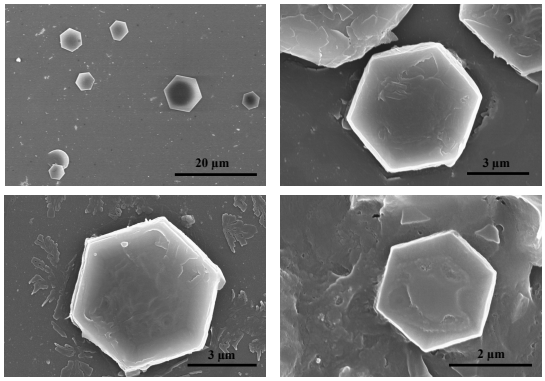

Figure 5.18. SEM images of **CCP-4** crystals after 24h reaction.

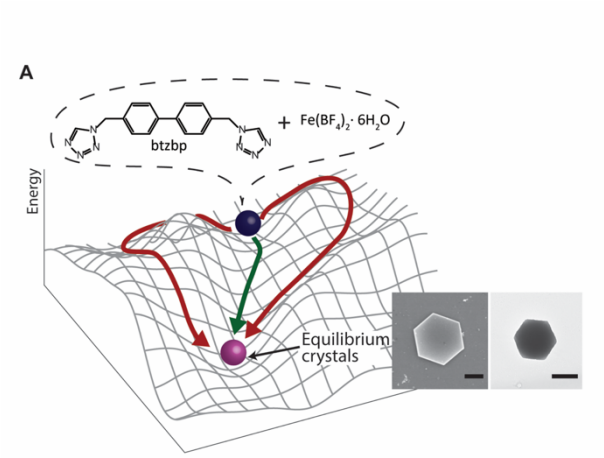

Figure 5.19. Schematic illustration of pathway complexity.

In addition, pathway C results in faster crystallization with no observation of particles in solution within 3 hours, having the possibility in the same system to select different pathways to obtain the same final structure. Pathway A and B (dominated by kinetics) progress under RD conditions for 40 ms, forcing the system to progress under the slower conditions.

5.3 CONCLUSIONS

In this *chapter* an unprecedent explanation of the crystal growth mechanism of a SCO coordination polymer gas sorption capacity has been presented. For this purpose, the use of the reaction-diffusion conditions present in the microfluidic reactor plays a key-role to obtain new pathways of growing that cannot be obtained in the bulk mixing conditions. The continuous feeding of reactants in the RD region favors an increase in the number of coordination events, allowing the system to go through pathways that are forbidden in the bulk mixing experiments. Controlled RD conditions present in microfluidic devices have been proved to be a useful tool for unveiling and studying crystallization processes that cannot be well-explained in the classic thermodynamic control syntheses. In addition, it has been shown crucial for pathway selection, isolating different metastable states that finally yield the same final hexagonal structure. The precise control of growing in coordination polymers with diverse and interesting properties like spin-crossover or gas sorption will be challenging for obtaining materials with desirable properties.

5.4. METHODS

Iron(II) tetrafluoroborate hexahydrate (97%) was purchased from Sigma-Aldrich and 4,4-bis((1H-tetrazol-1-yl)methyl)-1,1-biphenyl (btzbp) was synthesized following a three-step protocol. HPLC grade acetonitrile was obtained from Fisher Chemical. A polydimethylsiloxane (PDMS) kit containing base and curing agent was purchased from Dow Corning (Sylgard 184 Silicone elastomer kit). In all experiments, solutions were filtered using

syringe filters having a pore size of 0.45 μm (Titan Syringe Filter, Fisher Scientific) prior to use. This avoids pollution of precursor solutions with dust or dirt particles.

5.4.1. Microfluidic device fabrication

The microfluidic devices were fabricated by replica moulding of PDMS against a structured master mould. The master mould was prepared using standard photolithographic techniques as described in detail elsewhere. Briefly, the microfluidic device consisted of a structured PDMS slab attached to a glass coverslip using oxygen plasma activation. The PDMS device comprised four input channels cross-sectional dimensions of 50 μm × 50 μm. These input channels converged to form a 10 mm long channel (the main microfluidic channel) that was 250 μm wide and 50 μm high. Inlets were connected to reagent reservoirs, and the outlet to a collection vessel, using Teflon tubing (PKM SA, Switzerland).

5.4.2. Synthesis

Synthesis of MF-CCP-4. In a typical experiment, solutions of iron(II) tetrafluoroborate hexahydrate (15.7 mM) and 4,4′-bis((1Htetrazol-1-yl)methyl)-1,1′-biphenyl (31.4 mM) in acetonitrile were injected into the two middle input channels while two pure acetonitrile flows were injected into the sheath channels. All four input flows were injected at a flow rate of 50 $\mu L \cdot min^{-1}$ using a syringe pump system (neMESYS module, Cetoni GmbH) that provided for precise control over flow rates in all channels. The turbid effluent solution was continuously collected in a 5 mL glass vial for 10

minutes, resulting in 2 mL of sample. To study crystal growth at different time intervals, a drop of sample was poured over a TEM grid (200 mesh, gold-based carbon support film, Quantifoil®) for TEM analysis. The TEM grids were prepared at 1, 3, 6, 12, and 24 hours.

Synthesis of (CCP-4). A solution of iron(II) tetrafluoroborate hexahydrate (15.7 mM) was added into a solution of 4,4′-bis((1Htetrazol-1-yl)methyl)-1,1′-biphenyl (31.4 mM) in acetonitrile. A white crystalline precipitate appeared.

5.4.3. Structural characterization

5.4.3.1. X-ray powder diffraction, phase purity

X-ray powder diffraction measurements were performed on an Empyrean PANalytical powder diffractometer, using Cu Kα radiation (λ = 1.54056 Å). **MF-CCP-4** was filled into 0.5 mm borosilicate capillary prior to being mounted and aligned. Two repeated measurements were collected at room temperature (2θ = 2–40°) and merged in a single diffractogram.

5.4.3.2. Scanning electron microscopy

SEM images were performed on a Hitachi S-4800 microscope operating at an accelerating voltage of 10 kV after metallization of the samples (Au-Pd).

5.4.3.3. Transmission electron microscopy

Transmission electron microscopy (TEM) images were collected on a JEOL JEM-1010. All measurements were performed at the acceleration voltage of 100 kV. High-resolution transmission electron microscopy images and EDX

microanalysis were obtained using a TECNAI G2F20 S-TWIN HR microscope operating at 200 kV.

5.4.4. Magnetic measurements

Magnetic susceptibility measurements were carried out on single-phased polycrystalline samples with a Quantum Design MPMS-XL-5 SQUID susceptometer. The susceptibility data were all collected at 1 K min^{-1}, with an applied field of 0.1 T.

5.5 REFERENCES

1. Aida, T., Meijer, E. W. & Stupp, S. I. Functional Supramolecular Polymers. *Science* **335**, 813–817 (2012).
2. Llordés, A., Garcia, G., Gazquez, J. & Milliron, D. J. Tunable near-infrared and visible-light transmittance in nanocrystal-in-glass composites. *Nature* **500**, 323–326 (2013).
3. Yaghi, O. M. *et al.* Reticular synthesis and the design of new materials. *Nature* **423**, 705–714 (2003).
4. Coronado, E. & Mínguez Espallargas, G. Dynamic magnetic MOFs. *Chem. Soc. Rev.* **42**, 1525–1539 (2013).
5. Nagarkar, S. S., Desai, A. V. & Ghosh, S. K. Stimulus-Responsive Metal–Organic Frameworks. *Chem. – Asian J.* **9**, 2358–2376 (2014).
6. Lin, Z.-J., Lü, J., Hong, M. & Cao, R. Metal–organic frameworks based on flexible ligands (FL-MOFs): structures and applications. *Chem. Soc. Rev.* **43**, 5867–5895 (2014).
7. McConnell, A. J., Wood, C. S., Neelakandan, P. P. & Nitschke, J. R. Stimuli-Responsive Metal–Ligand Assemblies. *Chem. Rev.* **115**, 7729–7793 (2015).

8. Sato, O. Dynamic molecular crystals with switchable physical properties. *Nat. Chem.* **8**, 644–656 (2016).
9. Ohtani, R. & Hayami, S. Guest-Dependent Spin-Transition Behavior of Porous Coordination Polymers. *Chem. – Eur. J.* **23**, 2236–2248 (2017).
10. Lustig, W. P. *et al.* Metal–organic frameworks: functional luminescent and photonic materials for sensing applications. *Chem. Soc. Rev.* **46**, 3242–3285 (2017).
11. Yoreo, J. J. D. *et al.* Crystallization by particle attachment in synthetic, biogenic, and geologic environments. *Science* **349**, (2015).
12. Cölfen, H. Bio-inspired Mineralization Using Hydrophilic Polymers. in *Biomineralization II* 1–77 (Springer, Berlin, Heidelberg, 2006).
13. Li, L., Weaver, J. C. & Ortiz, C. Hierarchical structural design for fracture resistance in the shell of the pteropod *Clio pyramidata*. *Nat. Commun.* **6**, 6216 (2015).
14. Sevim, S. *et al.* Self-assembled materials and supramolecular chemistry within microfluidic environments: from common thermodynamic states to non-equilibrium structures. *Chem. Soc. Rev.* **47**, 3788–3803 (2018).
15. Elvira, K. S., Solvas, X. C. i, Wootton, R. C. R. & deMello, A. J. The past, present and potential for microfluidic reactor technology in chemical synthesis. *Nat. Chem.* **5**, 905–915 (2013).

16. Mason, T. O. *et al.* Synthesis of Nonequilibrium Supramolecular Peptide Polymers on a Microfluidic Platform. *J. Am. Chem. Soc.* **138**, 9589–9596 (2016).

17. Rubio-Martinez, M. *et al.* Freezing the Nonclassical Crystal Growth of a Coordination Polymer Using Controlled Dynamic Gradients. *Adv. Mater.* **28**, 8150–8155 (2016).

18. Calvo Galve, N. *et al.* Isostructural compartmentalized spin-crossover coordination polymers for gas confinement. *Inorg. Chem. Front.* **3**, 808–813 (2016).

General Conclusions

This thesis has been focused on the synthesis and study of spin-crossover compartmentalized coordination polymers (CCPs). This includes the crystallization of these materials, the tuning of its magnetic properties, the inclusion of gas molecules inside their isolated cavities, separation of gases and study of its crystallization processes.

Different strategies have been carried out to overcome the tuning of the spin transition. For example, in *chapter 2*, it has been demonstrated that the inclusion of gas molecules inside the isolated cavities can modify the spin transition temperature. The presence of gases with electric quadrupolar moment subtle modify the ligand field affecting the iron (II) center, thus modifying the spin transition temperature. Depending on the sign of the quadrupolar moment, the modification of the spin transition temperature occurs in different manners: stabilizing the low-spin state, then increasing the transition temperature or stabilizing the high-spin state, then decreasing the transition temperature. Gases with no permanent quadrupolar moment do not affect the transition. Gas sorption studies in compartmentalized coordination polymers are challenging from the point of view that the presence of no permanent channels could made the gas inclusion a difficult task. In *chapter 2* the gas sorption studies of diverse gases have been performed, observing the capacity of **CCP-1** and **CCP-2** to locate one molecule of diverse gas molecules inside their isolated cavities whereas other gases remain unabsorbed. This fact has been used performing gas breakthrough studies, obtaining good performances in separation for CO_2 over N_2 or CH_4. These results demonstrate that the strategy used in this thesis, that is, the use of discrete compartments to locate gas molecules, is a perfect approach to

consider in the field of gas mixtures purification. Further investigations in the synthesis of CCPs derivatives could be a useful way to perform effective gas separations in the future.

But not only with a chemical-stimuli the transition temperature can be modified. In *chapter 3*, it has been demonstrated that an easy and successful way to tune the spin transition temperature is the combination of different ligands, synthesizing chemical mixtures of coordination polymers with the presence of two different ligands. Both ligands are similar in structural features but by separately they afforded coordination compounds with so differentiate magnetic properties. The gradual inclusion of one ligand to form hybrid structures afforded new transitions when new coordination environments in the iron (II) centers appear.

But the gas sorption in these materials can be enhanced modifying the ligand topology. In *chapter 4*, a bis-tetrazole ligand has been synthesized, larger in size than the previous reported one. It afforded the synthesis of **CCP-3** and **CCP-4**, two CCPs than almost double the internal cavities of **CCP-1** and **CCP-2**. The gas capacity of CO_2 has been doubled in these materials, permitting the adsorption of two molecules of CO_2 per void. The magnetic properties of these materials have been maintained and could be modified by the inclusion of CO_2 molecules. In addition, the possibility to deposit compartmentalized coordination polymers in a 2D substrate has been performed, and it maintain its magnetic and crystalline properties. Further

investigations in the preparation of membranes to selective gas sorption with these types of materials could be studied.

Finally, in *chapter 5* the crystallization process of CCPs has been performed using microfluidics. **CCP-4** has been synthesized using a microfluidic device, permitting to "freeze" the crystallization process during the kinetic conditions. Two different pathways have been found but regardless the pathway, the final product is the same that the thermodynamic one: hexagonal microcrystal. In addition, some mesoscale assembly has been found in the analysis of the thermodynamic synthesis, with the perfect self-assembly of smaller hexagon particles forming a bigger hexagonal one. The possibility to pathway selection using microfluidics open the possibility to study the crystallization processes of other similar materials, selecting a desired growing pathway despite its forbidden nature in thermodynamic conditions on a laboratory.

Resumen de la Tesis Doctoral

Objetivos

El objetivo general de esta tesis es la preparación de polímeros de coordinación multifuncionales que presenten la propiedad de transición de espín y adsorción de gases. Respecto a la primera, se estudiará la manera de modificar a nuestro antojo la transición y para ello se utilizarán dos aproximaciones: la primera, ayudada por la segunda propiedad de adsorción de gases, será el aprovechar la adsorción de estas moléculas para influir en las propiedades electrónicas del centro de hierro (II), modificando el campo de ligandos que sufre este y por tanto, modificando la transición de espín; la segunda aproximación será la combinación de diferentes ligandos orgánicos que compartan la misma topología de coordinación y por separado den lugar a materiales de muy distinta índole magnética. La combinación de ambos será clave para generar nuevos entornos de coordinación en los centros de hierro (II), provocando la creación de nuevas transiciones de espín a distintas temperaturas. Además, otro objetivo adicional es el estudio del crecimiento cristalino de estos materiales.

Metodología

Síntesis

En esta tesis se han llevado a cabo diferentes técnicas de síntesis para completar los objetivos de la misma. Para empezar, los ligandos orgánicos utilizados en la construcción de polímeros de coordinación han sido sintetizados a partir de precursores previos. Para ello se han aplicado las distintas técnicas de síntesis orgánica aprendidas en la formación universitaria previa, afrontando los diversos problemas que estas presentan. Desde

sustituciones nucleofílicas aromáticas, pasando por reducciones de grupos azida a amina utilizando hidruro de aluminio y litio o ciclación de compuestos aromáticos, los ligandos orgánicos diseñados previamente "sobre el papel" para utilizar en esta tesis se han podido sintetizar sin problema.

Respecto a la parte más inorgánica de la tesis, la síntesis de los polímeros de coordinación, se han utilizado las diversas técnicas de crecimiento cristalinos aprendidas durante el doctorado. Se han llevado a cabo exitosamente la síntesis de diversos polímeros de coordinación utilizando métodos de "one pot", esto es, la mezcla directa a temperatura ambiente de los componentes básicos del polímero de coordinación (disoluciones de ligando orgánico y de la sal del metal a utilizar). Estas síntesis también se han llevado a cabo en otra variable, la del reflujo, cuando la mezcla de estos materiales necesita de temperatura para poder formar exitosamente los enlaces de coordinación. Esta última técnica en ocasiones puede resultar costosa en tiempo y materiales, por lo que en algunas de las síntesis presentadas en esta tesis se ha optimizado la síntesis de reflujo pudiendo realizar la formación del polímero de coordinación en un horno microondas. La optimización de este tipo de síntesis ha permitido reducir algunos tiempos de reacción de 4 horas a 5 minutos. Por último, los materiales de más alta cristalinidad han sido obtenidos gracias a las reacciones solvotermales, esto es, síntesis llevadas a cabo en hornos químicos dentro de unos viales especiales cerrados que permiten alcanzar temperaturas superiores a la temperatura de ebullición del disolvente.

Técnicas de caracterización

Rayos-X de monocristal

La cristalografía de rayos X de monocristal nos permite conocer las estructuras cristalinas de los compuestos siempre y cuando se disponga de un monocristal del material que difracten los haces de rayos X. Se basa en el principio de que los electrones de los átomos difractan los rayos X recibidos, este haz resultante y medido por el detector contiene información sobre el número de electrones y la posición del átomo de nuestro material. Análisis posteriores con métodos matemáticos nos permiten obtener las estructuras cristalinas de los compuestos.

En esta tesis, las estructuras cristalinas resueltas a partir de los respectivos monocristales han sido medidas a 120 y 240 K (debido al carácter de transición de espín y el cambio estructural que conlleva) en un difractómetro SUPERNOVA equipado con una fuente de rayos X monocromada (Mo). Para la resolución de las estructuras por métodos matemáticos se han utilizado el paquete de programas SHELXTL y como interfaz gráfica el programa OLEX-2. Los parámetros de recopilación y refinamiento de datos se muestran en cada capítulo correspondiente.

Rayos-X de polvo

Esta técnica se ha utilizado para comprobar la pureza de las distintas muestras cristalinas, comparando con los patrones obtenidos en el difractómetro de rayos X de monocristal. Es una técnica muy útil para poder detectar impurezas en el material. Se basa en la incidencia de los rayos X sobre una muestra del

material introducida en un capilar de 0.5 mm de diámetro de borosilicato (material amorfo, invisible a los rayos X por lo que no interfiere en la medida). Los rayos X salen difractados de la muestra con un ángulo theta (θ), y debido a la ley de Bragg de la diffracción ($n\lambda = 2 \cdot d \cdot \text{sen}\theta$), se pueden establecer las relaciones de las distancias interatómicas. El detector se mueve, recogiendo los distintos ángulos a los que difracta la muestra y recogiendo el difractograma de polvo que contiene información sobre la estructura cristalina de la muestra. Las medidas se realizaron en un equipo Empyrean PANalytical con dos barridos acumulados en el rango de θ de 2 a 60 º.

Medidas magnéticas

Las medidas magnéticas realizadas a los compuestos presentados en esta tesis se realizaron con un magnetómetro de tipo SQUID "Quantum Design MPMS-XL-5". SQUID es el acrónimo inglés para "Superconducting Quantum Interference Device" cuya traducción sería "Dispositivo Superconductor de Interferencia Cuántica". Estos susceptómetros son capaces de medir señales magnéticas muy pequeñas con muy poco ruido. Las medidas de este trabajo se realizaron generalmente en el intervalo de temperaturas entre 2 y 300 K y aplicando campos magnéticos de 0.1 T sobre las muestras poli-cristalinas de los compuestos. Después de realizar las medidas, los datos de susceptibilidad se corrigen para eliminar la contribución del porta-muestras donde se mide y de las contribuciones diamagnéticas mediante las constantes de Pascal.

Resumen y conclusiones

El trabajo descrito en esta tesis se enmarca dentro de los polímeros de coordinación compartimentalizados. Los polímeros de coordinación son materiales híbridos orgánicos-inorgánicos formados por un metal rodeado por unos ligandos orgánicos unidos mediante enlace de coordinación y se pueden obtener estructuras que se extienden en una, dos o tres direcciones del espacio. Las infinitas posibilidades que existen debido a la gran variedad de metales disponibles y especialmente, a la posibilidad de sintetizar múltiples ligandos orgánicos permite diseñar químicamente materiales con propiedades "a la carta", además de la posibilidad de presentar multifuncionalidad, esto es, la combinación de diversas propiedades haciendo el material mucho más interesante. Cuando un polímero de coordinación presenta la característica de porosidad, esto es, presenta canales internos capaces de alojar huéspedes, ya sean disolventes, gases u otras moléculas, al polímero de coordinación se le llama Metal-Organic Framework (MOF), redes metal-orgánicas.

Dentro de estas múltiples propiedades tenemos la estabilidad química, muchas veces necesaria para poder preparar un material útil ya que estará expuesto al ataque de diversos agentes químicos que pueden desgastarlo e inutilizar sus interesantes propiedades. Los MOFs además presentan altas áreas superficiales, haciéndolos candidatos perfectos para su uso en catálisis. La posibilidad de utilizarlos como células de combustible también se ha explorado, con la medida de sus propiedades conductoras. Pero la característica estrella de los MOFs como ya se ha comentado es la que les da su particular designación como sub-clase de polímero de coordinación y esta es la presencia de porosidad. La posibilidad de alojar huéspedes en el interior

de estos compuestos (y lo que puede conllevar en la modificación de otra de sus propiedades) ha hecho a estos materiales ser uno de los campos en auge desde hace 20 años. En 1998 se reportó el primer ejemplo de adsorción de gases en uno de estos materiales, midiendo la adsorción de dióxido de carbono y de nitrógeno en el llamado MOF-5. En los siguientes años, el intenso estudio en el campo de los MOFs permitió ir aumentando cada vez más la capacidad de almacenar cada vez más cantidad de gases.

Pero con el tiempo, la simple idea de almacenar cada vez más cantidad de gas dio paso a otra idea muy interesante, derivada de las necesidades medioambientales del planeta: la separación de gases. Se comenzó a estudiar otro tipo de MOFs, los llamados MOFs de ultramicroporo, donde en lugar de buscar una apertura de poro mayor para poder almacenar más cantidad de gas, se busca un poro más pequeño capaz de discriminar entre diferentes gases que compongan una mezcla. La producción de residuos en la industria petroquímica y electrónica lleva al desarrollo de nuevos materiales capaz de eliminar las impurezas originadas en la producción de sus materiales y los MOFs son candidatos perfectos para llevar a cabo esta tarea. Por ejemplo, la producción de acetileno puro es un problema debido a que se genera una mezcla gaseosa de acetileno/dióxido de carbono. En 2005 se reportó un MOF que podía separar eficientemente esta mezcla gaseosa. El MOF de cobre reportado podía adsorber el acetileno mucho mejor que el dióxido de carbono, permitiendo la separación de esta mezcla. Pero realmente la mayor utilidad sería poder adsorber la impureza de dióxido de carbono, ya que en este primer material luego es necesario el coste de liberar el acetileno del material. Por ello, en 2016 se demostró que esto era posible, con la publicación de un

trabajo donde se sintetizó un MOF de manganeso. A bajas presiones, se demostraba que este material podía adsorber dióxido de carbono preferentemente sobre acetileno. Los autores hipotetizaron sobre este comportamiento debido a la interacción entre el momento cuadrupolar del gas y la red metal-orgánica.

Otra mezcla de gases interesante de separar es la formada por etileno/acetileno. El etileno es utilizado ampliamente en la fructífera industria de los polímeros, pero en su producción se generan diversas impurezas, entre ellas acetileno. En 2017 se publicó sobre un MOF que permitía separar eficientemente mezclas de acetileno y etileno.

La otra propiedad estrella que pueden presentar los MOFs, además de su intrínseca porosidad, es el magnetismo. El magnetismo es una propiedad que pueden presentar los materiales basada en los portadores de espín. Los MOFs magnéticos se pueden dividir entre los que presentan interacciones magnéticas de largo rango, los que tienen centros single-molecule magnets (SMMs) y los que presentan spin-crossover.

La presencia de interacciones magnéticas de largo rango y porosidad es un desafío al que se han tenido que enfrentar los químicos para combinar estas dos propiedades contrarias: el magnetismo necesita distancias cortas entre los centros metálicos para poder propagar eficientemente el canje magnético y la porosidad necesita largas distancias para poder generar poros más grandes. Diversas estrategias se han llevado a cabo para poder sortear este inconveniente. Se han utilizado ligandos cortos que aún así generaban

estructuras porosas, de hecho, en 2002 se reportó un sistema usando uno de los grupos más cortos, el grupo CN, que presentaba magnetismo y además la adsorción de moléculas de oxígeno por el material modificaba sus propiedades magnéticas. Otra estrategia llevada a cabo es combinar dos tipos de ligandos: uno corto para obtener un canje magnético eficiente en la estructura y otro más largo a modo de "pilar" que permita obtener grandes poros. La familia del MOF-74 es un claro ejemplo de esta metodología, pudiendo haber sintetizado una gran variedad de derivados cambiando el centro metálico (zinc, cobalto, níquel, magnesio, manganeso, cobre, hierro...). El derivado de hierro se reportó en 2012, demostrando además que el canje magnético del MOF se podía modificar con la adsorción de distintos hidrocarburos. Dependiendo de lo fuerte que sea la interacción del hidrocarburo y la red metal-orgánica, el cambio en el magnetismo es diferente. Otra posibilidad es la utilización de radicales orgánicos como ligandos, debido a que la presencia de los espines individuales que poseen pueden promover interacciones de canje efectivas. En 2002 se publicó el primer ejemplo de un MOF con ligandos orgánicos radical y presentando propiedades magnéticas, aunque a muy baja temperatura.

Los single-molecule magnets (SMMs) son moléculas magnéticas que presentan baja relajación de la magnetización a bajas temperaturas. La inclusión de estas interesantes moléculas en los nodos de un MOF se produjo por primera vez en 2004, permitiendo estudiar eficientemente el magnetismo en estos materiales. Pero un derivado de los SMMs se desarrolló posteriormente y estos fueron los single-ion magnets (SIMs). Basados en complejos metálicos mononucleares con iones de alta anisotropía magnética,

tienen la particularidad que son interesantes en el campo de la computación quántica ya que pueden ser considerados como bits cuánticos. El primer ejemplo de MOFs presentando SIMs en los nodos metálicos se produjo en 2014 en nuestro propio grupo. Se sintetizó toda una familia de SIM-MOFs usando diferentes lantanoides.

La última propiedad magnética que pueden presentar los MOFs es la transición de espín. El primer ejemplo de este fenómeno se reportó en 1930, pero no pudo ser explicado eficientemente hasta años más tarde, cuando las teorías de campo cristalino y su evolución, la del campo de ligandos se establecieron. El fenómeno se puede explicar cuando un metal de transición sufre la degeneración energética de sus cinco orbitales d en presencia de un campo octaédrico de ligandos. Se forman tres orbitales no enlazantes de menor energía y dos orbitales antienlazantes de mayor energía. El fenómeno de la transición de espín puede aparecer en iones de metales de la primera serie de transición con configuraciones electrónicas de d^4 a d^7 pero el ion estrella estudiado en la transición de espín es el hierro II, presentando una configuración d^6. Estos 6 electrones tienen dos maneras de distribuirse entre los 5 orbitales degenerados comentados anteriormente y depende de la diferencia energética entre estos dos grupos de orbitales (llamada energía de campo cristalino) y la energía de apareamiento de los electrones, P. Cuando P es mucho mayor que la energía de campo cristalino, los electrones se colocan distribuidos entre todos los orbitales maximizando la multiplicidad y obteniendo un espín total a 2, llamado el estado de alto espín (AE). En el caso energético contrario, los seis electrones se aparean en los tres orbitales d de menor energía, resultando en un espín total a 0, llamado el estado de bajo

espín (BE). Cuando la energía del campo de ligandos y la energía de apareamiento son cercanas, puede haber una transición entre ambos estados mediante un estímulo externo, ya sea temperatura, presión o luz y entonces ocurre el fenómeno de la transición de espín, el cambio de AE a BE y viceversa.

La primera vez que se reportó un polímero de coordinación presentando transición de espín fue en 1995 y desde entonces el campo ha sido ampliamente estudiado. Para producir una buena transición de espín es necesaria una cooperatividad elástica, es decir, la transición de espín se genera inicialmente en un centro metálico y se extiende por toda la red. Para poder llevar a cabo esto en un polímero de coordinación infinito, es necesario tener unos ligandos orgánicos apropiados que conecten los centros metálicos además de una estructura cristalina sin defectos. Cuando se cumplen ambos requisitos, tenemos transiciones de espín abruptas. Un tipo de compuesto que cumple estas características son los llamados clatratos de Hofmann. La fórmula general de estos compuestos es $\{Ni(NH_3)_2[Ni(CN)_4]\} \cdot 2\ G$ siendo G un huésped interno. Se descubrieron a principios del siglo XX pero no fue hasta mediados cuando su estructura fue resuelta. Hasta 1996 no se introdujeron centros de hierro II en derivados de clatratos de Hofmann y fue entonces cuando apareció la transición de espín en este tipo de compuestos. En los años posteriores el desarrollo de derivados cambiando el resto de átomos de la fórmula introdujo ricas variaciones para el desarrollo y el estudio de la transición de espín en polímeros de coordinación.

Pero en esta tesis se han utilizado otro tipo de ligandos orgánicos con un grupo funcional determinado, los tetrazoles. Los tetrazoles son un tipo de compuesto orgánico heterocíclico aromático, compuesto por cuatro átomos de nitrógeno y uno de carbono. Tienen una buena capacidad de coordinación a centros metálicos debido a sus nitrógenos dadores de densidad electrónica. Además, cuando se coordinan en entornos de coordinación octaédricos a centros de hierro II, producen un campo de ligandos apropiado para obtener el fenómeno de la transición de espín. Los años 80 y 90 fueron muy fructíferos en la publicación de trabajos donde se presentaban complejos mononucleares de hierro II con tetrazoles coordinados exhibiendo transición de espín. No fue hasta el año 2000 que se publicó el primer polímero de coordinación basado en tetrazoles que presentaba transición de espín. El polímero en cuestión tenía una estructura linear que se extendía infinitamente en una dirección del espacio, presentando una transición de espín gradual.

En los años siguientes el campo se extendió en gran medida, publicando otros compuestos 1D pero también 2D y 3D basados en tetrazoles. Los estudios se centraron en principio en añadir cada vez más átomos de carbono alifáticos situados entre los dos grupos tetrazoles. Diversas topologías y transiciones de espín se fueron publicando a lo largo de la década de los 2000, aunque la mayoría mantenía la primera topología encontrada de cadenas 1D donde los centros metálicos de hierro II estaban conectados por tres ligandos bis-tetrazoles, extendiendo la estructura infinitamente.

Una vez establecida la transición de espín en los polímeros de coordinación, uno de los desafíos a los que se enfrentó el mundo científico fue la capacidad

para modificar esa transición de espín mediante un estímulo químico. La coexistencia de porosidad y transición de espín en los MOFs es una aproximación perfecta, pues la inclusión de moléculas huésped dentro del MOF puede llegar a modificar dicha transición. Nuestro grupo publicó en 2013 el primer trabajo donde la adsorción de un gas modificaba la transición de espín. El compuesto en cuestión es un polímero de coordinación de hierro II basado en ligando bis-tetrazol. La estructura está formada por cadenas 1D que se extienden infinitamente, donde los centros de hierro II están triplemente conectados por ligandos bis-tetrazoles, dejando cavidades aisladas donde se pueden alojar gases. El polímero de coordinación presenta transición de espín y los estudios de adsorción de gases demostraron que el material adsorbía preferentemente dióxido de carbono sobre nitrógeno. Además, esta adsorción de dióxido de carbono modificaba la transición de espín debido a la interacción del momento cuadrupolar del CO_2 con el anillo de tetrazol, cambiando ligeramente el campo de ligandos y por ello, la transición de espín.

En esta tesis se ha estudiado en profundidad la formación de estos sistemas de polímeros de coordinación compartimentalizados, es decir, que presentan cavidades aisladas en su interior capaces de alojar gases. La presencia de hierro II y ligandos tipo tetrazol ha permitido obtener transición de espín en todos los compuestos, además de poder modificar esta. También se ha estudiado el crecimiento cristalino.

En el *capítulo 2*, se trató la posibilidad de adsorber y separar distintos gases en dos polímeros de coordinación compartimentalizados previamente

reportados, **CCP-1** y **CCP-2**. Ambos son isoestructurales y presentan la fórmula $[Fe(btzx)_3](ClO_4)_2$ y $[Fe(btzx)_3](BF_4)_2$, respectivamente, siendo btzx un ligando bis-tetrazol. Ambos presentan cavidades aisladas en el interior de su estructura cristalina y una transición de espín centrada a unos 200 K. Previamente ya se reportó el estudio de adsorción de nitrógeno y dióxido de carbono en estos materiales, pero en este *capítulo* se repitió además de extenderse con CO (monóxido de carbono), CH_4 (metano), C_2H_6 (etano), C_2H_4 (etileno) y C_2H_2 (acetileno). En las isotermas de adsorción ya se aprecian algunos problemas de difusividad en algunos gases, observando como el polímero de coordinación puede adsorber aproximadamente una molécula de dióxido de carbono, metano, acetileno y etileno; por el contrario, el monóxido de carbono, el nitrógeno y el eteno quedan prácticamente sin adsorber. Los valores volumétricos en adsorción son bastante competitivos dentro del campo de los materiales para adsorción, debido a la estructura intrínseca del material, pues estos polímeros de coordinación compartimentalizados presentan una estructura "densa", debido a la ausencia de canales permanentes.

Se realizaron medidas en el sincrotrón ALBA, Barcelona, para poder determinar la localización de las moléculas gaseosas en el interior de las cavidades en colaboración con el Dr. I. J. Vitórica-Yrezábal. El uso de cavidades discretas conlleva la ventaja de que las moléculas de gas están confinadas en un menor espacio, favoreciendo la interacción entre estas y la red metal-orgánica. Los difractográmas de polvo de la muestra cargada con dióxido de carbono, acetileno y metano se midieron en el sincrotrón y mediante refinamiento Rietveld se pudo determinar la posición exacta de las

moléculas gaseosas en el interior de las cavidades, demostrando que estas interaccionan con el anillo de tetrazol. El magnetismo de la muestra con los distintos gases adsorbidos en su interior también se ha medido exitosamente, encontrando que diferentes gases modificaban la transición de espín de una manera diferente. Por ejemplo, el dióxido de carbono estabiliza el estado de bajo espín, desplazando la transición a mayores temperaturas; sin embargo, el etileno estabiliza el estado de alto espín, desplazando la transición a menores temperaturas. Esto puede ser explicado debido al distinto signo del momento cuadrupolar de ambos gases.

Por último, se realizaron medidas breakthrough de separación de mezclas gaseosas de dióxido de carbono/nitrógeno y dióxido de carbono/metano. Las medidas fueron exitosas, demostrando que el polímero de coordinación compartimentalizado podía separar eficientemente el dióxido de carbono de los otros gases en sus respectivas mezclas presentando selectividades competitivas respecto al resto de materiales del campo de separación de gases.

La conclusión de este capítulo es que se han sintetizado eficientemente dos polímeros de coordinación compartimentalizados que además de presentar interesantes propiedades magnéticas, estas pueden ser modificadas tras la inclusión de gases, además de ser capaz de separar dióxido de carbono respecto nitrógeno y metano, abriendo la posibilidad de ampliar el estudio de estos polímeros compartimentalizados como uno de los mejores materiales para estudiar la separación y purificación de mezclas gaseosas.

En el *capítulo 3* se estudió en profundidad la posibilidad de modificar la transición de espín. De todas las aproximaciones para poder modificar la transición de espín se utilizó una de las más efectivas: la posibilidad de combinar dos ligandos con ligeras diferencias estructurales pero que mantengan el mismo centro de coordinación. Dos polímeros de coordinación previamente reportados, $[Fe(btzx)_3](ClO_4)_2$ y $[Fe(btix)_3](ClO_4)_2$ presentan ligandos muy parecidos: btzx es un bis-tetrazol (4 átomos de nitrógeno en el heterociclo aromático) y btix es un bis-triazol (3 átomos de nitrógeno en el heterociclo aromático). Son isoestructurales, aunque el ligando btix adopta una conformación ligeramente diferente, obteniendo una estructura ligeramente más torsionada. El mayor cambio se observa en sus propiedades magneticas: mientras el derivado de tetrazol muestra una transición de espín centrada a 200 K el derivado de triazol se mantiene en alto espín en todo el rango de temperaturas. La posibilidad de crear una estructura híbrida con ambos ligandos presentes es el trabajo de este *capítulo*, donde se prepararon eficientemente una familia de polímeros de coordinación, usando diluciones de ligando. Así, se prepararon diferentes síntesis combinando distintas proporciones de ligando, empezando con una alta proporción de ligando tetrazol que es el que provoca la transición de espín y añadiendo poco a poco ligando triazol. También se preparó una mezcla física de ambos compuestos para comprobar la naturaleza química de las mezclas que se estaban sintetizando.

Los análisis Pawley de los difractogramas de polvo de las distintas diluciones químicas de ligando mostraron solo una fase cristalina hasta que el porcentaje de triazol utilizado llegó al 30%, donde empezó a verse ligando sin

reaccionar. Cuando el ligando triazol utilizado llegó al 50%, una mezcla física de ambos compuestos se encontró en el difractograma de polvo. El magnetismo de las muestras sintetizadas demostró que se había logrado crear una estructura híbrida de ambos ligandos: a bajas concentraciones de triazol utilizado, además de la transición de espín original, se genera una nueva transición de espín centrada a 140 K, además de un pequeño desplazamiento de la transición original de 200 K. En la red infinita de centros de hierro II con 3 ligandos tetrazol sirviendo de puentes, cuando se va introduciendo triazol en la mezcla inicial, el triazol se inserta en algunas partes de la cadena, generando un nuevo entorno de coordinación de 5 tetrazoles y 1 triazol en el hierro II, lo que provoca la aparición de la nueva transición. Además, el carácter torsionado del triazol hace que se ejerza una presión química interna en la estructura, la responsable de desplazar ligeramente la transición original. Conforme aumentamos la cantidad de triazol, la transición original disminuye en intensidad y la nueva aumenta, confirmando la teoría. Además, en cierto momento dos triazoles coincidirán uno al lado del otro, generando un nuevo entorno octaédrico de 4 tetrazoles y 2 triazoles, generando una nueva transición. Esto se observa cuando llegamos a un 20% de triazol, generando una nueva transición de espín a 60 K. Conforme aumentamos más la cantidad de triazol, se pierde la coherencia estructural debido a la presión a la que se ve sometida la estructura, y para un % de triazol igual a 50 se obtiene una mezcla física de ambos componentes separados.

Como conclusión a este capítulo se han sintetizado exitosamente toda una familia de diluciones químicas de un sistema de transición de espín original, observando como no solo se puede modificar la transición original, sino que

se pueden sintetizar sistemas con múltiples transiciones de espín, generando distintos entornos octaédricos en los centros metálicos de hierro II, siendo esta una aproximación sencilla de llevar a cabo y resolviendo muchos de los problemas encontrados en la búsqueda de la modificación de la curva de transición de espín en los polímeros de coordinación.

En el *capítulo 4* se sintetizaron exitosamente dos nuevos polímeros de coordinación compartimentalizados, isoestructurales a **CCP-1** y **CCP-2** y llamados **CCP-3** y **CCP-4**, de fórmula $[Fe(btzbp)_3](ClO_4)_2$ y $[Fe(btzbp)_3](BF_4)_2$ respectivamente. El ligando btzbp es otro ligando bis-tetrazol, pero con un anillo de benceno más, en total 2 anillos comparado con el anillo presente en btzx. La motivación de diseñar químicamente este ligando fue la posibilidad de generar cavidades discretas más grandes en los polímeros de coordinación compartimentalizados, pudiendo expandir la posibilidad de adsorción de gases y el estudio magnético. Mediante el diseño químico del ligando, se realizó la síntesis de este a partir de precursores comerciales, pudiendo llevarla a cabo en 3 pasos de síntesis orgánicas. En la primera, una reacción de sustitución nucleofílica permitía cambiar los grupos Br terminales por grupos N_3. Una reducción mediante hidruro de aluminio y litio en el segundo paso redujo el grupo azida a amina, y finalmente se realizó la ciclación aromática del anillo de tetrazol a partir de la amina, azida de sodio y trietil ortoformato. La pureza del ligando fue comprobada por resonancia magnética nuclear.

Se realizaron las síntesis inorgánicas a reflujo utilizando las cantidades adecuadas de ligando y de las correspondientes sales de hierro II, obteniendo

los materiales cristalinos **CCP-3** y **CCP-4**, comprobando su pureza, cristalinidad y carácter isoestructural de ambos por difracción de rayos X de polvo. Un monocristal de **CCP-4** se pudo obtener, resolviendo su estructura cristalina y comprobando que se obtenía el polímero de coordinación compartimentalizado, análogo a **CCP-1** y **CCP-2** pero con cavidades internas mayores.

Se realizó un estudio de adsorción de gases para dióxido de carbono, nitrógeno y metano. De las isotermas de adsorción de gases se desprende que nitrógeno y metano apenas se adsorben, pero mostrando una capacidad de adsorber dos moléculas de dióxido de carbono por cavidad interna. Como se quiso demostrar al diseñar químicamente este sistema, la capacidad de **CCP-1** y **CCP-2** se ha doblado, ya que en estos sistemas previos la capacidad era de una molécula de dióxido de carbono por cavidad.

El magnetismo de **CCP-3** y **CCP-4** se estudió, comprobando que mantienen una transición de espín relativamente abrupta a 195 y 199 K respectivamente, incluso para centros de hierro II tan separados en el espacio. Esto es debido a la buena cooperatividad elástica del sistema, debido al triple puente tetrazol que propaga efectivamente la transición de espín por toda la red cristalina. También se estudió la capacidad de modificar esta transición tras adsorber dióxido de carbono, estudiando que, para la adsorción parcial del sistema de una molécula, la transición podía moverse 7 K a temperaturas mayores, estabilizando el estado de bajo espín como en el caso de **CCP-1** y **CCP-2**. Sorprendentemente, cuando el sistema adsorbe dos moléculas de dióxido de carbono, la transición solo se desplaza 3 K respecto a la original. Inicialmente,

se podía esperar el efecto acumulativo, esto es, el momento cuadrupolar de una molécula de dióxido de carbono afecta a la densidad electrónica del anillo de tetrazol, modificando su transición y una segunda molécula podía desplazar todavía más esta transición. El efecto observado está relacionado con cierta interacción interna entre las moléculas de dióxido de carbono, disminuyendo el momento cuadrupolar total que afecta al anillo de tetrazol y por consiguiente, desplazando la transición de espín una menor temperatura.

Para acabar, se llevaron a cabo estudios de deposición del sistema en sustratos de silicio y cuarzo, pudiendo obtener una buena deposición de este en el de silicio. La caracterización por rayos X y el magnetismo revelan que el sistema mantiene sus propiedades cuando este es depositado sobre una superficie en dos dimensiones.

Como conclusión, el diseño químico de un ligando más largo para obtener un sistema con mayores cavidades internas y permitir una mayor adsorción de moléculas de gas y el estudio de sus propiedades magnéticas se ha realizado con éxito. Esto abre posibilidades al estudio de estos sistemas, incluyendo distintas funcionalidades en el diseño de nuevos ligandos con diferentes espaciadores entre los anillos de tetrazol, permitiendo cómo afecta esta característica a sus propiedades de adsorción de gases y magnéticas. Además, la posibilidad de depositar estos interesantes sistemas en dos dimensiones abre la posibilidad de poder fabricar membranas de adsorción de gases que contengan estos polímeros de coordinación compartimentalizados. Los estudios de separación de gases en este sistema con mayor cavidad interna también puede ser un interesante trabajo a realizar en el futuro.

Para finalizar, en el *capítulo 5*, se estudia el crecimiento cristalino de los polímeros de coordinación compartimentalizados, con ayuda de métodos microfluídicos y en colaboración con el Dr. Josep Puigmartí del instituto de química y bioingeniería del ETH Zurich. La microfluídica se ha demostrado como una herramienta útil para estudiar el crecimiento cristalino. Normalmente, los sistemas cristalinos sintetizados en el laboratorio se realizan bajo condiciones termodinámicas, esto es, temperatura, pH, composición del disolvente etc. Pero en sistemas de cristalización de sistemas vivos por ejemplo, los procesos ocurren bajo condiciones de no equilibrio, es decir, con gradientes químicos, difusión de los reactantes, efectos hidrodinámicos etc; lo que puede llevar a modos de crecimiento cristalino cinéticos. Normalmente, los efectos cinéticos pueden dominar sobre los termodinámicos, por lo que la microfluídica puede ser una herramienta excepcional para estudiar el crecimiento cristalino de los polímeros de coordinación, un campo bastante inexplorado a pesar de las interesantes propiedades que pueden presentar estos materiales. El polímero de coordinación compartimentalizado mostrado en el *capítulo 4*, **CCP-4**, se ha sintetizado bajo condiciones de microfluídica y se ha estudiado el crecimiento cristalino utilizando microscopio electrónico de transmisión. Como se ha dicho anteriormente, **CCP-4** presenta una capacidad de adsorber dióxido de carbono además de transición de espín. La morfología de los cristales sintetizados bajo condiciones termodinámicas en el laboratorio es de unas partículas hexagonales perfectas.

Utilizando la microfluídica se sintetizó el material **MF-CCP-4**, utilizando distintos tiempos de reacción. La caracterización de **MF-CCP-4** demostro por rayos X de polvo y magnetismo que mantenía las mismas características que

CCP-4, por lo que el material es análogo. Los estudios de microscopio electrónico de las 876 micropartículas obtenidas por microfluídica revelaron que el sistema puede crecer controlado cinéticamente a través de dos caminos de crecimiento cristalino: en el primero, una "semilla" cristalina crece a través de sus vértices, formando un hexágono incompleto que se va rellenando hasta completarse. Entonces una siguiente etapa del crecimiento ocurre, volviendo a crecer a través de los vértices. El otro camino de crecimiento cristalino ocurre cuando a partir de una "semilla cristalina", esta crece a partir de los laterales, hasta formar un hexágono incompleto también que se acaba rellenando. Entonces una siguiente etapa del crecimiento ocurre, volviendo a crecer a través de los laterales. Hay que hacer notar que ambos caminos llevan al mismo producto, el microcristal hexagonal.

Se estudió también el crecimiento termodinámico realizado en el laboratorio, recogiendo distintas alícuotas de la disolución de síntesis original para intentar "congelar" el crecimiento. El análisis por microscopio electrónico reveló que el crecimiento que se llevaba a cabo es el auto-ensamblamiento de pequeños hexágonos cristalinos, todos orientados en la misma dirección, formando un incompleto hexágono más grande.

Como conclusión, en este capítulo se ha revelado el crecimiento cristalino de un polímero de coordinación compartimentalizado con transición de espín. El uso de la microfluídica permite al sistema crecer hasta por dos caminos diferentes, pero obteniendo finalmente la misma estructura que en el producto termodinámico obtenido por la síntesis clásica. Pese a que los caminos encontrados por microfluídicas llevan a tiempos de reacción más largos que

por el método termodinámico, el uso de la microfluídica fuerza al sistema a evolucionar por estos caminos menos favorables energéticamente. Esto abre posibilidades de métodos de cristalización “a la carta” en materiales de similares características.

Resum de la Tesi Doctoral

Objectius

L'objectiu general d'aquesta tesi és la preparació de polímers de coordinació multifuncionals que presentin la propietat de transició d'espí i adsorció de gasos. Respecte a la primera, s'estudiarà la manera de modificar al nostre antull la transició i per això s'utilitzaran dues aproximacions: la primera, ajudada per la segona propietat d'adsorció de gasos, serà el aprofitar l'adsorció d'aquestes molècules per influir en les propietats electròniques del centre de ferro II, modificant el camp de lligands que pateix aquest i per tant, modificant la transició d'espí; la segona aproximació serà la combinació de diferents lligands orgànics que comparteixin la mateixa topologia de coordinació i per separat donen lloc a materials de molt diferent índole magnètica. La combinació de tots dos serà clau per generar nous entorns de coordinació en els centres de ferro II, provocant la creació de noves transicions d'Espí a diferents temperatures. A més, un altre objectiu addicional és l'estudi del creixement cristal·lí d'aquests materials.

Metodologia

Síntesi

En aquesta tesi s'han dut a terme diferents tècniques de síntesi per completar els objectius de la mateixa. Per començar, els lligands orgànics utilitzats en la construcció de polímers de coordinació han estat sintetitzats a partir de precursors previs. Per a això s'han aplicat les diferents tècniques de síntesi orgànica apreses en la formació universitària prèvia, afrontant els diversos problemes que aquestes presenten. Des de substitucions nucleofíliques

aromàtiques, passant per reduccions de grups azida a amina utilitzant hidrur d'alumini i liti o ciclació de compostos aromàtics, els lligands orgànics dissenyats prèviament "sobre el paper" per utilitzar en aquesta tesi s'han pogut sintetitzar sense problema.

Pel que fa a la part més inorgànica de la tesi, la síntesi dels polímers de coordinació, s'han utilitzat les diverses tècniques de creixement cristal·lins apreses durant el doctorat. S'han dut a terme amb èxit la síntesi de diversos polímers de coordinació utilitzant mètodes de "one pot", és a dir, la barreja directa a temperatura ambient dels components bàsics del polímer de coordinació (dissolucions de Lligand orgànic i de la sal del metall a utilitzar). Aquestes síntesi també s'han dut a terme en una altra variable, la del reflux, quan la barreja d'aquests materials necessita de temperatura per poder formar amb èxit els enllaços de coordinació. Aquesta última tècnica en ocasions pot resultar costosa en temps i materials, de manera que en algunes de les síntesis presentades en aquesta tesi s'ha optimitzat la síntesi de reflux i pot realitzar la formació del polímer de coordinació en un forn microones. L'optimització d'aquest tipus de síntesi ha permès reduir alguns temps de reacció de 4 hores a 5 minuts. Finalment, els materials de més alta cristal·linitat han estat obtinguts gràcies a les reaccions solvotermals, és a dir, síntesi dutes a terme en forns químics dins d´uns vials especials tancats que permeten assolir temperatures superiors a la temperatura d'ebullició del dissolvent.

Tècniques de caracterització

Raigs-X de monocristall

La cristal·lografia de raigs X de monocristall ens permet conèixer les estructures cristal·lines dels compostos sempre que es disposi d'un monocristall del material que difracten els raigs X. Es basa en el principi que els electrons dels àtoms difracten els raigs X rebuts, aquest resultant i mesurat pel detector conté informació sobre el nombre d'electrons i la posició de l'àtom del nostre material. Anàlisis posteriors amb mètodes matemàtics ens permeten obtenir les estructures cristal·lines dels compostos.

En aquesta tesi, les estructures cristal·lines resoltes a partir dels respectius monocristalls han estat mesurats a 120 i 240 K (a causa del caràcter de transició d'espí i el canvi estructural que comporta) en un difractòmetre SUPERNOVA equipat amb una font de raigs X de grafit monocromada (Mo). Per a la resolució de les estructures per mètodes matemàtics s'han utilitzat el paquet de programes SHELXTL i com a interfície gràfica el programa Olex-2. Els paràmetres de recopilació i refinament de dades es mostren en cada capítol corresponent.

Raigs-X de pols

Aquesta tècnica s'ha utilitzat per comprovar la puresa de les diferents mostres cristal·lines, comparant amb els patrons obtinguts en el difractòmetre de raigs X de monocristall. És una tècnica molt útil per poder detectar impureses en el material. Es basa en la incidència dels raigs X sobre una mostra del material introduïda en un capil·lar de 0,5 mm de diàmetre de vidre (material amorf,

invisible als raigs X pel que no interfereix en la mesura). Els raigs X surten difractats de la mostra amb un angle theta (θ), i a causa de la llei de Bragg de la diffracció ($\lambda = 2 \cdot d \operatorname{sen}\theta$), es poden establir les relacions de les distàncies interatòmiques. El detector es mou, recollint els diferents angles als quals difracta la mostra i recollint el difractograma de pols que conté informació sobre l'estructura cristal·lina de la mostra. Les mesures es van realitzar en un equip Empyrean PANalytical amb dos escombrats acumulats en el rang de θ de 2 a 60º.

Mesures magnètiques

Les mesures magnètiques realitzades als compostos presentats en aquesta tesi es van realitzar amb un magnetòmetre de tipus SQUID "Quantum Design MPMS-XL-5". SQUID és l'acrònim anglès per "Superconducting Quantum Interference Device" la traducció seria "Dispositiu Superconductor d'Interferència Quàntica". Aquests susceptómetres són capaços de mesurar senyals magnètiques molt petites amb molt poc soroll. Les mesures d'aquest treball es van realitzar generalment en l'interval de temperatures entre 2 i 300 K i aplicant camps magnètics de 0.1 T sobre les mostres poli-cristal·lines dels compostos. Després de realitzar les mesures, les dades de susceptibilitat es corregeixen per eliminar la contribució del porta-mostres on es mesura i de les contribucions diamagnètiques mitjançant les constants de Pascal.

Resum i conclusions

El treball descrit en aquesta tesi s'emmarca dins dels polímers de coordinació compartimentalitzats. Els polímers de coordinació són materials híbrids orgànics-inorgànics formats per un metall envoltat per uns lligands orgànics

units mitjançant enllaç de coordinació i es poden obtenir estructures que s'estenen en una, dues o tres direccions de l'espai. Les infinites possibilitats que existeixen a causa de la gran varietat de metalls disponibles i especialment, a la possibilitat de sintetitzar múltiples lligands orgànics permet dissenyar químicament materials amb propietats "a la carta", a més de la possibilitat de presentar multifuncionalitat, és a dir, la combinació de diverses propietats fent el material molt més interessant. Quan un polímer de coordinació presenta la característica de porositat, és a dir, presenta canals interns capaços d'allotjar hostes, ja siguin dissolvents, gasos o altres molècules, al polímer de coordinació se li crida Metal-Organic Framework (MOF), xarxes metall-orgàniques.

Dins d'aquestes múltiples propietats tenim l'estabilitat química, moltes vegades necessària per poder preparar un material útil ja que estarà exposat a l'atac de diversos agents químics que poden desgastar i inutilitzar les seves interessants propietats. Els MOFs a més presenten altes àrees superficials, fent-los candidats perfectes per al seu ús en catàlisi. La possibilitat d'utilitzar-los com a cèl·lules de combustible també s'ha explorat, amb la mesura de les seves propietats conductores. Però la característica estrela dels MOFs com ja s'ha comentat és la que els dóna la seva particular designació com sub-classe de polímer de coordinació i aquesta és la presència de porositat. La possibilitat d'allotjar hostes al interior d'aquests compostos (i el que pot comportar en la modificació d'una altra de les seves propietats) ha fet a aquests materials ser un dels camps en auge des de fa 20 anys. El 1998 es va reportar el primer exemple d'adsorció de gasos en un d'aquests materials, mesurant l'adsorció de diòxid de carboni i de nitrogen en l'anomenat MOF-5. En els següents anys,

l'intens estudi en el camp dels MOFs va permetre anar augmentant cada vegada més la capacitat d'emmagatzemar cada vegada més quantitat de gasos.

Però amb el temps, la simple idea d'emmagatzemar cada vegada més quantitat de gas va donar pas a una altra idea molt interessant, derivada de les necessitats mediambientals del planeta: la separació de gasos. Es va començar a estudiar un altre tipus de MOFs, els anomenats MOFs de ultramicroporus, on en lloc de buscar una obertura de porus més gran per poder emmagatzemar més quantitat de gas, es busca un porus més petit capaç de discriminar entre diferents gasos que componen una barreja. La producció de residus en la indústria petroquímica i electrònica porta al desenvolupament de nous materials capaç d'eliminar les impureses originades en la producció dels seus materials i els MOFs són candidats perfectes per dur a terme aquesta tasca. Per exemple, la producció d'acetilè pur és un problema a causa de que es genera una barreja gasosa d'acetilè / diòxid de carboni. El 2005 es va reportar un MOF que podia separar eficientment aquesta barreja gasosa. El MOF de coure reportat podia absorbir l'acetilè molt millor que el diòxid de carboni, permetent la separació d'aquesta barreja. Però realment la major utilitat seria poder absorbir la impuresa de diòxid de carboni, ja que en aquest primer material després és necessari el cost d'alliberar l'acetilè del material. Per això, en 2016 es va demostrar que això era possible, amb la publicació d'un treball on es va sintetitzar un MOF de manganès. A baixes pressions, es demostrava que aquest material podia absorbir diòxid de carboni preferentment sobre acetilè. Els autors pensaren sobre aquest comportament a causa de la interacció entre el moment quadrupolar del gas i la xarxa metall-orgànica.

Una altra barreja de gasos interessant de separar és la formada per etilè / acetilè. L'etilè és utilitzat àmpliament en la fructífera indústria dels polímers, però en la seva producció es generen diverses impureses, entre elles acetilè. En 2017 es va publicar sobre un MOF que permetia separar eficientment mescles d'acetilè i etilè.

L'altra propietat estrela que poden presentar els MOFs, a més de la seva intrínseca porositat, és el magnetisme. El magnetisme és una propietat que poden presentar els materials basada en els portadors d'espí. Els MOFs magnètics es poden dividir entre els que presenten interaccions magnètiques de llarg rang, els que tenen centres single-molecule magnets (SMMS) i els que presenten spin-crossover.

La presència d'interaccions magnètiques de llarg rang i porositat és un desafiament al qual s'han hagut d'enfrontar els químics per combinar aquestes dues propietats contràries: el magnetisme necessita distàncies curtes entre els centres metàl·lics per poder propagar eficientment el bescanvi magnètic i la porositat necessita llargues distàncies per poder generar porus més grans. Diverses estratègies s'han dut a terme per poder sortejar aquest inconvenient. S'han utilitzat lligands curts que tot i així generaven estructures poroses, de fet, el 2002 es va reportar un sistema amb un dels grups més curts, el grup CN, que presentava magnetisme i a més l'adsorció de molècules d'oxigen pel material modificava les seves propietats magnètiques. Una altra estratègia duta a terme és combinar dos tipus de lligands: un de curt per obtenir un bescanvi magnètic eficient en l'estructura i un altre més llarg a manera de "pilar" que permeti obtenir grans porus. La família del MOF-74 és un clar

exemple d'aquesta metodologia, podent haver sintetitzat una gran varietat de derivats canviant el centre metàl·lic (zinc, cobalt, níquel, magnesi, manganès, coure, ferro ...). El derivat de ferro es va reportar el 2012, demostrant a més que el bescanvi magnètic del MOF es podia ajustar fent servir l'adsorció de diferents hidrocarburs. Depenent del fort que sigui la interacció de l'hidrocarbur i la xarxa metall-orgànica, el canvi en el magnetisme és diferent. Una altra possibilitat és la utilització de radicals orgànics com lligands, a causa de que la presència dels espins individuals que posseeixen poden promoure interaccions de bescanvi efectives. El 2002 es va publicar el primer exemple d'un MOF amb lligands orgànics radical i presentant propietats magnètiques, encara que a molt baixa temperatura.

Els single-molecule magnets (SMMS) són molècules magnètiques que presenten baixa relaxació de la magnetització a baixes temperatures. La inclusió d'aquestes interessants molècules en els nodes d'un MOF es va produir per primera vegada el 2004, permetent estudiar eficientment el magnetisme en aquests materials. Però un derivat dels SMMS es va desenvolupar posteriorment i aquests van ser els single-ió magnets (SIMs). Basats en complexos metàl·lics mononuclears amb ions d'alta anisotropia magnètica, tenen la particularitat que són interessants en el camp de la computació quàntica ja que poden ser considerats com bits quàntics. El primer exemple de MOFs presentant SIMs en els nodes metàl·lics es va produir en 2014 en el nostre propi grup. Es va sintetitzar tota una família de SIM-MOFs usant diferents lantanoides.

L'última propietat magnètica que poden presentar els MOFs és la transició d'Espí. El primer exemple d'aquest fenomen es va reportar en 1930, però no va poder ser explicat eficientment fins anys més tard, quan les teories de camp cristal·lí i la seva evolució, la del camp de lligands es van establir. El fenomen es pot explicar quan un metall de transició pateix la degeneració energètica dels seus cinc orbitals d en presència d'un camp octaèdric de lligands. Es formen tres orbitals no enllaçants de menor energia i dos orbitals antienllaçants de major energia. El fenomen de la transició d'Espí pot aparèixer en ions de metalls de la primera sèrie de transició amb configuracions electròniques de d^4 a d^7 però el ió estrela estudiat en la transició d'espí és el ferro II, presentant una configuració d^6. Aquests 6 electrons tenen dues maneres de distribuir-se entre els 5 orbitals degenerats comentats anteriorment i depèn de la diferència energètica entre aquests dos grups d'orbitals (anomenada energia de camp cristal·lí) i l'energia d'aparellament dels electrons, P. Quan P és molt més gran que l'energia de camp cristal·lí, els electrons es col·loquen distribuïts entre tots els orbitals maximitzant la multiplicitat i obtenint un espí total a 2, anomenat l'estat d'alt espí (AE). En el cas energètic contrari, els sis electrons s'aparellen en els tres orbitals d de menor energia, resultant en un espí total a 0, anomenat l'estat de baix espí (BE). Quan l'energia del camp de lligands i l'energia d'aparellament són properes, pot haver una transició entre els dos estats mitjançant un estímul extern, ja sigui temperatura, pressió o llum i llavors passa el fenomen de la transició d'espí, el canvi d'AE a BE i viceversa.

La primera vegada que es va reportar un polímer de coordinació presentant transició d'espí va ser el 1995 i des de llavors el camp ha estat àmpliament

estudiat. Per produir una bona transició d'espí cal una cooperativitat elàstica, és a dir, la transició d'espí es genera inicialment en un centre metàl·lic i s'estén per tota la xarxa. Per poder dur a terme això en un polímer de coordinació infinit, cal tenir uns lligands orgànics apropiats que connectin els centres metàl·lics a més d'una estructura cristal·lina sense defectes. Quan es compleixen ambdós requisits, tenim transicions d'espí abruptes. Un tipus de compost que compleix aquestes característiques són els anomenats clatrats de Hofmann. La fórmula general d'aquests compostos és $\{Ni(NH_3)_2[Ni(CN)_4]\} \cdot 2H$ sent H un hoste intern. Es van descobrir a principis del segle XX però no va ser fins a mitjans quan la seva estructura va ser resolta. Fins a 1996 no es van introduir centres de ferro II en derivats de clatrats de Hofmann i va ser llavors quan va aparèixer la transició d'espí en aquest tipus de compostos. En els anys posteriors el desenvolupament de derivats canviant la resta d'àtoms de la fórmula introduir riques variacions per al desenvolupament i l'estudi de la transició d'espí en polímers de coordinació.

Però en aquesta tesi s'han utilitzat un altre tipus de lligands orgànics amb un grup funcional determinat, els Tetrazols. Els Tetrazols són un tipus de compost orgànic heterocíclic aromàtic, compost per quatre àtoms de nitrogen i un de carboni. Tenen una bona capacitat de coordinació a centres metàl·lics a causa dels seus nitròsgens dadors de densitat electrònica. A més, quan es coordinen en entorns de coordinació octaèdrics a centres de ferro II, produeixen un camp de lligands apropiat per obtenir el fenomen de la transició d'espí. Els anys 80 i 90 van ser molt fructífers en la publicació de treballs on es presentaven complexos mononuclears de ferro II amb Tetrazols coordinats exhibint transició d'Espí. No va ser fins l'any 2000 que es va

publicar el primer polímer de coordinació basat en Tetrazols que presentava transició d'Espí. El polímer en qüestió tenia una estructura lineal que s'estenia infinitament en una direcció de l'espai, presentant una transició d'Espí gradual.

En els anys següents el camp es va estendre en gran mesura, publicant altres compostos 1D però també 2D i 3D basats en Tetrazols. Els estudis es van centrar en principi a afegir cada vegada més àtoms de carboni alifàtics situats entre els dos grups Tetrazols. Diverses topologies i transicions d'Espí es van anar publicant al llarg de la dècada dels 2000, encara que la majoria mantenia la primera topologia trobada de cadenes 1D on els centres metàl·lics de ferro II estaven connectats per tres lligands bis-Tetrazols, estenent l'estructura infinitament .

Un cop establerta la transició d'Espí en els polímers de coordinació, un dels desafiaments als quals es va enfrontar el món científic va ser la capacitat per a modificar aquesta transició d'Espí mitjançant un estímul químic. La coexistència de porositat i transició d'Espí en els MOFs és una aproximació perfecta, ja que la inclusió de molècules hoste dins el MOF pot arribar a modificar aquesta transició. El nostre grup va publicar el 2013 el primer treball on l'adsorció d'un gas modificava la transició d'Espí. El compost en qüestió és un polímer de coordinació de ferro II basat en Lligand bis-tetrazol. L'estructura està formada per cadenes 1D que s'estenen infinitament, on els centres de ferro II estan triplement connectats per lligands bis-Tetrazols, deixant cavitats aïllades on es poden allotjar gasos. El polímer de coordinació presenta transició d'Espí i els estudis d'adsorció de gasos van demostrar que

el material adsorbía preferentment diòxid de carboni sobre nitrogen. A més, aquesta adsorció de diòxid de carboni modificava la transició d'Espí causa de la interacció del moment quadrupolar del CO_2 amb l'anell de tetrazol, canviant lleugerament el camp de lligands i per això, la transició d'Espí.

En aquesta tesi s'ha estudiat en profunditat la formació d'aquests sistemes de polímers de coordinació compartimentalitzats, és a dir, que presenten cavitats aïllades en el seu interior capaços d'allotjar gasos. La presència de ferro II i lligands tipus tetrazol ha permès obtenir transició d'Espí en tots els compostos, a més de poder modificar aquesta. També s'ha estudiat el creixement cristal·lí.

En el capítol 2, es va tractar la possibilitat d'adsorbir i separar diferents gasos en dos polímers de coordinació compartimentalitzats prèviament reportats, **CCP-1** i **CCP-2**. Tots dos són isoestructurals i presenten la fórmula [Fe (btzx)$_3$] (ClO_4)$_2$ i [Fe (btzx)$_3$] (BF_4)$_2$, respectivament, sent btzx un Lligand bis-tetrazol. Tots dos presenten cavitats aïllades a l'interior de la seva estructura cristal·lina i una transició d'Espí centrada a uns 200 K. Prèviament ja es va reportar l'estudi d'adsorció de nitrogen i diòxid de carboni en aquests materials, però en aquest capítol es va repetir més d'estendre amb CO (monòxid de carboni), CH_4 (metà), C_2H_6 (età), C_2H_4 (etilè) i C_2H_2 (acetilè). A les isotermes d'adsorció ja s'aprecien alguns problemes de difusivitat en alguns gasos, observant com el polímer de coordinació pot adsorbir aproximadament una molècula de diòxid de carboni, metà, acetilè i etilè; per contra, el monòxid de carboni, el nitrogen i el etè queden pràcticament sense adsorbir. Els valors volumètrics en adsorció són bastant competitius dins el

camp dels materials per adsorció, a causa de l'estructura intrínseca del material, ja que aquests polímers de coordinació compartimentalitzats presenten una estructura "densa", a causa de l'absència de canals permanents.

Es van realitzar mesures en el sincrotró ALBA, Barcelona, per poder determinar la localització de les molècules gasoses a l'interior de les cavitats en col·laboració amb el Dr. I. J. Vitórica-Yrezábal. L'ús de cavitats discretes comporta l'avantatge que les molècules de gas estan confinades en un menor espai, afavorint la interacció entre aquestes i la xarxa metall-orgànica. Els difractogrames de pols de la mostra carregada amb diòxid de carboni, acetilè i metà es van mesurar al sincrotró i mitjançant refinament Rietveld es va poder determinar la posició exacta de les molècules gasoses a l'interior de les cavitats, demostrant que aquestes interaccionen amb l'anell de tetrazol. El magnetisme de la mostra amb els diferents gasos adsorbits en el seu interior també s'ha mesurat amb èxit, trobant que diferents gasos modificaven la transició d'Espí d'una manera diferent. Per exemple, el diòxid de carboni estabilitza l'estat de baix espí, desplaçant la transició a majors temperatures; però, l'etilè estabilitza l'estat d'alt Espí, desplaçant la transició a menors temperatures. Això pot ser explicat a causa del diferent signe del moment quadrupolar d'ambdós gasos.

Finalment, es van realitzar mesures breakthrough de separació de mescles gasoses de diòxid de carboni / nitrogen i diòxid de carboni / metà. Les mesures van ser reeixides, demostrant que el polímer de coordinació compartimentalitzat podia separar eficientment el diòxid de carboni dels altres gasos en les seves respectives mescles presentant selectivitats

competitives respecte a la resta de materials del camp de separació de gasos.

La conclusió d'aquest capítol és que s'han sintetitzat eficientment dos polímers de coordinació compartimentalitzats que a més de presentar interessants propietats magnètiques, aquestes poden ser modificades després de la inclusió de gasos, a més de ser capaç de separar diòxid de carboni respecte nitrogen i metà, obrint la possibilitat d'ampliar l'estudi d'aquests polímers compartimentalitzats com un dels millors materials per estudiar la separació i purificació de mescles gasoses.

En el capítol 3 es va estudiar en profunditat la possibilitat de modificar la transició d'Espí. De totes les aproximacions per poder modificar la transició d'Espí es va utilitzar una de les més efectives: la possibilitat de combinar dues lligands amb lleugeres diferències estructurals però que mantinguin el mateix centre de coordinació. Dos polímers de coordinació prèviament reportats, $[Fe(btzx)_3](ClO_4)_2$ i $[Fe(btix)_3](ClO_4)_2$ presenten lligands molt semblants: btzx és un bis-tetrazol (4 àtoms de nitrogen en el heterocicle aromàtic) i btix és un bis-Triazol (3 àtoms de nitrogen en el heterocicle aromàtic). Són isoestructurals, encara que el Lligand btix adopta una conformació lleugerament diferent, obtenint una estructura lleugerament més torsionada. El major canvi s'observa en les seves propietats magnètiques: mentre el derivat de tetrazol mostra una transició d'Espí centrada a 200 K el derivat de Triazol es manté en alt Espí en tot el rang de temperatures. La possibilitat de crear una estructura híbrida amb dos lligands presents és la feina d'aquest capítol, on es van preparar eficientment una família de polímers de coordinació, usant dilucions de Lligand. Així, es van preparar diferents síntesi

combinant diferents proporcions de lligand, començant amb una alta proporció de lligand tetrazol que és el que provoca la transició d'Espí i afegint a poc a poc Lligand Triazol. També es va preparar una barreja física de tots dos compostos per comprovar la naturalesa química de les mescles que s'estaven sintetitzant.

Les anàlisis Pawley dels difractogrames de pols de les diferents dilucions químiques de Lligand van mostrar només una fase cristal·lina fins que el percentatge de Triazol utilitzat va arribar al 30%, on va començar a veure Lligand sense reaccionar. Quan el Lligand Triazol utilitzat va arribar al 50%, una barreja física de tots dos compostos es va trobar al difractograma de pols. El magnetisme de les mostres sintetitzades va demostrar que s'havia aconseguit crear una estructura híbrida de tots dos lligands: a baixes concentracions de Triazol utilitzat, a més de la transició d'Espí original, es genera una nova transició d'Espí centrada a 140 K, a més d'un petit desplaçament de la transició original de 200 K. a la xarxa infinita de centres de ferro II amb 3 lligands tetrazol servint de ponts, quan es va introduint Triazol en la barreja inicial, el Triazol s'insereix en algunes parts de la cadena, generant un nou entorn de coordinació de 5 Tetrazols i 1 Triazol en el ferro II, el que provoca l'aparició de la nova transició. A més, el caràcter torsionat del Triazol fa que s'exerceixi una pressió química interna en l'estructura, la responsable de desplaçar lleugerament la transició original. D'acord augmentem la quantitat de Triazol, la transició original disminueix en intensitat i la nova augmenta, confirmant la teoria. A més, en cert moment 2 triazols coincidiran un al costat de l'altre, generant un nou entorn octaèdric de 4 Tetrazols i 2 triazols, generant una nova transició. Això s'observa quan vam

arribar a un 20% de Triazol, generant una nova transició d'Espí a 60 K. D'acord augmentem més la quantitat de Triazol, es perd la coherència estructural a causa de la pressió a què es veu sotmesa l'estructura, i per 1% de Triazol igual a 50 s'obté una barreja física de tots dos components separats.

Com a conclusió a aquest capítol s'han sintetitzat amb èxit tota una família de dilucions químiques d'un sistema de transició d'Espí original, observant com no només es pot modificar la transició original, sinó que es poden sintetitzar sistemes amb múltiples transicions d'Espí, generant diferents entorns octaèdrics en els centres metàl·lics de ferro II, sent aquesta una aproximació senzilla de dur a terme i resolent molts dels problemes trobats en la recerca de la modificació de la corba de transició d'Espí en els polímers de coordinació.

En el capítol 4 es van sintetitzar amb èxit dos nous polímers de coordinació compartimentalitzats, isoestructurals a **CCP-1** i **CCP-2** i anomenats **CCP-3** i **CCP-4**, de fórmula $Fe(btzbp)_3](ClO_4)_2$ i $[Fe(btzbp)_3](BF_4)_2$ respectivament. El Lligand btzbp és un altre Lligand bis-tetrazol, però amb un anell de benzè més, en total 2 anells comparat amb l'anell present en btzx. La motivació de dissenyar químicament aquest Lligand va ser la possibilitat de generar cavitats discretes més grans en els polímers de coordinació compartimentalitzats, podent expandir la possibilitat d'adsorció de gasos i l'estudi magnètic. Mitjançant el disseny químic del Lligand, es va realitzar la síntesi d'aquest a partir de precursors comercials, podent dur-la a terme en 3 passos de síntesi orgàniques. A la primera, una reacció de substitució nucleofílica permetia canviar els grups Br terminals per grups N_3. Una

reducció mitjançant hidrur d'alumini i liti en el segon pas va reduir el grup azida a amina, i finalment es va realitzar la ciclació aromàtica de l'anell de tetrazol a partir de l'amina, azida de sodi i trietil ortoformat. La puresa del Lligand va ser comprovada per ressonància magnètica nuclear.

Es van realitzar les síntesis inorgàniques a reflux utilitzant les quantitats adequades de Lligand i de les corresponents sals de ferro II, obtenint els materials cristal·lins **CCP-3** i **CCP-4**, comprovant la seva puresa, cristal·linitat i caràcter isoestructural de tots dos per difracció de raigs X de pols. Un monocristall de **CCP-4** es va poder obtenir, resolent la seva estructura cristal·lina i comprovant que s'obtenia el polímer de coordinació compartimentalitzat, anàleg a **CCP-1** i **CCP-2** però amb cavitats internes grans.

Es va realitzar un estudi d'adsorció de gasos per diòxid de carboni, nitrogen i metà. De les isotermes d'adsorció de gasos es desprèn que nitrogen i metà gairebé no s'adsorbeixen, però mostrant una capacitat d'adsorbir dues molècules de diòxid de carboni per cavitat interna. Com es va voler demostrar al dissenyar químicament aquest sistema, la capacitat de **CCP-1** i **CCP-2** s'ha doblat, ja que en aquests sistemes previs la capacitat era d'una molècula de diòxid de carboni per cavitat.

El magnetisme de **CCP-3** i **CCP-4** es va estudiar, comprovant que mantenen una transició d'Espí relativament abrupta a 195 i 199 K respectivament, fins i tot per a centres de ferro II tan separats en l'espai. Això és a causa de la bona cooperativitat elàstica del sistema, a causa del triple pont tetrazol que propaga

efectivament la transició d'Espí per tota la xarxa cristal·lina. També es va estudiar la capacitat de modificar aquesta transició després d´adsorbir diòxid de carboni, estudiant que, per l'adsorció parcial del sistema d'una molècula, la transició es podia moure 7 K a temperatures majors, estabilitzant l'estat de baix Espí com en el cas de **CCP -1** i **CCP-2**. Sorprenentment, quan el sistema adsorbeix dues molècules de diòxid de carboni, la transició només es desplaça 3 K respecte a l'original. Inicialment, es podia esperar l'efecte acumulatiu, és a dir, el moment quadrupolar d'una molècula de diòxid de carboni afecta la densitat electrònica de l'anell de tetrazol, modificant la seva transició i una segona molècula podia desplaçar encara més aquesta transició. L'efecte observat està relacionat amb certa interacció interna entre les molècules de diòxid de carboni, disminuint el moment quadrupolar total que afecta a l'anell de tetrazol i per tant, desplaçant la transició d'Espí una menor temperatura.

Per acabar, es van dur a terme estudis de deposició del sistema en substrats de silici i quars, podent obtenir una bona deposició d'aquest al de silici. La caracterització per raigs X i el magnetisme revelen que el sistema manté les seves propietats quan aquest és dipositat sobre una superfície en dues dimensions.

Com a conclusió, el disseny químic d'un Lligand més llarg per obtenir un sistema amb majors cavitats internes i permetre una major adsorció de molècules de gas i l'estudi de les seves propietats magnètiques s'ha realitzat amb èxit. Això obre possibilitats a l'estudi d'aquests sistemes, incloent diferents funcionalitats en el disseny de nous lligands amb diferents espaiadors entre els anells de tetrazol, permetent com afecta aquesta

característica a les seves propietats d'adsorció de gasos i magnètiques. A més, la possibilitat de dipositar aquests interessants sistemes en dues dimensions obre la possibilitat de poder fabricar membranes d'adsorció de gasos que continguin aquests polímers de coordinació compartimentalitzats. Els estudis de separació de gasos en aquest sistema amb major cavitat interna també pot ser un interessant treball a realitzar en el futur.

Per acabar, en el capítol 5, s'estudia el creixement cristal·lí dels polímers de coordinació compartimentalitzats, amb ajuda de mètodes microfluídics i en col·laboració amb el Dr. Josep Puigmartí de l'institut de química i bioenginyeria de l'ETH Zurich. La microfluídica s'ha demostrat com una eina útil per estudiar el creixement cristal·lí. Normalment, els sistemes cristal·lins sintetitzats al laboratori es realitzen sota condicions termodinàmiques, això és, temperatura, pH, composició del dissolvent etc. Però en sistemes de cristal·lització de sistemes vius per exemple, els processos ocorren sota condicions de no equilibri, és a dir, amb gradients químics, difusió dels reactants, efectes hidrodinàmics etc; el que pot portar a maneres de creixement cristal·lí cinètics. Normalment, els efectes cinètics poden dominar sobre els termodinàmics, de manera que la microfluídica pot ser una eina excepcional per estudiar el creixement cristal·lí dels polímers de coordinació, un camp força inexplorat tot i les interessants propietats que poden presentar aquests materials. El polímer de coordinació compartimentalitzat mostrat en el capítol 4, **CCP-4**, s'ha sintetitzat sota condicions de microfluídica i s'ha estudiat el creixement cristal·lí utilitzant microscopi electrònic de transmissió. Com s'ha dit anteriorment, **CCP-4** presenta una capacitat d'adsorbir diòxid de carboni a més de transició d'Espí. La morfologia dels

cristalls sintetitzats sota condicions termodinàmiques al laboratori és d'unes partícules hexagonals perfectes.

Utilitzant la microfluídica es va sintetitzar el material **MF-CCP-4**, utilitzant diferents temps de reacció. La caracterització de **MF-CCP-4** va demostrar per raigs X de pols i magnetisme que mantenia les mateixes característiques que **CCP-4**, de manera que el material és anàleg. Els estudis de microscopi electrònic de les 876 micropartícules obtingudes per microfluídica van revelar que el sistema pot créixer controlat cinèticament a través de dos camins de creixement cristal·lí: en el primer, una "llavor" cristal·lina creix a través dels seus vèrtexs, formant un hexàgon incomplet que es va omplint fins completar-se. Llavors una següent etapa del creixement passa, tornant a créixer a través dels vèrtexs. L'altre camí de creixement cristal·lí passa quan a partir d'una "llavor cristal·lina", aquesta creix a partir dels laterals, fins a formar un hexàgon incomplet també que s'acaba omplint. Llavors una següent etapa del creixement passa, tornant a créixer a través dels laterals. Cal fer notar que els dos camins porten al mateix producte, el microcristal hexagonal.

Es va estudiar també el creixement termodinàmic realitzat al laboratori, recollint diferents alíquotes de la dissolució de síntesi original per intentar "congelar" el creixement. L'anàlisi per microscopi electrònic va revelar que el creixement que es duia a terme és l'auto-ensamblament de petits hexàgons cristal·lins, tots orientats en la mateixa direcció, formant un incomplet hexàgon més gran.

Com a conclusió, en aquest capítol s'ha revelat el creixement cristal·lí d'un polímer de coordinació compartimentalizat amb transició d'Espí. L'ús de la microfluídica permet al sistema créixer fins per dos camins diferents, però obtenint finalment la mateixa estructura que en el producte termodinàmic obtingut per la síntesi clàssica. Malgrat que els camins trobats per microfluídiques porten a temps de reacció més llargs que pel mètode termodinàmic, l'ús de la microfluídica força al sistema a evolucionar per aquests camins menys favorables energèticament. Això obre possibilitats de mètodes de cristal·lització "a la carta" en materials de similars característiques.

This text collects the work developed by the author as a PhD student in the Institute of Molecular Science (ICMol) under the supervision of Prof. Eugenio Coronado and Dr. Guillermo Mínguez Espallargas.

Compartmentalized coordination polymers (CCPs) are a specific type of metal-organic materials that present isolated cavities accessible for host molecules. The work described in this thesis is motivated by the intention of developing multifunctional compartmentalized coordination polymers and study their magnetic and gas sorption properties besides the interplay between them.

ICMol
Institut de Ciència Molecular

VNIVERSITAT DE VALÈNCIA